JPRS L/9884

31 July 1981

USSR Report

METEOROLOGY AND HYDROLOGY

No. 3, March 1981

FBIS FOREIGN BROADCAST INFORMATION SERVICE

NOTE

JPRS publications contain information primarily from foreign newspapers, periodicals and books, but also from news agency transmissions and broadcasts. Materials from foreign-language sources are translated; those from English-language sources are transcribed or reprinted, with the original phrasing and other characteristics retained.

Headlines, editorial reports, and material enclosed in brackets [] are supplied by JPRS. Processing indicators such as [Text] or [Excerpt] in the first line of each item, or following the last line of a brief, indicate how the original information was processed. Where no processing indicator is given, the information was summarized or extracted.

Unfamiliar names rendered phonetically or transliterated are enclosed in parentheses. Words or names preceded by a question mark and enclosed in parentheses were not clear in the original but have been supplied as appropriate in context. Other unattributed parenthetical notes within the body of an item originate with the source. Times within items are as given by source.

The contents of this publication in no way represent the policies, views or attitudes of the U.S. Government.

APPROVED FOR RELEASE: 2007/02/09: CIA-RDP82-00850R000400030065-3

JPRS L/9884

31 July 1981

USSR REPORT

METEOROLOGY AND HYDROLOGY

No. 3, March 1981

Translation of the Russian-language monthly journal METEOROLOGIYA I GIDROLOGIYA published in Moscow by Gidrometeoizdat.

CONTENTS

Structure and Conditions of Development of Thunderstorm Clouds..... 1

Anthropogenic Changes in Atmospheric CO_2 Concentration During the Next Fifty Years..... 19

Experimental Investigation of the Correlation Between the Meteorological Range of Visibility and Altitude of the Lower Cloud Boundary..... 36

Running Control and Evaluation of Alternative Models..... 45

Determination of Turbulent Diffusion Coefficients..... 52

Computation of Transport of Substances Contaminating the Atmosphere..... 60

Two-Frequency Microwave Radiometric Method for Determining Wind Velocity From a Satellite..... 65

Diagnostic Model of Water and Ice Circulation in the Arctic Basin..... 76

Complex Prediction of the Interannual Variability of Inflow of North Sea Waters Into the Baltic According to Shore Observation Data..... 86

Status of the Study of the Element-Salt Composition of Sea Waters Using Nuclear-Physical Methods..... 91

Use of Radar Data in a Hydrodynamic Model of Rainwater Runoff With Distributed Parameters..... 99

Experimental Substantiation of Computations of the Rate of Water Flow Along the Cultivated Surface of Slopes..... 107

Determination of Damage to Cotton Plants in Different Development Stages Resulting From Hailfalls..... 112

Improvement in the Method for Predicting the Intensity and Quantity of Precipitation in a Warm Period..... 119

Possibility of Prediction of Lightning Discharges..... 125

Determination of Filtration Coefficients of Cohesive Soils in a Frozen State Through Their Kinetic Specific Surface..... 128

Evaluation of Applicability of Different Methods for Determining Evaporation From a Water Surface in a Zone of Hummocked Swamps..... 134

Reconciling of Mesospheric Temperature Values Measured by Different Rocket Sounding Systems..... 138

Radio Device of a System for Thermal Sounding of the Atmosphere by the Radioacoustic Sounding Method..... 146

Review of Monograph by V. R. Alekseyev and B. L. Sokolov: Polevyye Issledovaniya Naledey (Field Investigations of Ice Encrustations), Leningrad, Gidrometeoizdat, 1980..... 151

Fiftieth Anniversary of the Leningrad Hydrometeorological Institute..... 154

Notes From Abroad..... 157

Obituary of Maksim Savvich Kulik (1907-1980)..... 159

UDC 551.(594.21:576.1)

STRUCTURE AND CONDITIONS OF DEVELOPMENT OF THUNDERSTORM CLOUDS

Moscow METEOROLOGIYA I GIDROLOGIYA in Russian No 3, Mar 81 pp 5-17

[Article by I. M. Imyanitov, Main Geophysical Observatory, manuscript received 2 Jul 80]

[Text]

Abstract: Investigations of recent years have demonstrated that the electric properties of thunderstorm clouds differ appreciably from those postulated only 10 years ago. It has been established that thunderstorm phenomena occur in stratiform clouds, that there is a high level of electric losses in active thunderstorm clouds, and that there are electric currents exceeding by orders of magnitude those which were surmised. It was postulated that the critical conditions for the occurrence of a discharge include energy factors. Existing models were inadequate for explaining the observed electric characteristics. Two schemes are presented: for the process of electrification of a part of the clouds, based on the contact electrification process, and macroelectrification of the clouds, based on the effect of falling of charged precipitation. Both schemes make it possible to explain the effects discovered during the last decade.

Man's acquaintanceship with thunderstorms can be divided into four stages. In the first stage man attempted to answer the question "what is this?"; in the second stage "how?"; in the third stage "why?"; and finally, now, in the fourth stage "how to control it?" However, the answers to the preceding two questions are by no means complete.

A solution of the problem of how thunderstorm clouds are structured and why thunderstorm phenomena develop should also be the basis for predicting thunderstorms and for foreseeing the local and global consequences of industrial activity and for understanding the physics of a high-voltage discharge in aerosol clouds. Although no other phenomenon is expressed so sharply in the atmosphere as a thunderstorm in relation to the dependence of man on natural forces with the development of technology and industry, the principal electric characteristics of clouds have become known, and indeed, only in a general way, only now. Accordingly, there are mutually exclusive theories of thunderstorm electricity [22] because thunderstorms develop under conditions which meteorologists not only do not consider dangerous for the development of thunderstorms, but even conditions which are hypothetically impossible for their occurrence [4].

1. Electric Model of Thunderstorm Cloud

A simple model of the electric structure of a thunderstorm cloud as formulated by Simpson (for example, see [9, 14, 17] was not capable of explaining the new facts (Table 1). This was also true of the Kuettner model (for example, see [17]).

A new model was developed and an attempt has been made to examine its statistical and dynamic aspects [9-27]. A model of a thunderstorm cloud in the maturity stage is shown in Fig. 1. As long as the stage of a well-developed cumulus cloud prevails the electric charge 3 is absent and the charges 1, 2 and 4 are several orders of magnitude less than those existing in the maturity stage. In the period of transition from the Cu cong stage to the stage of mature Cb, conventionally designated Cu cong→Cb, the charge 2 is small in comparison with the charge 1 and therefore the field strength over the cloud has a different direction than in the maturity stage. The charge 3 is associated for the most part with the charge of falling precipitation. In the decay stage the charge 3 is considerably decreased and the charges 1 and 2 become less than in the preceding stage.

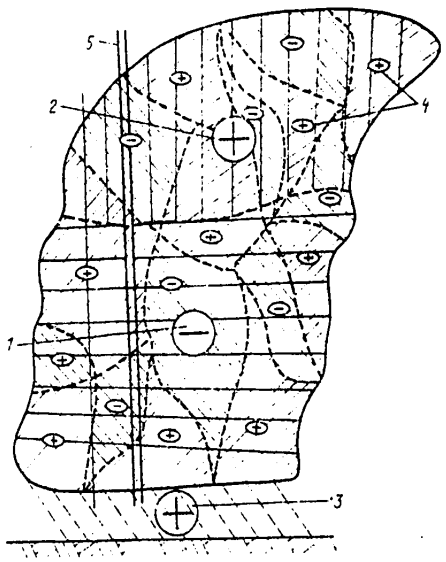

Fig. 1. Static model of thunderstorm cloud in maturity stage. 1) main electric charge in cloud; 2) charge arising under influence of atmospheric conductivity; 3) precipitation charge; 4) charge of electric inhomogeneities in cloud; 5) column of unit section.

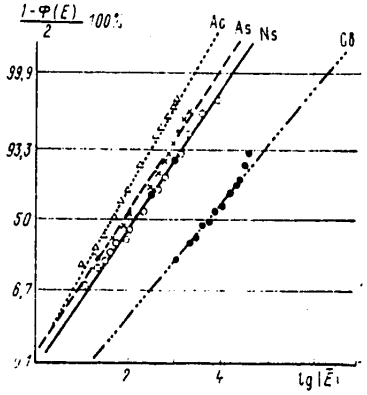

Fig. 2. Probability 1 - Φ(E) of occurrence of fields with the strength E less than the stipulated level in clouds of different species.

The characteristics of the electric field outside the cloud are determined for the most part by the charges 1, 2, 3. The charges in zones of inhomogeneity 4 can create local field strengths exceeding by an order of magnitude those created by the

Table 1

Electric Properties of Thunderstorm Clouds

Characteristics or parameter	Data to 1970	New Data
Electric structure created by organized electrification	Remains constant in all stages and can be approximated by a three-charge structure	Changes in different stages of cloud development, undergoing transition from two- to three-charge with simultaneous existence of strongly charged small zones
Stage of charge accumulation in convective clouds	Cu cong., Cu cong. → Cb, Cb	Cu cong. → Cb, Cb
Clouds in which electric discharges can occur	Cb	Cb, Ns and some other stratiform clouds
Mean value of principal cloud charges, Kl	10-30 (static model) 100-500 (dynamic model)	10-30
Average electric currents, A:		
over cloud	0.5-1	0.05-1
in cloud	0.5-1	10-100
Conductivity, cm/m	10^{-16}-10^{-15}	10^{-13}-10^{-12}
Limiting field strengths, V/m:		
average for cloud	10^5	10^5
in zones of inhomogeneities	?	10^6
Minimum field strength at which discharge begins, V/m	?	10^6
Minimum energy of zone in which discharge begins, J	10^6-10^8	10^3
Minimum extent of zone in which discharge begins, m	10^{-2}-100	20
Minimum field strength necessary for maintaining discharge, V/m	?	10^5
Number of possible elementary mechanisms for electrification of particles leading to cloud charging	20	2 (contact electrification and capture of ions from air)

Table 2

Mean Values of Principal Charges in Clouds in Maturity Stage

Latitude, degrees	Mean electric moment created by charges 1 and 2, Kl·km	Charges 1 and 2, Kl	Distance between charges 1 and 2 a, km	$\alpha = h/a$ (h is cloud thickness, in km)
60-50 N	35	23	1.5	4-6
50 N	70	24	3	3-4
35 N	230	39	6	1.5-2.5
35 S	200	40	5	1.5-2.5

main charges. The value of the main charges 1 and 2 is different for different clouds and has a tendency, on the average, to increase toward the equator (Table 2).

The probability of encountering field strength values less than the average value in clouds of the temperate latitudes is shown in Fig. 2, taken from [9]. This probability is approximated satisfactorily by a log-normal distribution. The principal electric macrocharacteristics of clouds are given in Table 1. In the analysis of the data in Table 1 it must be taken into account that it gives estimated data since the precise parameterization of the properties of clouds, a discrimination of the peculiarities introduced by the specifics of aerosynoptic processes and the influence of characteristic physiographic conditions require the carrying out of prolonged systematic measurements which for the time being have not been made.

In summarizing what has been stated above, it should be noted that recently essentially new data have been obtained on the meteorological conditions for the occurrence of thunderstorm phenomena, on the electric structure of thunderstorm clouds and its changes, on the principal electric characteristics of clouds and on the conditions for the occurrence of lightning in clouds. It was found that the theories and hypotheses formulated up to the late 1960's are incapable of explaining the observed phenomena, and the question naturally arose: what processes cause them?

2. Thunderstorm Cloud as an Electric Generator

We will represent a thunderstorm cloud as an electric generator in which particles, having different velocities of motion, can be charged in large part with different signs and thereafter, due to the difference in velocities, large volumes are formed in space which are charged primarily by electricity of one sign or another. The charges of these volumes should create electric fields whose strength and extent are sufficiently great for the appearance of lightning. The answers to the questions of how the processes of micro- and macroelectrification occur and what the term "adequacy" of strength and extent for the occurrence of lightning means will provide a key to the understanding of the true electric activity of a cloud.

2.1. Charging of particles in clouds.

Among the many difficulties facing investigators of the processes of charging of particles in clouds the greatest complexities are probably caused by three circumstances: the measured charges on precipitation particles were considerably greater than those arising in laboratory experiments (for example, see [9, 14, 17, 28]); the charges of particles of both clouds and precipitation could be both positive and negative; as a rule, if the particles of one sign are encountered in a greater quantity, the mean value of their charges is less than the mean value of the charges of particles present in a lesser quantity (for example, see [14, 28]); finally, the conditions for the charging of particles in different stages of cloud development and in its different parts are so dissimilar that it seemed that tens of elementary electrification processes developed, the relationship of whose activities was extremely difficult to determine (for example, see [9, 14, 28]). Investigators of any of these processes almost invariably attempted to put "their" process as the basis for the

next theory of thunderstorm electricity, but it was invariably found that the electroproductivity of the processes was inadequate. For example, induction charging with the breaking of a contact in an electric field was inadequately effective because measurements in clouds [5, 24] indicated that the real field strength in clouds cannot ensure the necessary charges. Investigations of the Workman and Reynolds mechanism and its modifications, on which great hopes were also laid, led to the unexpected conclusion that although this effect creates great potentials the charges created by them are less than the charges appearing with the breaking of the contact (rupture of the film) of ice and water particles [6]. Accordingly, M. Brook [22] even proposed that moratoria be imposed on new and old investigations of the processes of elementary electrification until there was a more precise clarification of the characteristics of clouds in order to avoid the appearance of noncomparable hypotheses, theories and models. A solution to this problem was found when it was possible to reduce all the principal processes of electrification of particles in clouds to two (for example, see [9]):

-- charge exchange between particles separated in space (after the contact of different particles, during destruction of a particle), so-called contact electrification;

-- transfer of charges from an ionized gas medium to particles.

Both processes can be substantially influenced by external strong electric fields, changing both the electrification at the contact and the ionization level and creating reverse positive and negative feedbacks having a significant effect on the electrification of particles.

Contact electrification arises in every case when there is a break in the contact between two particles, during the destruction of particles, detachment of a water film from solid particles, escape of splinters from a freezing drop and similar effects (for example, see [9]).

If a neutral particle collides with another neutral particle and the difference in their electrochemical potentials is $\varphi_{1,2}$, after breaking of the contact the charges $+q_1$ and $-q_1$ arise on the particles

$$|q_1| = \varphi_{1,2}\, c_{1,2}, \qquad (1)$$

where $c_{1,2}$ is the mutual capacitance of the particles at the time of breaking of the electrical contact between them [3].

The difference in the electrochemical potentials $\varphi_{1,2}$ is dependent on the chemical composition of the particles, their phase state and surface properties; the capacitance $c_{1,2}$ is dependent on the geometry of the particles, their elasticity properties and on the concentration and mobility of the charge carriers in the particles and also on temperature. Under these conditions virtually any breaking of the contact of particles results in their electrification, which will be the greater the more diverse the particles. A paradox appears: it is more difficult to explain why the particles in an aerosol cloud are uncharged than to explain their charging.

If a large particle collides with small particles, similar in their properties, the charge q of the large particle will increase exponentially. We will assume as a simplification that the large and small particles are spherical and their radii

are equal to R and r respectively, $R \gg r$, and the difference in their electrochemical potentials is $\varphi_{1,2}$. Then the charge acquired by the large particle is

$$q = \frac{(R+r)^2}{1{,}5\,r^2}\, q_1\,(1 - e^{-\frac{t}{\tau}}). \qquad (2)$$

The limiting charge q_{lim} arising on the large particle will be equal to [2, 3]

$$q_{lim} \approx \varphi_{1,2} c_{1,2} \frac{R^2}{r^2} \approx q_1 \frac{R^2}{r^2}. \qquad (2a)$$

In this case $c_{1,2} \approx Ar$, where $A = 3\text{-}8 \approx 5$, and q_1 is the charge imparted to the particle at the time of the first contact. The relaxation time of the process will be equal to $\tau \approx R^2/r^2N$, where N is the number of collisions of large and small particles per unit time.

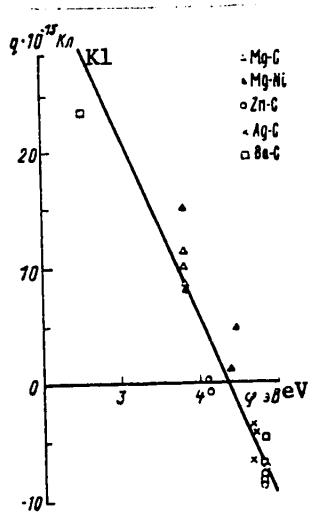

Fig. 3. Dependence of charge with breaking of contact of two particles having an electric potential difference $\Delta\varphi$.

As a result of this effect, in clouds during collisions of precipitation particles and cloud droplets a charge can be formed on the first which exceeds by a factor of 10^2-10^4 that obtained in a single collision and usually observed in the laboratory. In the experiments of Buser and Aufdermaur [18] it was demonstrated that the charge imparted in this case in actuality is proportional to the difference in electrochemical potentials (Fig. 3). Formulas (2) and (3) have been confirmed in numerous experiments [2, 11, 18]. Thus, collective effects can play a major role in the electrification of particles in a cloud.

If $\varphi_{1,2}$ and the sizes of particles are random values, the charges accumulated on small and large particles are imparted with some distributions [11, 12]. Two extreme cases are possible: if large and small particles (precipitation particles

and cloud particles) with equal probability acquire both positive and negative charges no organized electrification will occur in the cloud, although the particles in it will be charged, but if the large particles are charged with one electric sign and the small particles are charged with another, organized electrification of the cloud arises which is intensified with the falling of precipitation particles. In a general case, when the total values of the charges of large and small particles are displaced in different directions from the zero value, organized electrification is combined with the charging of particles of any sizes with different electric signs.

The magnitude of the charge imparted during contact is dependent on the strength of the external field E. However, the role of the induction mechanism of charging occurs only in very strong fields. The fact is that induction charging is comparable with contact charging and exceeds it only when

$$\gamma E\delta \geqslant \varphi_{1,2},$$

where δ is the gap between the particles 1 and 2 at the time of breaking of the contact and γ is the coefficient of intensification of the external field in the gap between the particles; the γ value is close to A, that is, $\gamma \approx$ 5-10. Since for liquid particles the value $\delta = 10^{-7}$-10^{-4} cm, whereas for solid particles it is close to $\delta = 10^{-8}$-10^{-6} cm, in fields $\geqslant 10^4$ V/cm the induction mechanism begins to prevail over the contact mechanism. This effect is clearly manifested in experiments [18] and explains the noncorrespondence between the Sartor, Zhiv and Levin and other models to the observed results.

Superposed on the contact electrification process is the capture of ions from the air, usually lessening the charge acquired with the breaking of the contacts [12] and also the charging of particles by the capture of ions from the surrounding air (for example, see [9, 14, 17, 28]). However, these processes, even in the modern interpretation [34], do not make it possible to obtain the charges required in the cloud during the time of its development.

The reduction of the numerous processes of particle electrification in clouds to two made it possible to simplify the problem of experimental and theoretical modeling of the process of electrification of particles in clouds. However, such modeling must include allowance for the coagulation of particles, the influence of electric forces on the interaction of particles, the influence of medium conductivity, the change in cloud ionization in strong electric fields and allowance for the positive and negative feedbacks caused by these effects.

2.2. Accumulation of space charges in clouds. The literature describes two models of the process of accumulation of electric charges in clouds. In the first of these, representing a development of the concepts of El'ster and Geytel' and Wilson (for example, see [9, 14, 17, 28]), the principal reason for the separation of regions charged with the same sign in clouds is the falling of particles of precipitation charged with the same electric sign relative to smaller particles charged with the other sign. The energy already accumulated in the cloud as a result of ascent of its water part in the gravity field in this model is realized in an electric cloud generator during the falling of particles. This model initially seemed to contradict the facts because the charges of precipitation particles measured at the

earth's surface did not confirm the models of predominant charging of precipitation. Only after measurements aloft -- in clouds and directly under them -- was it found that in clouds there are extremely extended zones in which virtually all the precipitation particles are charged with the same sign [5, 26] and only at the ground level, due to the charge exchange effect, will the observed + and - charging be observed.

In the second model, developed by Green and Vonnegut (for example, see [9, 17, 28]), the charging of clouds is created due to convective transfer of the space charge accumulating near the earth into a cloud by vertical air movements; this charge, passing through the cloud, settles on its droplets. The charge accumulating in the cloud with its field causes an outflow of charges of the other sign toward the boundaries of the cloud, primarily toward its upper part, creating a dipole electric structure. In this model the cloud acts as a singular electric filter. The energy realized in the cloud electric generator appears due to vertical air movements.

Vonnegut, developing the Green scheme, postulated that the corona discharge of pointed objects or features on the ground under the influence of the cloud field leads to an intensified charging of the latter, which in turn intensifies the entry of space charges into the cloud, etc. The possible positive correlation between the rate of entry of the charge into the cloud and the intensity of its generation made it possible to regard the cloud as an induction type electrostatic machine.

At the last, Fifth International Conference on Atmospheric Electricity the principal reports [29, 30] represented the points of view set forth above and the main problems were concentrated in them. Without dwelling on the details of the discussed problems [22], we note only that the supporters of the Green-Vonnegut model have pointed out that the model of charging of clouds by precipitation does not explain the high value of the observed charges of precipitation, the noncoincidence of the zone of falling of precipitation and the zone of generation of lightning, thunderstorm phenomena in warm clouds and the appearance of a space charge layer (electrode effect) in the upper part of the cloud. The opponents of the Green-Vonnegut theory noted, in particular, that the sign of the charge accumulated by the cloud in the initial stage of the process is opposite that predicted by theory.

In the experiments carried out for solution of the problem of the possibilities of the convective mechanism, carried out under our direction [9, 10], it was demonstrated that in well-developed cumulus clouds with their tops at a level of 6 and even 7 km, there is no appreciable electric charge as predicted by the convection theory, the magnitude of the cloud charges is virtually not dependent on its thickness, and only with the appearance of large droplets in the cloud ($\bar{\Phi} > 100\,\mu m$) do the electric processes begin to intensify. At the same time the data in Table 1 show that the absence of appreciable electrification in the Cu cong stage does not make it possible to accumulate the observed charges as a result of convection in the few minutes separating this stage from the thunderstorm stage. It can therefore be assumed that the first and foremost reason for the charging of a cloud is the falling of precipitation, although in the stage Cu cong→Cb and Cb air movements can play a substantial role, although differing from that predicted by convection theory.

Since the process of electrification of clouds in general, the same as for individual particles, transpires in a conducting medium, in all computations of an electric cloud generator it is necessary to take into account the relationship of intensity of charging and discharging processes. Failure to take this circumstance into account made it impossible to use the schemes and models of electrification of clouds, which are being developed even recently [14, 22], and required the development of a new model.

We will attempt to convey the principal features of this model using a simple scheme. A complication of the model (for example, see [13]) leads to more precise data, but deprives the model of graphic features.

Mow we will examine the change with time t of the charge Q of a unit column 5 (see Fig. 1) of an initially neutral cloud present in a conducting medium due to the falling of precipitation whose particles acquire an electric charge as a result of the contact mechanism [9, 27]

$$dQ/dt - I_{ch} - 4\pi(\lambda_{a_{up}} + \lambda_{a_{low}} + \lambda_{eff})Q, \tag{3}$$

where I_{ch} is the current created by falling charged precipitation, $\lambda_{a_{up}}$ and $\lambda_{a_{low}}$ are the atmospheric conductivities at the upper and lower boundaries of the cloud, λ_{eff} is the effective conductivity in the cloud.

The electric current in the precipitation is

$$I_{ch} = \sum_i n_i q_i V_i - \sum_j n_j q_j V_j. \tag{4}$$

where n_i, V_i and q_i are the concentration and velocity of particles carrying a charge of the same sign and n_j, V_j and q_j are the corresponding notations for particles carrying a charge of a different sign.

The effective conductivity is

$$\lambda_{eff} = \lambda_0 + Pk, \tag{5}$$

where λ_0 is conductivity within the cloud, k is the mean value of the coefficient of turbulent exchange within the cloud, P is a coefficient dependent on the geometry of the distribution of charges and turbulence within the cloud.

The first term on the right-hand side of equation (3) describes the electric currents charging the clouds; the second term describes its discharge currents I_{dis} through the upper and lower boundaries.

The solution of equation (3) is given for a one-dimensional case on the assumption of a constancy of the currents I_{ch} and I_{dis} with time in the form

[3 = ch]

$$Q = I_{ch}\tau\left(1 - e^{-\frac{t}{\tau}}\right), \tag{6}$$

where τ is the relaxation time,

$$\tau = \frac{\varepsilon}{4\pi(\lambda_{a_{up}} + \lambda_{a_{low}} + \lambda_{eff})} \tag{7}$$

Under the conditions of the problem which we adopted equation (6) can be represented in the form

$$Q_{cloud} = I_{ch} S \tau I_3 S \left(1 - e^{-\frac{t}{\tau}}\right), \quad (8)$$

where S is the cross-sectional area of the active part of the cloud and Q_{cloud} is the charge 1 in Fig. 1.

The upper charge 2 (Fig. 1) is created by a conductivity current bringing from the atmosphere a charge which settles on the particles of the upper part of the cloud. Since usually $\lambda_{a_{up}} \gg \lambda_{a_{low}}$, the corresponding charging exerts no appreciable effect in the lower part of the cloud and the charge 2 of the cloud in the maturity stage can become close in absolute value to the charge 1.

The electric moment M of the cloud in the maturity stage can accordingly be represented by the expression

$$M = \alpha h Q_{cloud}, \quad (9)$$

where h is cloud thickness and α is a dimensionless coefficient showing by how many times the cloud thickness exceeds the distance between the centers of the charges 1 and 2 (Table 2).

The lower charge 3 (Fig. 1) is created by the charge of precipitation and is equal to

$$Q_{ch} = \sum_i n_i q_i - \sum_j n_j q_j. \quad (10)$$

It is important to note that the charges 1 and 2 accumulated in the cloud can exceed the charge 3 by many times. If there are significant changes in wind velocity with height this can lead to an appreciable displacement of the region of lightning generation relative to the precipitation zone (for example, see [23]).

The stage of decline of electric activity in the cloud is characterized, in particular, by the fact that the cloud charging current I_{ch} begins to decrease with time. Usually this moment is close to the onset of attenuation of precipitation. In this case the solution of (8) is somewhat modified: it contains a cofactor characterizing this process. If the precipitation ceases suddenly, the charge and the electric moment of the cloud decrease at a rate determined by the relaxation time τ.

If electric simulations are used, the model resembles a Van Graff generator situated in a conducting medium. The role of a "conveyor belt," carrying the charges, is played by precipitation and the role of an electrode is played by the cloud itself.

The considered model shows that the cloud electrification changes:
-- proportionally to the increase in the electric current of the precipitation, which in turn changes proportionally to: a) the change in the charges on the individual precipitation particles, b) change in the difference in the concentrations of precipitation particles charged with different signs, c) the increase in the relative rate of falling of precipitation particles charged with different signs;
-- proportionally to the horizontal and vertical extents of the active part of the cloud;

-- inversely proportionally to the increase in electric losses of the cloud, in particular to: a) the increase in cloud conductivity, b) the increase in turbulence within the cloud, c) the increase in atmospheric conductivity at the upper boundary of the cloud, dependent primarily on the altitude of the upper boundary.

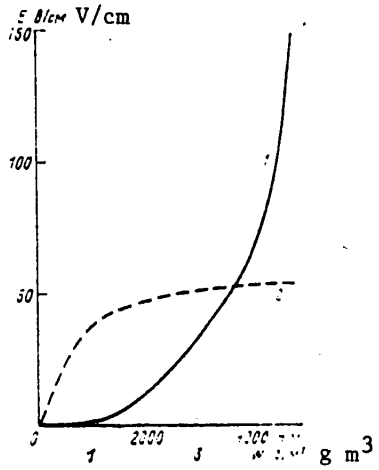

Fig. 4. Computed dependence of field strength E in cloud on thickness H (1) and liquid-water content w (2) of the latter.

The model leads to the unexpected conclusion that one electrification process ensures a three-charge cloud structure. The adopted scheme for the electrification of individual particles and allowance for collective effects ensure electric currents corresponding to the data in Table 1. The measured relaxation time values indicated (for example, see [9]) that the principal losses arise in a thunderstorm cloud and are related to a considerable degree to the turbulence in it. In clouds developing over water areas the mean τ values exceed by a factor greater than 3 the τ values characteristic for continental clouds, that is, thunderstorm phenomena over the oceans can appear in clouds whose thickness and liquid-water content are much less than for clouds over the land. If τ in clouds is very small, weak electrification processes (for example, in stratonimbus clouds) can lead to the appearance of thunderstorms [27]. Similarly, even charging processes in warm clouds, attenuated due to small $\varphi_{1,2}$ can, if the losses in them are small, as is the case in breeze clouds, lead to the appearance of a thunderstorm.

Figure 4 shows the correlations between the electrification of a cloud and its thickness [22] and liquid-water content [9], computed using a refined model [13].

Without dwelling in detail on the mechanism of the appearance of zones of inhomogeneities in clouds (Fig. 1) we note only that their existence is closely associated with air currents in clouds, with the circumstance that cloud turbulence

Table 3

Correlation of Electric Characteristics of Clouds and Other Meteorological Characteristics

Electric characteristics	Meteorological characteristics	Degree of correlation
1. Large charges of precipitation and cloud particles	Degree of icing of part of cloud	Average
	of mixed phase composition	
	Intensity of precipitation	Average
	Size of precipitation particles	High
2. Concentration and rate of falling of charged precipitation particles	Cloud thickness	Average
	Liquid-water content	Average
	Degree of icing	Weak
	Cloud thickness+liquid-water content	Average
	Cloud thickness+liquid-water content +degree of icing	High
	Intensity of precipitation	Average
	Intensity of precipitation	Average
3. Electric current of precipitation	Lightning	Very high
4. Large space charges filling considerable part of cloud	Cloud volume	Weak
	Vertical extent of cloud	Weak
	Development of cloud top above isotherm -20 - -25°C	High
	Intensity of precipitation	Average
5. Turbulent conductivity	Macroscale turbulence	High?
6. Electric field strength	See 2, 3 and 4	See 2, 3 and 4
	Orientation of crystals	High?

leads to its homogeneity, creating local, relatively short-lived inhomogeneities. As was demonstrated in [9], the lifetime of these inhomogeneities is sufficiently great so that the electric fields in them considerably increase the rate of growth of particles and the latter is reflected in the growth of the electric field in the inhomogeneity. Lightning discharges can begin in zones of inhomogeneities. It was recently found [7] that the zone in which the discharge begins should not only create a field with a strength greater than the critical value, but also store an adequate electric energy (see Table 1). Accordingly, the prevailing (for example, see [20]) concept that a lightning discharge can begin with a discharge on a particle (or several particles) is incorrect. The criticality of field strength and energy determines the minimum extent of the region from which the discharge can begin.

In general, the considered model eliminates the objections advanced against the theory of cloud electrification as a result of the falling of charged precipitation [30]. For conversion from the examined model to a model of a real cloud it is necessary to develop two- and then three-dimensional models, introduce time dependences for the charging current and losses in a cloud and introduce feedbacks taking into account the reciprocal influence of electric forces and microphysical processes in clouds.

3. Correlation Between Electric and Other Meteorological Characteristics of Clouds

A short-range forecast and diagnosis of the possibility of the appearance of thunderstorm phenomena in a specific cloud or small region is based on the measurement of characteristics only indirectly related to the electric characteristics of a thunderstorm and therefore it is desirable to be able to evaluate the reliability of these correlations. On the other hand, a direct comparison of the electric characteristics of different clouds without allowance for the conditions of their development in application to a specific cloud electrification model can lead to seemingly contradictory results.

According to the data published by Few, et al. [23], for example, projections onto the earth of regions of the falling of intensive precipitation and the generation of lightning are considerably displaced relative to one another, whereas according to data published by Proctor [31] and Carter and Kidder [19] they coincide. Above we noted the fundamental importance of solution of the problem of the relative location of these regions. The arising contradiction disappears when one considers the genesis of the investigated clouds. If the theory of charging by precipitation is correct, for thunderstorms developing in the atmosphere, where there is no appreciable change in wind velocity with altitude (for example, warm thunderstorms), characteristic for the region of investigations [31], the regions of falling of precipitation and generation of lightning should coincide. When there is a considerable wind shear with altitude (for example, frontal, rapidly moving thunderstorms characteristic for [19, 23]) these regions can differ considerably.

The appearance of thunderstorm phenomena in stratiform clouds without the presence of masked convective clouds was impossible because there were no meteorological conditions corresponding to the indirect indicators of a thunderstorm [27]. The vigorous processes of enlargement of particles and the falling of precipitation in cumulonimbus clouds still seem inexplicable.

Now we will examine the physical principles of the developing relationships between electric and other meteorological characteristics of clouds from the point of view of the considered model. The appearance of large electric charges on particles is associated with high values of the difference in electrochemical potentials between them and a substantial difference in the size of cloud and precipitation particles (see formulas (1) and (2)). The greatest potential differences usually arise between water and ice particles, that is, in mixed clouds. This circumstance explains the usually observed relationship between thunderstorm phenomena and the vertical extent of clouds (size of precipitation particles) and the presence of a well-developed zone with negative temperatures in clouds. However, the organized electrification of precipitation particles can be observed both in warm clouds and in clouds with a small supercooled thickness; despite the fact that the electric losses in clouds are small the occurrence of thunderstorm phenomena in the latter is not uncommon.

In order for significant charging currents to appear there must also be a great intensity of precipitation (see formula (4)), which in turn is associated with the great liquid-water content of the clouds and their vertical development. A correlation between the intensity of precipitation and thunderstorm activity was already noted in the last century (for example, see [14, 17, 28]). However, in the case of small electric losses thunderstorm phenomena appear when there is relatively light precipitation [27], but in the case of great losses they do not arise even in heavy showers (for example, see [19]). Therefore, probably, although radar criteria for thunderstorms during the summer over the continents [15, 16] structurally coincide with formulas (8)-(9), they cease to be valid when determining thunderstorm conditions during the cold season of the year, over water areas, etc. On the basis of the data in this article it can be postulated that in addition to the necessity for making an allowance for turbulent conductivity in the correlation between the intensity of precipitation and its electrification it is also necessary to take into account the possibility of a strong but relatively symmetric electrification of particles (for example, see [29]) without appreciable organized electrification.

Table 3 gives a summary of evaluations of the reliability of the correlation of different meteorological elements with electric elements in clouds. It must be remembered that the correlation in Table 3 is given for some mean conditions. In individual regions and and seasons these correlations may be strengthened or weakened due to the fact that in some mountainous region a thunderstorm with a high degree of reliability can correlate with the appearance of a small cloud over a certain peak in the morning hours, although similar correlations are absent in other areas.

When evaluating the role of electric forces in the specifics of development of a cloud it must be remembered that the interaction of particles under the influence of these forces radically changes the effectiveness of collision of particles, especially small particles. According to the computations in [25, 32], the relative coefficient of collision of particles measuring microns and tens and hundreds of microns can increase by hundreds and thousands of times (attaining the value 1) with fields and charges really existing in clouds in comparison with the value of this coefficient in the absence of fields. In very strong fields the region of weak (forbidden) coagulation virtually disappears. As indicated experimentally, the values of the relative collision coefficient can attain even 20-30 [33]. Due to the change in the rate of motion of particles in the electric field the length of the

column of small particles with which a large particle collides during a given time interval can increase by several times [25]. In other words, under the influence of electric forces the process of enlargement of particles for the most part is reduced to the coagulation process. The processes of collision, amalgamation and separation of particles transpire as they would in clouds without the influence of electric forces but having a liquid-water content of hundreds, thousands and even more g/m^3, that is, the rate of development of thunderstorm clouds is determined to a great extent by the electric forces in them.

In the life of each science there are latent ("autumn" and "winter") periods when facts are accumulated and compared. This is followed by a period of generalization and interpretation (the "spring" and "summer" of science), leading in the long run to a new level of comprehension. Our understanding of thunderstorm processes has probably entered into this second stage.

BIBLIOGRAPHY

1. Danilov, Yu. I., Yevteyev, B. F., Kazak, R. R., Kaprans, A. A. and Selvikyan, Ya. V., "Investigation of Electrification of Bodies in Water Flows," TRUDY GGO (Transactions of the Main Geophysical Observatory), No 350, 1977.

2. Imyanitov, I. M., ELEKTRIZATSIYA SAMOLETOV V OBLAKAKH I OSADKAKH (Electrification of Aircraft in Clouds and Precipitation), Leningrad, Gidrometeoizdat, 1970.

3. Imyanitov, I. M., "On the Problem of the Electrostatic Charging Mechanism," DOKLADY AN SSSR (Reports of the USSR Academy of Sciences), Vol 121, No 1, Issue 93, 1958.

4. Imyanitov, I. M., Yevteyev, B. F. and Kamaldina, I. I., O PRICHINAKH, PRIVODYASHCHIKH K PORAZHENIYU SAMOLETOV MOLNIYAMI V KHOLODNOYE VREMYA GODA (Factors Leading to the Damage of Aircraft by Lightning During the Cold Season of the Year), Leningrad-Moscow, Gidrometeoizdat, 1976.

5. Imyanitov, I. M. and Mikhaylovskaya, V. V., "Experience in Investigating the Charging of Precipitation Particles in the Free Atmosphere," TRUDY GGO, No 97, 1960.

6. Imyanitov, I. M. and Mordovina, L. S., "Reason for the Appearance of Large Potentials in the Process of Freezing of Some Aqueous Solutions," DOKLADY AN SSSR, Vol 190, No 3, 1970.

7. Imyanitov, I. M., Pavlova, G. P., Ponomarev, Yu. F. and Chubarina, Ye. V., "Analysis of Conditions for the Damage of an Aircraft by an Atmospheric Electric Discharge Outside Cumulonimbus Clouds," TRUDY GGO, No 424, 1979.

8. Imyanitov, I. M., Chubarina, Ye. V. and Shvarts, Ya. M., "Effect of Electric Forces on Cloud Development," TRUDY GGO, No 301, 1974.

9. Imyanitov, I. M., Shvarts, Ya. M. and Chubarina, Ye. V., ELEKTRICHESTVO OBLAKOV (Cloud Electricity), Leningrad, Gidrometeoizdat, 1971.

10. Markchev, N. T. and Fedchenko, A. M., "Possibility of Damage to Aircraft by Electric Discharges in Nonthunderstorm Convective Clouds," NAUCHNO-TEKHN. REFERAT. SBORNIK. SISTEMY NAVIGATSII, POSADKI I UPRAVLENIYA VOZD. DVIZH. (Collection of Scientific and Technical Abstracts. Systems for Navigation, Landing and Control of Air Traffic), No 1, Moscow, 1977.

11. Mordovina, L.S., "Electrification in a Flow of Aerosols," TRUDY GGO (Transactions of the Main Geophysical Observatory), No 277, 1972.

12. Mordovina, L. S., "Random Electrification of Particles During Collisions," TRUDY GGO, No 301, 1974.

13. Mordovina, L. S., "Electrification of Stratonimbus Clouds as a Result of Interaction of Particles With One Another," TRUDY GGO, No 323, 1974.

14. Muchnik, V. M., FIZIKA GROZY (Thunderstorm Physics), Leningrad, Gidrometeoizdat, 1975.

15. Sal'man, Ye. M., Gashina, S. B. and Divinskaya, B. Sh., "Radar Parameters of Separation of Thunderstorm and Shower Activity," METEOROLOGIYA I GIDROLOGIYA (Meteorology and Hydrology), No 4, 1969.

16. Stepanenko, V. D., RADIOLOKATSIYA V METEOROLOGII (Radar in Meteorology), Leningrad, Gidrometeoizdat, 1973.

17. Chalmers, G. A., ATMOSFERNOYE ELEKTRICHESTVO (Atmospheric Electricity), Leningrad, Gidrometeoizdat, 1974.

18. Buser, O. and Aufdermaur, "Electrification of Collisions of Ice Particles on Ice or Metal Targets," ELECTRICAL PROCESSES IN ATMOSPHERE, Darmstadt, Dietrich Steinkopf, 1977.

19. Carte, A. E. and Kidder, R. E., "Lightning in Relation to Precipitation," J. ATMOS. TERREST. PHYS., Vol 39, 1977.

20. Crabb, J. A., Griffiths, R. F. and Latham, J., "Triggering of Lightning by Corona From Ice Hydrometeors or Colliding Raindrops," ELECTRICAL PROCESSES IN ATMOSPHERE, Darmstadt, Dietrich Steinkopf, 1977.

21. Dolezalek, H., "Report on the Fifth Conference," ELECTRICAL PROCESSES IN ATMOSPHERE, Darmstadt, Dietrich Steinkopf, 1977.

22. ELECTRICAL PROCESSES IN ATMOSPHERE, Darmstadt, Dietrich Steinkopf, 1977.

23. Few, A. A., Teer, T. L. and MacGorman, D. R., ADVANCES IN A DECADE OF THUNDER RESEARCH, In [22].

24. Gaskell, W., Illingworth, A. J. and Latham, J., "Airborne Studies of Electric Fields and the Charge and Size of Precipitation Elements in Thunderstorms," QUART. J. ROY. METEOROL. SOC., Vol 104, 1978.

25. Grover, S. N., "A Numerical Determination of the Effect of Electric Fields and Charges on the Efficiency With Which Cloud Drops and Small Raindrops Collide With Aerosol Particles," Pageopd 114, 1976.

26. Gunn, R., "The Electrical Charge on Precipitation at Various Altitudes and Its Relation to Thunderstorms," PHYS. REV., Vol 71, 1947.

27. Imyanitov, I. M., Evteev, B. F. and Kamaldina, I. I., "The Thunderstorm Cloud," PLANETARY ELECTRODYNAMICS, Gordon and Breach, Vol 1, New York, 1969.

28. Israel, H., ATMOSPHERIC ELECTRICITY, Volumes 1 and 2, Jerusalem, 1971, 1973.

29. Magono, Ch., "Precipitation Electricity of Thunderclouds and Showerclouds," in [22].

30. Moore, C. B., "An Assessment of Thunderstorm Electrification Mechanism," in [22].

31. Proctor, D. E., "VHF Radio Pictures of Lightning," in [22].

32. Schlamp, R. J., Grover, S. N. and Pruppacher, H. R., "A Numerical Investigation of the Effect of Electric Charges and Vertical External Electric Field on the Collision Efficiency of Cloud Drops," J. ATMOS. SCI., Vol 33, 1976.

33. Smith, M. H., "The Influence of Electric Forces Upon Droplet Collection Efficiencies," in [22].

UDC 551.(510.4+588.7)

ANTHROPOGENIC CHANGES IN ATMOSPHERIC CO_2 CONCENTRATION DURING THE NEXT FIFTY YEARS

Moscow METEOROLOGIYA I GIDROLOGIYA in Russian No 3, Mar 81 pp 18-31

[Article by E. K. Byutner, doctor of physical and mathematical sciences, O. K. Zakharova and I. Ye. Turchinovich, candidates of physical and mathematical sciences, and A. G. Lapenis, State Hydrological Institute, manuscript received 17 Jun 80]

[Text]

Abstract: The percentage distribution of carbon content was computed for three reservoirs (biomass of the land, ocean and atmosphere) for the next 50-year period (to 2030) for determining the most probable rate of industrial CO_2 emission. For use in computation of CO_2 absorption by the ocean a correlation was derived between the partial pressure of CO_2 in the atmosphere and its content in the upper quasihomogeneous layer of the ocean (UQHL) in a broad range of temperatures. The computations were made for a fixed mean global temperature of the UQHL equal to 16.8°C. A dependence of the CO_2 concentration in the atmosphere on time was derived for the period up to 2030.

Introduction. The combustion of fossil fuel (petroleum, coal and natural gas) is an essential part of modern power production. The supplies of organic carbon accumulated in the course of hundreds of millions of years are oxidized and enter the atmosphere in the form of carbon dioxide. Data from the monitoring of CO_2 initiated in 1958 indicate a constant increase in the content of atmospheric CO_2 (see Fig. 1). Over a 20-year period, from 1958 to 1978, the quantity of CO_2 increased from 315 million^{-1} to 335 million^{-1} parts in volume, that is, by 42.5 Gt of carbon. [The quantity 1 million^{-1} CO_2 is equivalent to $2.124 \cdot 10^{15}$ g of carbon in the atmosphere; in the text which follows the masses of the reservoirs in all cases are given in gigatons, that is, in 10^{15} g of carbon.] If this figure is compared with the quantity of CO_2 entering the atmosphere during these same years as a result of industrial activity, it is found that about half of the anthropogenic carbon has remained in the atmosphere. The remaining quantity was distributed among the other carbon reservoirs of the so-called "mobile store," that is, the biomass and the ocean.

The total planetary carbon cycle includes three interrelated cycles which differ, in particular, with respect to the intensity of the characteristic values of the exchange fluxes, and accordingly, the time scales as well. In the first cycle, the so-called cycle of carbon in the "mobile reserve," which includes the processes of photosynthesis, respiration and oxidation of organic matter, as well as gas exchange between the atmosphere and ocean, the magnitude of the exchange fluxes is tens Gt/year (see Fig. 2). Within the limits of the second cycle there is weathering, dissolving and precipitation of carbonates with an intensity of the corresponding fluxes from 0.1 to 1 Gt/year. Finally, the third cycle, geological, includes the processes of carbon entry into the atmosphere from the earth's deep layers and the accumulation of calcareous rocks; the rates of these processes in order of magnitude are 10^{-2} Gt/year and the changes in carbon content associated with them have a characteristic time scale of 10^7 years in the different reservoirs [5, 15]. The characteristic times of change in the content of carbon in the atmosphere, the upper quasihomogeneous layer (UQHL) of the ocean and in the biomass with impairments in equilibrium in the first cycle are about 10 years, the time scale during which the combustion of reserves W_∞ of fossil fuel available for exploitation is estimated at 200-300 years, and the W_∞ value is considered to fall in the range from 8 to 16 times the CO_2 content in the atmosphere. Accordingly, impairments of equilibrium due to the combustion of fuel arise, in particular, in the course of the first cycle. In the prediction of changes in the carbon content in different reservoirs which can occur in the course of the next 50 years it is possible to limit ourselves to an examination of the processes transpiring within the limits of only the first cycle because the second cycle is characterized by far greater inertia: its scale is estimated at 10^3-10^4 years [32].

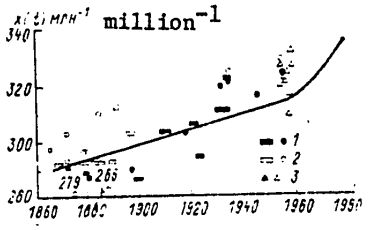

Fig. 1. Results of observations of atmospheric CO_2 content. From 1860 to 1960 [20]: 1) reliable data, 2) doubtful data, 3) data from aircraft observations. The solid curve to 1958 represents dependence (9) for $A = 8.2 \cdot 10^{-4}$ from 1958 to 1978 -- mean monitoring data for stations in the northern hemisphere.

The problem of the distribution of anthropogenic carbon dioxide between the atmosphere, ocean and biomass with a stipulated temporal variation of the rate of industrial effluent and the total quantity W_∞ of fossil fuel which can be burned has been formulated and solved during recent years by a whole series of authors [20, 21, 26, 30, 31, 34, 37, 40]. All these computations naturally contain the parameters characterizing gas exchange among the principal reservoirs, as shown in Fig. 2. The values of all these parameters are now known with some degree

of error. The type of equations used in different studies for describing the CO_2 cycle is also somewhat different.

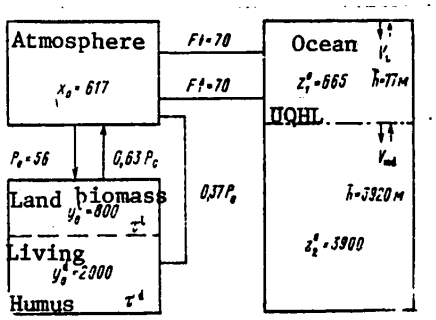

Fig. 2. Carbon content in three reservoirs, Gt in atmosphere, biomass and ocean, and also exchange fluxes between them, Gt/year.

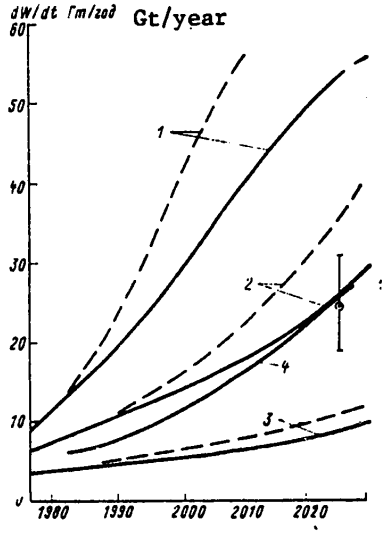

Fig. 3. Rates of industrial discharge of carbon Gt/year as function of time [26]. 1) r = 0.0653; 2) r = 0.0453; 3) r = 0.0253; 4) most probable rate of discharge and its discharge in 2025. n = 0.5 (solid curves), n = 1 (dashed curves).

The purpose of our study was more limited: it sets forth the results of computations of changes in atmospheric CO_2 concentration which can occur during the next 50 years. In such a relatively short time interval the principal interaction occurs between the atmosphere, biomass and upper quasihomogeneous layer of the ocean and the deep ocean can be regarded as an infinitely large reservoir absorbing excess carbon dioxide from the upper quasihomogeneous layer. In addition, a whole series of nonlinear effects can be neglected and a simplified system of equations for the cycling of the carbon of the mobile reserve affords a possibility for evaluating to what degree the inaccuracy in determining different parameters can exert an effect on the results of computations.

Rate of Industrial Discharge

Figure 3 shows the prognostic functions dW/dt for different scenarios of energy development in the future in the form in which they were used in [20]. The vertical line drawn at the level of the abscissa t = 2025 years was taken from [36] and shows the extent to which the range of possible rates of industrial discharge had narrowed as a result of an analysis of data on the development of world energy production during recent years. The dot on this curve designates the most probable dW/dt value for the year 2025. The principal results of our computations are represented by curve 4, which corresponds to the rate of industrial growth

$$r = \frac{1}{W}\frac{dW}{dt} = 4.5\%/\text{year}$$

in 1975. A decrease in this value due to the finite nature of the reserves of available fossil fuel and changeover to other types of energy sources will still have a weak effect in the next 50 years, although a rate of industrial discharge in 2025 which is 1.8 times less than the rate corresponding to the constant value $r = 0.045\ \text{year}^{-1}$ is predicted.

Even at the present time the intensity of the anthropogenic carbon dioxide source dW/dt is 5 Gt/year and by 2025 will attain 26 Gt/year; accordingly, it should result in strong changes in the cycling of carbon of the mobile reserve.

Principal Reservoirs of Carbon in the Mobile Reserve

a) Atmosphere. The overwhelming part of carbon present in the atmosphere is present there in the form of carbon dioxide. For the interval 1958-1978 Figure 1 shows the mean values of the CO_2 concentration according to data for a number of stations situated in the northern hemisphere. The concentrations observed in the southern hemisphere are less than in the northern hemisphere by 3-4 million^{-1} but have a similar dependence on time [29]. Until 1958 there had been no monitoring of the CO_2 content and there are only data from individual measurements which differ from one another primarily due to the imperfection of the measurement method. As a result of analysis of such data Callender [29] concluded that the carbon dioxide concentration in the mid-19th century was close to 290 million^{-1}. A similar conclusion was drawn in [23]. In most models of the carbon cycle this figure is used as the initial equilibrium concentration up to the beginning of anthropogenic disturbances. It corresponds to an x_0 value of the atmospheric carbon reservoir equal to 617 Gt. It goes without saying that this figure cannot be regarded as absolutely precise, but its mean square error probably falls in the range 5-8 million^{-1}.

The estimates obtained on the basis of an analysis of data on the ratio of the isotopes $^{13}C/^{12}C$ in tree rings, from which substantially lesser x_0 values follow, are based on an inadequately complete statistical material and can scarcely be assigned a great weight.

b) Ocean. In the ocean inorganic carbon is present in the form of CO_2 in both dissolved gas and also the ions HCO_3^- and $CO_3^=$.

The upper quasihomogeneous layer (UQHL) of the ocean on the average under stationary conditions should be in chemical equilibrium with atmospheric carbon dioxide. The total carbon content z_1^0 in all three forms, that is, CO_2, HCO_3^- and $CO_3^=$ (the quantity of nondissociated H_2CO_3 is negligible) is determined by the temperature, salinity and alkalinity of the water. If the values for the UQHL [1] t = 16.8°C, s = 34.7°/oo, Alk = 2.44 meq/liter and a depth h = 77 m are used as the mean global values, then with x_0 = 290 million^{-1} the z_1^0 value is equal to 665 Gt. The remaining ocean as a whole is 6-7% supersaturated with carbon dioxide in comparison with the UQHL as a result of activity of the ocean biomass. The basic functioning of biomass occurs in the upper 200-m layer, but the dead organic remains settle into the deeper layers, being oxidized as they descend. As a result of this process, the ocean in general is doubly undersaturated with oxygen. This is known from both experimental observations [35] and from theoretical computations [8, 9]. Such an O_2 undersaturation is about 6000 Gt and should correspond to a CO_2 supersaturation of about 6000 (12/32), that is, 2200 Gt. Accordingly, the total quantity of inorganic carbon z_2^0 in the deep ocean is evidently close to 39 000 Gt [21]. The existing uncertainty in this figure will not be reflected in the results of the computations as long as the deep ocean can be considered an infinitely great reservoir for the "runoff" of anthropogenic carbon dioxide. There are carbonates in the sediments of the ocean floor. For the time being the interaction of ocean waters with precipitated carbonates need not be taken into account because this is an inertial process with a characteristic time scale not less than 10^3 years and the alkalinity Alk of water can be considered constant. According to the data in [1, 14], the mean global value of the Alk/Cl ratio is 0.12 and therefore with a salinity S equal to 34.7°/oo we have Alk = 2.44 meq/liter.

The exchange flux F_0 between the ocean and the atmosphere can be represented in the form

$$F_0 = V_L S k_0 (p_a - p_w) = F\downarrow - F\uparrow, \quad (1)$$

where the V_L value has the dimensionality of velocity and accordingly is called the characteristic rate of gas exchange through the discontinuity atmosphere-UQHL, S is the area of the world ocean, k_0 is the coefficient of solubility of CO_2 in sea water. The product k_0p_w is the limiting value of the CO_2 concentration in water and k_0p_w is the concentration of dissolved CO_2 gas in the UQHL, since the "partial pressure of CO_2 in water" p_w by definition is the ratio of its concentration c to the k_0 value. As demonstrated in [12, 13], the difference $p_0 - p_w$ has a latitudinal and seasonal dependence and for the most part due to change in the p_w value. The characteristic values of this difference are 30-40 million^{-1}. Its mean annual value is close to zero within the limits of accuracy of observational data and the corresponding hydrochemical computations. The state of dynamic equilibrium between the UQHL and the atmosphere comes about by the evening-out of two oppositely

directed fluxes $F\uparrow$ and $F_{\downarrow}$. Each of these can be obtained if the mean global value of the V_L parameter is known. Such a value has now been obtained on the basis of data from laboratory experiments for determining the dependence of the V_L parameter on wind velocity with subsequent statistical averaging of this dependence using the probability distribution functions for different wind velocity values and for the surface of the world ocean. As a result, with storm effects taken into account it was found that the mean global value V_L is equal to $39 \cdot 10^{-4}$ cm/sec. The $F\uparrow$ and $F\downarrow$ fluxes are 70 Gt/year. The amplitude of the seasonal values of the exchange flux F_0 is almost an order of magnitude less [2].

c) Biomass. The principal reservoir of organic carbon is in the continental biomass. The magnitude of the living biomass of the land, according to the presently most commonly published estimates [28], is 827 Gt. Its greater part is in forests. The data in [3] give a close figure: 2420 for dry organic matter (the mean molecular weight is considered equal to 30). A detailed analysis of the presently available evaluations of the y_0^1 parameter and the possible reasons for the discrepancies between different authors was presented in [28]. But the conclusion of the author of [28] that the figure 827 can be exaggerated by a factor of 2 is probably too critical. There is far greater uncertainty in estimates of the content of soil humus y_0^d. As demonstrated in [22], the figure used until recently, equal to 710 Gt, was taken from publications dated 1915.

The mean global value y_0^d, according to the estimates of the author of [22], is 3000 ± 500 Gt; according to the data in [28] it is half as great -- 1500 Gt. In the 3000 figure the author of [22] included 800 Gt of peat which is oxidated very slowly. Accordingly, we used a y_0^d value equal to 2000 Gt, the same as in [34].

The mean annual primary productivity of the continental phytomass, according to the estimates in [34], is $P_0 = 56$ Gt/year. The data obtained in [7], 1410 Gt/year for dry organic matter, virtually coincide with this P_0 value. In a state of equilibrium the P_0 value should be compensated by expenditures on oxidation transpiring in vital functioning processes with the dying of rapidly oxidizing organic matter and with the decomposition of humus. A mean global value [10] was obtained for the last part of so-called "soil respiration"; it was $0.37\ P_0$. Accordingly, the characteristic time of oxidation of continental humus is

$$P_0 = 2000/(0.37 \cdot 56) = 96 \text{ years.}$$

The corresponding "turnover time" for the living biomass is

$$\tau^1 = 800/56 = 14.5 \text{ years.}$$

The living biomass of the ocean is primarily in the form of zooplankton [19] and is approximately 20 Gt, that is, almost two orders of magnitude less than the continental biomass. The humus content in the ocean is reckoned at 1380 Gt [17], which is not much less than the y_0^d value. The mean annual productivity of the ocean is about half the productivity of continental plants, but there are many investigations [39] according to which ocean productivity is limited by the nutrients received from the depths, and not by the carbon dioxide, of which there are considerable quantities in the ocean. On the basis of these considerations only the continental biomass was included in our computation scheme.

Oceanic Reaction to Anthropogenic Disturbances

The equation describing oceanic reaction to changes in the atmospheric content of carbon dioxide is naturally written in the following form:

$$h\frac{d\bar{c}}{dt} = V_L Sk_0 (p_a - p_w) - V_{mix} S (\bar{c} - c_0). \qquad (2)$$

Here the term situated on the left-hand side describes the change in the content of total inorganic carbon in the UQHL and on the right-hand side there are terms describing gas flows through the upper and lower boundaries of the UQHL respectively. The principal feature of this equation is that gas exchange for CO_2 through the upper boundary of the UQHL is proportional to the difference in the partial pressures of CO_2 in the air p_a and in the water p_w (the p_w value is determined as the quotient by division of the concentration of dissolved CO_2 in water by the solubility coefficient k_0). The p_w value with stipulated temperature, salinity and alkalinity values for sea water is unambiguously related to the total concentration of inorganic carbon in the UQHL, that is, to the c value. The exchange flux of the UQHL with depth is proportional to the deviation of c from the equilibrium value c_0 which prevailed in the UQHL prior to the onset of anthropogenic disturbances. Accordingly, for the solution of equation (2) it is necessary to compute the function $p_w(c)$. Such computations were made from the known k_0 values, and also the first k_1 and second k_2 constants of dissociation of carbonic acid cited in [14] on the basis of data from Liman, and a series of other known hydrochemical constants. The results of computations with Alk = 2.44 meq/liter, S = 35°/oo and different UQHL temperature values are cited in Fig. 4. It follows from the graphs that chemical equilibrium with the atmosphere, in which the p_a value varies greatly, is attained with an extremely small change in the content of inorganic carbon in the UQHL. An increase in p_a by a factor of 2 causes an increase in c by several percent. This is a well known fact specifically for the reason that the UQHL in its time was known as a "bottleneck" through which there is an exchange of the carbon dioxide between the atmosphere and the ocean. The characteristic time for the setting-in of chemical equilibrium, that is, the equality of the p_a and p_w values between the atmosphere and the UQHL, does not exceed 1.2-2 years [24] and the time interval in computing the mean CO_2 content trend is equal to 10 years. Accordingly, with the use of equation (2) for computing the absorption of anthropogenic CO_2 by the ocean it can be assumed that $p_a = p_w$, but the total concentration c(t) of carbon in the UQHL in this case must be taken from the results of precise computations of the hydrochemical relationships cited in Fig. 4 without recourse to linearizations.

The curves in Fig. 4 demonstrate the dual role of temperature in the process of exchange of CO_2 between the ocean and atmosphere: with an increase in temperature the transmissivity of the UQHL as a buffer layer between the atmosphere and the main layer of the ocean increases (the relative values $(\bar{c} - c_0)/c_0$ increase), but its inherent capacity decreases. The computations indicated that the resultant influence of temperature of the UQHL on the rate of absorption of CO_2 by the ocean is small. A warmer UQHL leads to more intensive transfer of excess carbon dioxide from the atmosphere into the ocean; a temperature increase by 1°C increases the quantity of absorbed carbon dioxide by 2%. However, it must be noted that such an effect is obtained when the characteristics of exchange between the UQHL and the underlying layers are not dependent on the temperature of the UQHL. It is evident

that this is not the case and the total temperature effect can be computed only after obtaining the corresponding dependences for the characteristic rate V_{md} of gas exchange with depth. We carried out all subsequent computations for a fixed mean global temperature of the UQHL equal to 16.8°C [18].

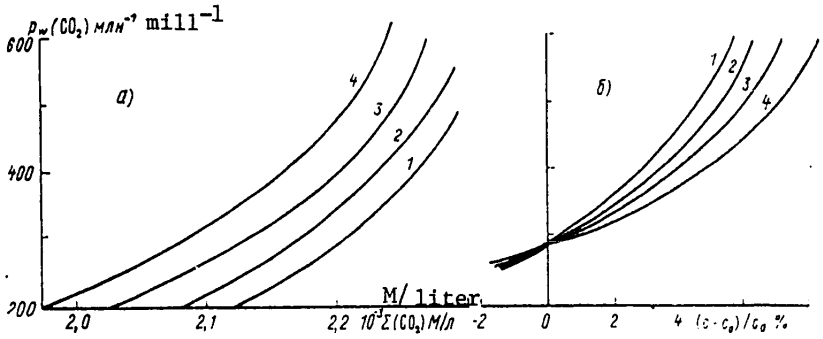

Fig. 4. Absolute (a) and relative (b) concentrations of total inorganic carbon (x-axis) in ocean as a function of the partial pressure of CO_2 (y-axis) at a temperature of 5°C (1), 10°C (2), 15°C (3), 20°C (4).

The flux of excess total inorganic carbon from the UQHL in depth in equation (2) is considered to be proportional to the deviation of the concentration c(t) from the equilibrium value c_0 which prevails in the UQHL at the time t = 0. Such an assumption is usually made in box models for describing the cycling of carbon between different reservoirs. The principal feature of box models is the hypothesis that the flux from the box i into the box j at each particular moment in time is proportional to the deviation of the content of the impurity in the i-th box n_i from the equilibrium content N_i^0 in this same box: $I_{ij} = k_{ji}n_i = k_{ji}(N_i - N_i^0)$. The very same applies to the flux from the box j into the box i: $I_{jk} = k_{ji}n_j$. For fluxes associated with photosynthesis and the biological release of CO_2 during the oxidation of humus such a hypothesis is natural. However, in describing the processes of transfer through the discontinuity between the ocean and the atmosphere and exchange between the UQHL and the deeper layers it is necessary to take into account the conditional character of the box models. The k_{ij} coefficients are conditional parameters and in a general case do not satisfy the principle of reciprocity of the kinetic coefficients: in order that at equilibrium the content of the impurity remain constant in each box it is necessary to satisfy the condition

$$k_{ij}/k_{ji} = N_j^0/N_i^0,$$

which is compatible with the equality $k_{ij} = k_{ji}$ only when $N_i^0 = N_j^0$. However, if $k_{ij} \neq k_{ji}$, the total exchange flux $I_{ij} - I_{ji}$ in the last analysis is not found to be proportional to the difference in the concentrations of the impurity near the discontinuity.

Equation (2) contains the real, rather than conditional diffusion parameters V_L and V_{md}.

The assumption that there is a proportionality between the flux in depth to the $\bar{c}-c_0$ value is related to the fact that, first of all, the ocean below the UQHL is considered an infinitely large reservoir in which the concentration retains an equilibrium value, and second, since the activity of the oceanic biomass is not taken into account in the computations, this equilibrium value should be equal to c_0.

In actuality, since the settling of particles of organic carbon from the surface into the deep layers was excluded from our computations, the presence of a small compensatory flux of total inorganic carbon, directed upward and caused by the supersaturation of deep waters is also excluded.

For V_{md}, which represents a value inverse of the diffusion resistance of the blocking stratified layer directly adjoining the lower boundary of the UQHL, at the present time the mean global value has not yet been ascertained. It is known that the turbulence characteristics in this layer are highly dependent on the temperature and salinity drops and have a very great spatial and seasonal variability.

A V_{md} evaluation can be obtained using data on the relationship between the content of radiocarbon ^{14}C in the UQHL and in the deeper layers of the ocean obtained in numerous measurements prior to the beginning of nuclear tests in the 1960's, as a result of which the natural distribution of ^{14}C was disrupted. These data are usually used in evaluations either of the coefficients describing gas exchange with the atmosphere or the effective thickness of the upper layer of the ocean [40]. Since the effective rate of gas exchange with the atmosphere V_L was determined in [2] on the basis of independent considerations, and the natural thickness of the UQHL is used as the thickness of the upper layer of the ocean, the ^{14}C distribution can be used for evaluating the V_{md} parameter (and also for checking the V_L value).

Radiocarbon was formed in the atmosphere from nitrogen ^{14}N under the influence of cosmic rays with a mean intensity Q from 1.8 to 2.5 atoms/(cm^2·sec) or from $0.58 \cdot 10^4$ to $1.05 \cdot 10^4$ g/year. Its relative content by mass in the atmosphere prior to nuclear shots was $^{14}C/^{12}C = 1.24 \cdot 10^{-12}$. The decay constant for radiocarbon λ is 8000 years. The relative content

$$\delta_1 = \frac{(^{14}C/^{12}C)_{UQHL}}{(^{14}C/^{12}C)_{atm}} \tag{3}$$

is somewhat less than unity and the corresponding ratio in the deeper layers δ_2 is less than δ_1. With maintenance of a stationary ^{14}C content this ensures a continuous radiocarbon flux from the atmosphere compensating its radioactive decay in the ocean.

Accordingly, the following relationships must be satisfied

$$F \uparrow (1 - \delta_1) = \frac{1}{\lambda} (z_1 \delta_1 + z_2 \delta_2), \tag{4}$$

$$V_{md} \frac{z_1}{h} (\delta_1 - \delta_2) = \frac{z_2 \delta_2}{\lambda}. \tag{5}$$

According to data in [35], δ_1 is equal to 0.96, δ_2 = 0.84. Formula (4) gives a V_L value equal to $64 \cdot 10^{-4}$ cm/sec. This is somewhat greater than the value $39 \cdot 10^{-4}$ cm/sec which we used, but it is necessary to take into account that the error in computing the V_L value in accordance with formula (4) is very great: a change in δ_1 by ±0.02 changes the result by ±40%.

Using formula (5) it is possible to compute the V_{md} value. It is equal to 4.75 m/year or $1.5 \cdot 10^{-5}$ cm/sec.

Similar estimates ($1.25 \cdot 10^{-5}$ cm/sec) of vertical velocities V_{md} in some circulation models of the ocean are given in [9]. In [34], on the basis of data on the propagation of tritium in the ocean, which had been formed in the atmosphere as a result of nuclear tests, it was found that $V_{md} = 2.5 \cdot 10^{-5}$ cm/sec with a thickness h equal to 100 m. Evidently the effective global mean value of the parameter V_{md} for gas exchange processes fell within these limits, that is, from 1 to $2.5 \cdot 10^{-5}$ cm/sec.

Biomass Reaction

The continental biomass, like the ocean, probably should also be an absorber of anthropogenic CO_2. An increase in the intensity of photosynthesis with an increase in the CO_2 concentration under laboratory (greenhouse) conditions is a well-established fact.

In the time interval during which the system did not change greatly the equations for the carbon content in living y^l and dead biomass (humus) can be written in the following way:

$$\frac{dy^l}{dt} = P_n\left(1 + \beta \ln \frac{x}{x_0}\right) - \frac{y^l}{\tau^l}; \tag{6}$$

$$\frac{dy^d}{dt} = 0{,}37\ \frac{y^l}{\tau^l} - \frac{y^d}{\tau^d}, \tag{7}$$

where τ^l and τ^d are the characteristic times of relaxation of living biomass and humus respectively, β is a coefficient characterizing the reaction of the biomass to a change in the carbon dioxide content in the atmosphere. Under natural conditions the value of this coefficient cannot be judged on the basis of data from laboratory experiments since the increment of biomass can be limited by a whole series of factors such as moistening, the quantity of nutrients, etc. However, in general the continental phytomass must increase the increment with an increase in the x(t) function, since the present-day content of atmospheric carbon dioxide is considerably below the optimum for the photosynthesis process.

The methods for describing the biomass reaction adopted in different models [21, 31, 34] differ rather significantly from one another.

The system of equations (6) and (7) adopted in our computations is close to that used in [34] with the difference that we assume the mean rate of oxidation of soil humus is known on the basis of estimates of the global mean values of "soil respiration" [10]. The same as in [34], equations (5) and (7) contain the assumption of an invariability of the photosynthesizing green mass since the plants strive to have an optimum surface.

The breakdown of biomass into living and dead with the choice of a characteristic "turnover" time for each of them seems to us to be justified in a problem in which the biota is considered only from the point of view of its properties as a CO_2 source and user. It is evident that only living biomass can be a user of CO_2. In general, both living and dead biomass serves as a source, but since it is the mean annual primary productivity, and not total assimilation, which serves as an index of intensity of use, the principal CO_2 source is soil humus and the intensity of this source should be proportional to y^d. With such a formulation the times τ^l and τ^d are determined somewhat more reliably than with the breakdown of biomass into two parts with small and large characteristic "turnover" times, as was done, for example, in [26].

Naturally, the y^l value consists of a whole set of populations, to each of which it is possible to assign its characteristic "turnover" time, but an elementary analysis of the equation for y^l indicates that under the condition of retention of the total y_0^l value and productivity P_0 the details of such a breakdown exert little effect on the computation results.

In solving the problem of biomass reaction to any changes in atmospheric gas composition it is necessary to take into account the fundamental circumstance that whatever increase there may be in the carbon dioxide concentration the biomass cannot continue to increase indefinitely. There are restrictions on its increase due to internal factors which must be reflected in the equation by the appearance therein of the term $y^l(y^l - y_0^l)$. The authors of [16] simply imposed a limitation of the magnitude of the biomass. Keeling and Bacastow [26] introduced the function $\beta(t)$, whereas the authors of [34] obtained a limited increase in y^l only due to a limitation on the W(t) function.

The introduction of a quadratic term into equation (6) leads to a natural limitation on the biomass due to internal factors, but for the time interval during which the increment is small this limiting term can be discarded. In this case system (6)-(7) contains only one unknown parameter, for whose determination it is possible to use the results of CO_2 monitoring.

Use of Monitoring Data for Determining the β Coefficient

If ΔW is used to denote the total industrial discharge of CO_2 into the atmosphere during the time interval Δt, the following expression must be satisfied

$$\Delta W = \Delta x + \Delta y^l + \Delta y^d + \Delta z_1 + \Delta z_2. \tag{8}$$

Interval	ΔW	$(1+\alpha)\Delta W$	Δx	$\frac{\Delta y}{3}$	Δz_1	Δz_2	Δz_1	Δz_2
					$V_{md} = 1,25 \cdot 10^{-5}$		$V_{md} = 2,5 \cdot 10^{-5}$	
I	84	113,4	53	104,4	9	22	9	44
II	79	91	42,5	54,4	6	14	6	28

Data on the ΔW value for the years 1860-1958 (I) and 1958-1978 (II), in accordance with [36], are given in the table. This table gives the corresponding Δx values taken from the graph (Fig. 1) with a value x_0 = 290 million^{-1}. In computing the Δy and Δz values by use of equations (2), (6) and (7) during these same time intervals the x(t) function was approximated by two segments of the exponential curve:

for interval I $$\frac{x}{x_0} e^{A_1 (t-1860)}, \quad A_1 = 8{,}2 \cdot 10^{-4} \text{ year}^{-1}; \tag{9}$$

for interval II $$\frac{x}{x_1} = e^{A_2 (t-1958)}, \tag{10}$$

where x_1 = 315 million^{-1}, $A_2 = 3.08 \cdot 10^{-3}$ year^{-1}.

The system of equations (6)-(7) is such that the increment of biomass, both living and dead, is proportional to β. An analysis of its solution with functions x/x_0 of the type (9) and (10) shows that variation of the parameters y_0^l and y_0^d in the range ±25% exerts little effect on the results of computation of Δy (in the limits 10%). In addition to combustion of fossil fuel, some additional CO_2 quantity will enter the atmosphere as a result of cutting of forests.

The entry of CO_2 into the atmosphere accompanying the procurement of wood represents some part of the annihilated biomass. There is also the uncontrollable annihilation of forests. According to estimates [31], the existence of uncontrollable factors in human activity means that the real quantity of anthropogenic CO_2 entering the atmosphere will be $\Delta W(1+\alpha)$, where α falls in the range 0.35-0.15. If it is assumed that in interval I $\alpha_I = 0.35$, and in interval II $\alpha_{II} = 0.15$, then the reduction of the balance in the table with a mean value V_{md} will give $\beta_I = 0.18$ and $\beta_{II} = 0.40$. It is evident that the error in determining β by this method is very great; it is even difficult to estimate quantitatively because the parameters α_I and α_{II} are very uncertain.

The value of the β parameter can also be determined by another independent method by monitoring the atmospheric content of the isotope ^{13}C. The atmosphere and the biosphere, as well as fossil fuel, contain different quantities of the nonradioactive isotope of carbon ^{13}C ($\delta^{13}C_{atm} = -7^o/oo$, $\delta^{13}C_{bio} = \delta^{13}C_{fuel} = -25^o/oo$, where $\delta^{13}C$ is the deviation of the ^{13}C content in different reservoirs from the standard (1.237%)). Since fossil fuel and biomass contain ^{13}C in a volume 18°/oo less than the atmosphere, the discharge of CO_2 in the combustion of fuel, and also any change in the biosphere cause changes in the content of ^{13}C in the atmosphere.

The measurements made by Keeling, et al. [27] indicated that from 1956 through 1978 the atmospheric content of ^{13}C decreased from -6.69 to -7.24°/oo, that is, by 0.55°/oo. During this period the atmosphere received 79 Gt of CO_2 due to the carbon in fossil fuel. The total reservoir which received this excess CO_2 with a reduced ^{13}C quantity is approximately 3.3 x_0 (without allowance for the fractionation of isotopes). These data make it possible to estimate the change in biomass in these 22 years. In actuality, if the atmospheric content of ^{13}C changed only as a result of industrial effluent, then during the 22 years the change in the content of ^{13}C $\Delta(\delta^{13}C_{atm})$ would be determined by the difference $\Delta(\delta^{13}C_{fuel} - \delta^{13}C_{atm}) = -18^o/oo$, and also by the effluent and the total reservoir:

$$(-18^{0}{}_{00})\frac{79}{3{,}3\,x_0} = -0{,}7^{0}/_{00}.$$

According to data in [27], during these years the decrease in atmospheric ^{13}C content was only -0.55°/oo. This means that the biomass partially replenished the ^{13}C deficit due to its growth:

$$(-18^{0}{}_{00})\frac{\Delta y}{3{,}3\,x_0} \approx (-0{,}7+0{,}55)^{0}/_{00}, \quad \Delta y = 17 \text{ Gt}.$$

Using the results of computations for Δy on the basis of equations (6)-(7), we assume Δy for these years to be equal to $24.6\beta + 29.8\beta = 54.4\beta$. Then the estimate of β on the basis of the change in atmospheric ^{13}C content gives 0.31.

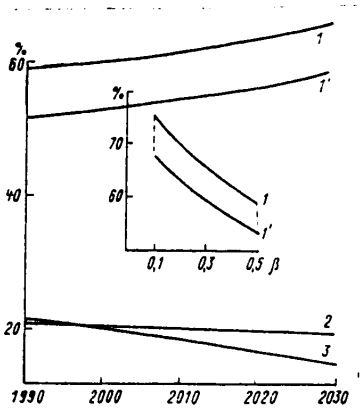

Fig. 5. Distribution of anthropogenic carbon dioxide between atmosphere (1), continental biomass (2) and ocean (3) with $\beta = 0.3$, $V_{md} = 1.25 \cdot 10^5$ cm/sec. The curve 1' corresponds to $V_{md} = 2.5 \cdot 10^{-5}$ cm/sec. The inset shows the $\Delta x/\Delta W$ values in % for the year 2030 as a function of β.

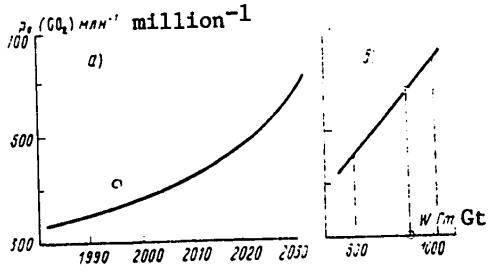

Fig. 6. Temporal variation of CO_2 concentration in atmosphere (a) and dependence of concentration in 2030 on quantity of combusted fossil fuel within limits of range defined in Fig. 3 (b).

Results of Computations of Changes in Atmospheric CO_2 Concentration to 2030

Computations of the distribution of anthropogenic carbon dioxide between the atmosphere, ocean and biomass were made on the assumption that the entry of CO_2 into the atmosphere occurs at the rate dW/dt corresponding to the most probable curve shown in Fig. 3. Accordingly, the total discharges Δ W beginning in 1980 will be as follows: in 1990 -- 63 Gt, in 2000 -- 155 Gt, in 2010 -- 297 Gt, in 2020 -- 494 Gt, in 2030 -- 788 Gt. The basic computations were made for a β value obtained using data from the monitoring of ^{13}C, that is, 0.3, and for two V_{md} values: $1.25 \cdot 10^{-5}$ cm/sec and $2.5 \cdot 10^{-5}$ cm/sec. The results are given in Figures 5 and 6. Figure 5 illustrates the percentage distribution of Δ W among the three reservoirs. Its characteristic feature is that in that time interval when dW/dt is increasing the fraction of industrial CO_2 remaining in the atmosphere is increasing. This occurs due to the great inertia of the ocean reaction to atmospheric disturbances. The fraction from the biomass remains approximately constant. The ratio $\Delta x/\Delta W$, equal, according to monitoring data, to 43.5% in 1970, agrees well with extrapolation of computations for $V_{md} = 2.5 \cdot 10^{-5}$.

Variants of calculations with $V_{md} = 1.25 \cdot 10^{-5}$ and $\beta = 0.3$ and with $V_{md} = 2.5 \cdot 10^{-5}$ and $\beta = 0.15$ give values of the temporal variation of atmospheric CO_2 content coinciding within the limits 5 million^{-1}. This function is also shown in the last graph (Fig. 6). This also illustrates the influence of the total quantity of industrial discharge in 2030 on the x values for this same year. The influence of independent variations of the β and V_{md} parameters is illustrated by the inset in Fig. 5. The results of computations by the models of the carbon cycle for 2020-2040 mentioned at the beginning of the article fit approximately into this same $\Delta x/\Delta W$ range.

In one of the recent studies of this subject [37] there is an analysis of limiting variants of the development of energy during the next 50 years. In the first variant the rate dW/dt of industrial effluent ceases to increase beginning in 1975 and remains equal to approximately 5 Gt/year. In the second the mean annual increment remains constant and is equal to 4.5% per year. In this case the dW/dt value by 2030 will become $e^{2.25}$, that is, 9.5 times greater than at the present time, that is, 50-60 Gt/year. The doubling of the CO_2 concentration in the atmosphere by 2030 which we obtained corresponds to an intermediate variant in which the rate of industrial effluent will increase by 2030 to 26-30 Gt/year. In this case the total magnitude of the anthropogenic CO_2 effluent will be about 800 Gt, which is considerably less than the reserves of fossil fuel available for use, the quantity of which is estimated at from 5000 to 10 000 Gt.

The authors express their appreciation to M. I. Budyko for initiating this study.

****

BIBLIOGRAPHY

1. ATLAS OKEANOV. T 1. TIKHIY OKEAN; T 2. ATLANTICHESKIY I INDIYSKIY OKEANY (Atlas of the Oceans. Vol 1. Pacific Ocean; Vol 2. Atlantic and Indian Oceans), VMF SSSR, 1974, 1977.

2. Ariel', N. Z., Bortkovskiy, R. S., Byutner, E. K. and Strokina, L. A., "Influence of Ocean Contamination by an Ocean Film on the Exchange of Oxygen With the Atmosphere," METEOROLOGIYA I GIDROLOGIYA (Meteorology and Hydrology), No 2, 1979.

3. Bazilevich, N. I, Rodin, L. Ye. and Rozov, N. N., GEOGRAFICHESKIYE ASPEKTY IZUCHENIYA BIOLOGICHESKOY PRODUKTIVNOSTI (Geographical Aspects of Study of Biological Productivity), Izd. Geogr. Obshch-va SSSR, Moscow, 1970.

4. Budyko, M. I., PROBLEMA UGLEKISLOGO GAZA (Problem of Carbon Dioxide), Leningrad, Gidrometeoizdat, 1979.

5. Budyko, M. I. and Ronov, A. B., "Evolution of the Chemical Composition of the Atmosphere in the Phanerozoic," GEOKHIMIYA (Geochemistry), No 5, 1979.

6. Budyko, M. I. and Vinnikov, K. Ya., "Global Warming," METEOROLOGIYA I GIDROLOGIYA, No 7, 1976.

7. Yefimova, N. A., RADIATSIONNYYE FAKTORY PRODUKTIVNOSTI RASTITEL'NOGO POKROVA (Radiation Factors in the Productivity of the Plant Cover), Leningrad, Gidrometeoizdat, 1977.

8. Kagan, B. A. and Ryabchenko, V. A., "Mean Concentration and Budget of Dissolved Oxygen in the World Ocean," DOKLADY AN SSSR (Reports of the USSR Academy of Sciences), Vol 233, No 4, 1977.

9. Kagan, B. A. and Ryabchenko, V. A., TRASSERY V MIROVOM OKEANE (Tracers in the World Ocean), Leningrad, Gidrometeoizdat, 1978.

10. Kobak, K. N., "Carbon Dioxide Supply for Forest Biogeocoenoses," PROBLEMY EKOLOGII I FIZIOLOGII LESNYKH RASTENIY (Problems in the Ecology and Physiology of Forest Plants), Leningrad, LTA, No 2, 1965.

11. Koblents-Mishke, O. I., Volkovinskiy, V. V. and Kabanova, Yu. G., "New Data on the Magnitude of Primary Production in the World Ocean," DOKLADY AN SSSR, Vol 183, No 3, 1968.

12. Lyakhin, Yu. I. and Ivanenkov, V. N., "Elements of the Carbonate System in Atlantic Ocean Waters," KHIMIKO-OKEANOGRAFICHESKIYE ISSLEDOVANIYA MOREY I OKEANOV (Chemical-Oceanographic Investigations of Seas and Oceans), Moscow, Nauka, 1975.

13. Lyakhin, Yu. I., Aleksandrov, V. P. and Pal'shin, I. I., "Computation of the Balance of CO_2 Exchange Between the Ocean and Atmosphere Over the Atlantic, Pacific and Indian Oceans," TRUDY LGMI (Transactions of the Leningrad Hydrometeorological Institute), No 65, 1978.

14. MORSKAYA VODA (Sea Water), edited by A. S. Monin, Moscow, Nauka, 1979.

15. Ronov, A. B., "Volcanism, Carbonate Accumulation and Life," GEOKHIMIYA, No 8, 1976.

16. Svirezhev, Yu. M and Tarko, A. N., "Modeling of the Global Biogeochemical Cycle of Carbon," VESTNIK AN SSSR (Herald of the USSR Academy of Sciences), No 12, 1979.

17. Skopintsev, B. A., "Oxygen Consumption in the Deep Waters of the Ocean," OKEANOLOGIYA (Oceanology), 15, No. 5, 1975.

18. Stepanov, V. N., "Temperature Field of Waters in the World Ocean," OKEANOLOGIYA, Vol 20, No 1, 1980.

19. Suyetova, I. A., "Patterns of Quantitative Distribution of Biomass of the Land and Ocean," VESTNIK MGU: SERIYA GEOGRAF. (Herald of Moscow State University: Geography Series), No 6, 1973.

20. Bacastow, R. B. and Keeling, C. D., "Models to Predict Future Atmospheric CO_2 Concentrations," WORKSHOP ON THE GLOBAL EFFECTS OF CARBON DIOXIDE FROM FOSSIL FUELS, Miami Beach, Florida, 1977.

21. Bjorkstrom, A., "A Model of the CO_2 Interaction Between Atmosphere, Oceans and Land Biota," SCOPE REPORT 13. THE GLOBAL CARBON CYCLE, Ch 15, 1979.

22. Bohn, H., "On Organic Soil Carbon and CO_2," TELLUS, Vol 30, 1978.

23. Bray, J. R., "An Analysis of the Possible Recent Change in Atmospheric CO_2 Concentration," TELLUS, Vol 11, 1959.

24. Broecker, W. S. and Peng, T. H., "Gas Exchange Between Air and Sea," TELLUS, Vol 26, 1974.

25. Eriksson, E., "The Atmospheric Carbon Dioxide Problem," TELLUS, Vol 30, 1978.

26. Keeling, C. D. and Bacastow, R. B., "Impact of Industrial Gases on Climate," ENERGY AND CLIMATE, 1977.

27. Keeling, C. D., Mook, W. G. and Tans, P. P., "Recent Trends in the $^{13}C/^{12}C$ Ratio of Atmospheric Carbon Dioxide," NATURE, Vol 277, No 5692, 1979.

28. Loomis, R. S., "CO_2 and Biosphere," CONF-770385. WORKSHOP ON THE GLOBAL EFFECTS OF CARBON DIOXIDE FROM FOSSIL FUELS, 44-50.

29. Machta, L., "Atmospheric Measurements of Carbon Dioxide," CONF-770385. WORKSHOP ON THE GLOBAL EFFECTS OF CARBON DIOXIDE FROM FOSSIL FUELS, 44-50.

30. Oeschger, H., Siegenthaler, U., Schotterer and Gugelmann, A., "A Box Diffusion Model to Study the Carbon Dioxide Exchange in Nature," TELLUS, Vol 27, 1975.

31. Olson, J. S., CHANGES IN THE GLOBAL CARBON CYCLE AND THE BIOSPHERE, Oak Ridge National Laboratory, 1978.

32. Pytkowicz, R. M., "Carbonate Cycle and the Buffer Mechanism of Recent Oceans," GEOCHIM. ET COSMOCHIM. ACTA, Vol 31, 1967.

33. Pytkowicz, R. M. and Small, L. F., "Fossil Fuel Problem and Carbon Dioxide: An Overview," THE FATE OF FOSSIL FUEL CO_2 IN THE OCEAN, edited by N. Andersen and A. Malahoff, 1977.

34. Revell, R. and Munk, W., "The Carbon Dioxide Cycle and the Biosphere," ENERGY AND CLIMATE, 1977.

35. Riley, J. P. and Skirrow, R. W., CHEMICAL OCEANOGRAPHY, Vol 2, 1975.

36. Rotty, R. M., "Present and Future Production of CO_2 From Fossil Fuels. A Global Appraisal," CONF-770385. WORKSHOP ON THE GLOBAL EFFECTS OF CARBON DIOXIDE FROM FOSSIL FUELS: 36-43.

37. Siegenthaler, U. and Oeshger, H., "Predicting Future Atmospheric Carbon Dioxide Levels," SCIENCE, Vol 199, No 4327, 1978.

38. Takahashi, T., "Carbon Dioxide Chemistry on Ocean Water," 1977. CONF-770385. WORKSHOP ON THE GLOBAL EFFECTS OF CARBON DIOXIDE FROM FOSSIL FUELS: 63-71.

39. Vooys, C. G. N., "The Carbonate System of the Ocean," Ch 10, SCOPE Report 13, THE GLOBAL CARBON CYCLE, 1979.

40. Ziemen, K. E., Offerman, P. and Hartman, G., "Source Functions of CO_2 and Future CO_2 Burden in the Atmosphere," Z. NATURFORSCH., No 12.

UDC 551.(591.2+576.4)

EXPERIMENTAL INVESTIGATION OF THE CORRELATION BETWEEN THE METEOROLOGICAL RANGE OF VISIBILITY AND ALTITUDE OF THE LOWER CLOUD BOUNDARY

Moscow METEOROLOGIYA I GIDROLOGIYA in Russian No 3, Mar 81 pp 32-38

[Article by Ye. R. Milyutin, candidate of technical sciences, and Yu. I. Yeremenko, Leningrad Electrotechnical Institute of Communication, manuscript received 24 Jun 80]

[Text]

Abstract: On the basis of an analysis of experimental data a study was made of analytical representations of real probabilistic distributions of the altitude of the lower boundary and the quantity of clouds. The correlation and regression relationships between the meteorological range of visibility and the altitude of the lower cloud boundary are determined.

The results of measurements of atmospheric transparency in horizontal and vertical directions are used extensively in a number of technical applications (optical communication, aviation, etc.). A universal characteristic of transparency in a horizontal direction is the meteorological range of visibility S_M (MRV), the finding of whose analytical form of the probabilistic distribution law was the subject of a study by the authors [15].

In many cases (in optical sounding, in optical communication on slant paths, in aviation, etc.) a knowledge of the altitude of the lower cloud boundary H_{low} is also of great practical interest. Accordingly, attempts at determining the statistical correlation of S_M, measured at many meteorological stations, and H_{low}, that is, in other words, attempts to find the correlation between horizontal and vertical atmospheric transparency in the presence of a cloud cover, are extremely timely. This problem was examined in a number of investigations [2, 7, 8, 12] in which the influence of low-lying clouds on the MRV was noted, but the correlation between S_M and H_{low} was evaluated only qualitatively.

In this study we will determine the empirical probabilistic distribution functions for H_{low} and the quantity of clouds N (in tenths) and a study is made of their seasonal and annual changes. On the basis of an analysis of the experimental data a study is made of analytical representations of the real distributions and the correlation and regression relationships between the random S_M and H_{low} values are found.

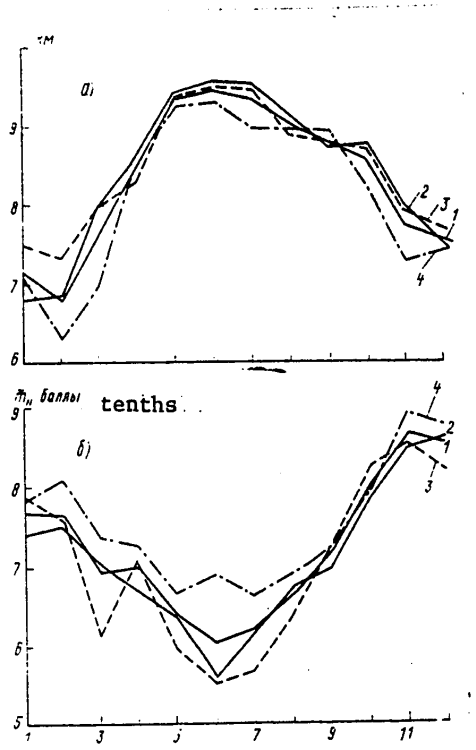

Fig. 1. Variation of monthly changes $\bar{m}_S$ and $\bar{m}_N$ for 14 years (1) for first (2), second (3) and third (4) periods.

As initial data we used the results of MRV observations for 14 years (1964-1977) made at Leningrad meteorological station. During the first period (1964-1968) the observations were made visually and in the second period (1969-1972) both visually and by means of a range-of-visibility recorder. During a third period (1973-1977) only a range-of-visibility recorder was employed. The total number of observations was n_S = 122 736.

Curves of the monthly changes in the sample mean $\bar{m}_S$ both for individual periods and for 14 years are shown in Fig. 1a, where the sequence number for the month of the year is plotted along the x-axis.

At the same time we processed observational data on the quantity of clouds (N) which was registered eight times a day. The total number of observations was n_N = 40 912. The results of space and aerological observations in this case could not be used because we were interested in the state of the cloud cover within a stipulated solid angle of the celestial hemisphere viewed from a definite point on the earth's surface.

On the basis of data on N we computed the frequencies of occurrence of the quantity of clouds in the range from 0/10 to 10/10 with a 1/10 interval for each month and as an average for the year, after which we constructed graphs of the accumulated

frequencies (Fig. 2a), representing statistical analogues of the distribution functions F(N) and making it possible to find the probability P that N will be greater than some level. The empirical distribution functions shown in Fig. 2a at the points N = 0 and N = 10 have discontinuities of the first kind, which makes their analytical description quite difficult. These peculiarities in the behavior of the distribution are attributable to the fact that in temperate and polar climates it is most common to observe values N = 0 and N = 10 [23]. In addition, we computed sample mean $\bar{m}_N$ and unbiased competent evaluations of the dispersion $\bar{D}_N$. The results are given in the table and Fig. 1b shows the curves illustrating the monthly changes $\bar{m}_N$.

An analysis of the results for 14 years indicated that the minimum quantity of clouds is observed in June and the maximum quantity is observed in November; even in June $\bar{m}_N > 6$, and $P(N > 5) > 0.61$, which confirms a considerable influence of cloud cover on atmospheric transparency in a vertical direction. However, as indicated in Fig. 1b, there are also deviations from the mean values, for example, in the first period the cloud cover maximum fell in December, which agrees with the conclusion presented in [4] on the basis of the results of observations of clouds in approximately these same years.

Then we determined the distribution function for the altitude of the lower cloud boundary, the quantity of which exceeds 5/10. We processed data from monthly observations of H_{low} during 1964-1968 made using a cloud-altitude measuring apparatus; n_H = 43 848. All H_{low} in accordance with ICAO recommendations are put into 12 intervals in order that in the subsequent computations it would be possible to use data from meteorological stations at the international airports of the ICAO member countries.

The sequence for the further statistical processing of observations was the same as in the preceding case. The determined $\bar{m}_H$ values are given in the table, from which it follows that the minimum mean altitude of the lower cloud boundary was observed in January and the maximum altitude was observed in June. In an analytical description of the distribution function H_{low} we used the same set of distributions as for S_M [15].

The computations made on an electronic computer indicated that according to the Kolmogorov consistency test the most acceptable approximation of the real distributions for the spring and autumn months, and also the mean annual distribution, is a truncated normal distribution (Fig. 3), whereas for the summer and winter months it is a Rayleigh distribution (Fig. 3b). The derived dependences make it possible, using the data in [4] on the relationships between cloud altitude and type, to evaluate the attenuation of optical radiation in the cloud layer.

By comparing the behavior of the curves of monthly changes of the parameters $\bar{m}_S$, $\bar{m}_N$ and $\bar{m}_H$ during the first period (Fig. 1,a,b and the table) it can be seen that the maxima of the $\bar{m}_S$ and $\bar{m}_H$ curves and the minimum of the $\bar{m}_N$ curve are observed in June, whereas the $\bar{m}_S$ and $\bar{m}_H$ minima coincide in January and the $\bar{m}_N$ maximum is displaced to December.

For a quantitative evaluation of the degree of correlation between S_M and H_{low} we compiled correlation tables with gradations of S_M and H_{low}, established earlier, for each month and as an average for the year. Using the data in the table we

computed the corresponding correlation coefficients $\bar{r}$ and the correlation ratios $\bar{\eta}$ using the known formulas [1]

$$\bar{r} = \frac{\sum_{i=1}^{14}\sum_{j=1}^{11} n_{ij} S_{M\,i} H_{H\,j} - n_H \bar{m}_s \bar{m}_H}{(n_H - 1)\sqrt{\bar{D}_s \bar{D}_H}}, \tag{1}$$

$$\bar{\eta}_1 = \sqrt{\frac{1}{(n_H - 1)\bar{D}_H}\sum_{i=1}^{14} n_i [\bar{m}_H (S_{M\,i}) - \bar{m}_H]^2}, \tag{2}$$

where $[H_H = H_{low}]$

$$\bar{m}_H (S_{M\,i}) = M\left[\frac{H_H}{S_M} = S_{M\,i}\right] = \frac{1}{n_i}\sum_{j=1}^{11} n_{ij} H_{H\,j}$$

is the conventional mean H_{low} value with $S_M = S_{M\,i}$, $H_{low\,j}$ is the middle of the j-th intervals of the H_{low} values, n_{ij} are the frequencies of combinations of the values $S_M = S_{M\,i}$ with $H_{low} = H_{low\,j}$.

The results of computations using formulas (1) and (2) are given in the table.

The significance of the correlation was determined in the following way. According to [14], in the case of large volumes of the sample n_H ($n_H > 80$) the $\bar{r}$ value is considered considerably different from zero if the following inequality is observed

$$\bar{r} > \left[1 + \frac{n_H - 2}{t_\alpha^2}\right]^{-\frac{1}{2}}, \tag{3}$$

where t_α is the critical value of the Student t-distribution with $(n_H - 2)$ degrees of freedom, corresponding to the selected significance level α_3 $(0 < \alpha_3 < 0.5)$.

The critical value $t_\alpha = t_{n_H - 2}(\alpha_3)$ is a solution of the equation

$$S_{n_H - 2}(t_\alpha) = 1 - \frac{\alpha_3}{2}, \tag{4}$$

where $s_{n_H-2}(t_\alpha)$ is the Student distribution function.

We note that with $n_{H-2} > 80$ it is possible to use the approximate equation

$$S_{n_H - 2}(t_\alpha) \simeq 0{,}5 + \Phi_0 (t_\alpha), \tag{5}$$

where $\Phi_0(t_\alpha)$ is the tabulated integral of probabilities.

In addition, with large n_H the $\bar{r}$ value approximately corresponds to a normal distribution with the dispersion $\bar{D}_r \simeq 1/n_H(1 - \bar{r}^2)^2$, which makes it possible to evaluate the $\bar{r}$ value using the confidence coefficient γ [8],

$$\gamma = P\{\bar{r} - \beta\sqrt{\bar{D}_r} < \bar{r} < \bar{r} + \beta\sqrt{\bar{D}_r}\} \simeq 2\Phi_0(\beta). \tag{6}$$

Computations made using formulas (3)-(6) show that for all months the $\bar{r}$ and $\bar{\eta}$ values differ considerably from zero even with small $\alpha_3 = 10$ and a high confidence coefficient $\gamma = 0.99$, which demonstrates the presence of a stable correlation.

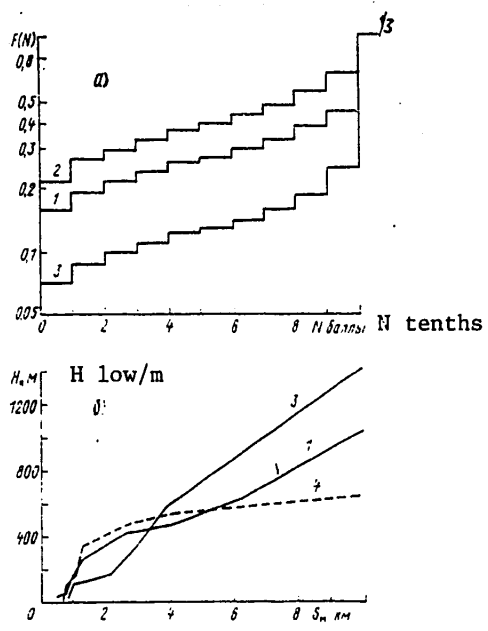

Fig. 2. Empirical distribution functions N (a) and regression dependence of H_{low} on S_M (b). 1) mean annual, 2) for November, 3) for June, 4) for January.

	$\bar{m}_S$ км				$\bar{m}_N$ tenths				$\bar{m}_H$ м	$\bar{r}$	$\bar{r}_1$
	I	II	III	14 yrs	I	II	III	14 yrs			
January	6,81	7,49	7,09	7,10	7,40	7,88	7,84	7,70	560,89	0,219	0,239
February	6,84	7,32	6,33	6,80	7,53	7,59	8,09	7,64	638,88	0,358	0,372
March	8,01	8,00	6,99	7,64	7,02	6,08	7,38	6,92	723,59	0,475	0,477
April	8,63	8,31	8,50	8,49	6,68	7,07	7,23	6,99	917,12	0,614	0,619
May	9,39	9,36	9,24	9,33	6,38	5,97	6,64	6,37	1238,82	0,411	0,415
June	9,54	9,50	9,30	9,44	5,57	5,51	6,90	6,03	1318,13	0,495	0,495
July	9,52	9,48	8,96	9,33	6,16	5,68	6,62	6,19	1313,55	0,426	0,433
August	9,14	8,88	8,96	9,00	6,70	6,36	6,89	6,67	1211,26	0,509	0,516
September	8,72	8,75	8,93	8,81	6,95	7,25	7,24	7,14	1024,04	0,505	0,508
October	8,75	8,69	8,22	8,55	7,84	8,24	7,98	8,00	787,68	0,425	0,429
November	7,95	7,93	7,27	7,70	8,49	8,54	8,93	8,66	618,01	0,412	0,418
December	7,50	7,68	7,42	7,53	8,59	8,24	8,76	8,55	579,89	0,364	0,383
Mean annual	8,41	8,45	8,12	8,32	7,10	7,03	7,52	7,23	886,72	0,499	0,503

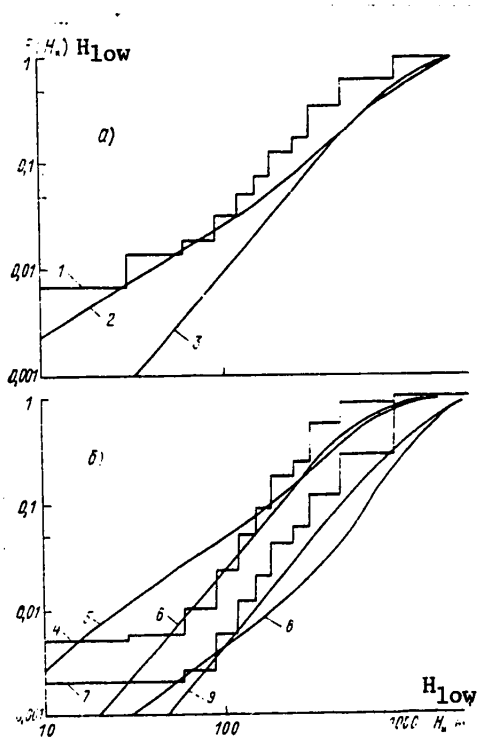

Fig. 3. Probabilistic distributions of lower cloud boundary. 1) mean annual, b) mean monthly; 1, 4, 7) empirical, 2, 5, 8) truncated normal, 3, 6, 9) Rayleigh; 4-6) for January, 7, 9) for June.

It follows from an analysis of these results that the greatest $\bar{r}$ and $\bar{\eta}$ values are attained in April and the minima are attained in January. In general, however, the correlation in a number of spring and autumn months exceeds the mean annual values, whereas in the summer and especially in the winter months it drops below the mean annual level. This phenomenon is evidently explicable on a physical basis as follows: in summer the altitude of the clouds is greater and therefore the cloud cover exerts a lesser influence on the meteorological range of visibility measured in the surface layer of the atmosphere, whereas in winter, despite the low cloud cover, and in part also due to this circumstance, such phenomena as snowfalls, etc. frequently occur which exert a stronger influence on the MRV than do the lowest clouds directly.

Regression lines for H_{low} and S_M were constructed in the form

$$H(S_{M\,i}) = \left[M \frac{H_{low}}{S_M} = S_{M\,i} \right]$$

for each month and as an average for the year, shown in Fig. 2b, in order to be able, on the basis of the measured S_M values, to estimate the H_{low} value and thus determine atmospheric transparency in vertical and slant directions.

The regression lines have the property that among all the real f(S) functions the minimum of the mathematical expectation

$[H_H = H_{low}]$ $$M\{[H_H - f(S)]^2\} = \overline{D}_H (1 - r^2) \quad (7)$$

is attained for $f(S) = H(S_{M\,i})$, that is, the H_{low}-S_M regression gives the best (with respect to the minimum of the standard deviation) representation of the H_{low}-S_M value [14].

It is known that on the basis of the difference in $\overline{r}$ and $\overline{\eta}$ ($\overline{\eta} \geq \overline{r}$) it is then possible to evaluate the closeness of the two-dimensional distribution of S_M and H_{low} to a normal distribution, that is, the closeness of the regression curve to a linear dependence. From an analysis of the graphs shown in Fig. 2b and the data from the correlation tables it follows that the regression curves for the summer, and also for some spring and autumn months can be satisfactorily approximated, using the Kolmogorov test, by a linear dependence in the form

$$H(S_{M\,i}) = \overline{m}_H + \overline{r}\sqrt{\frac{\overline{D}_H}{\overline{D}_S}}(S_{M\,i} - \overline{m}_S). \quad (8)$$

The dispersion of the H_{low} distribution relative to the regression line (8) is determined by expression (7).

For the winter months the regression becomes essentially nonlinear. This circumstance indirectly confirms the above-mentioned explanation of the peculiarities of seasonal changes of the $\overline{r}$ and $\overline{\eta}$ parameters.

The following conclusions can be drawn from the materials cited above:

1. The minimum mean quantity of clouds for a 14-year period is observed in June-July when it is about 6/10; then the $\overline{m}_N$ values increase monotonically, attaining a maximum in November-December ($\overline{m}_N > 8.5/10$), after which they also monotonically decrease. The corresponding mean probabilities of appearance of considerable cloud cover $P(N>5) = P_N$ vary from $P_N = 0.61$ with minimum cloud cover to $P_N = 0.87$ when there is maximum cloud cover.

2. During the period from 1864 to 1968 the minimum mean altitude of the lower cloud boundary was observed in December-January ($\overline{m}_H < 600$ m), and the maximum -- in June-July ($\overline{m}_H > 1300$ m). For the summer and winter months a satisfactory approximation of the real distributions of the altitude of the lower cloud boundary is a Rayleigh distribution, whereas for all the remaining months a truncated normal distribution is best.

3. It was established that there is a considerable correlation between the S_M and H_{low} random values. For the entire analyzed period this correlation (correlation coefficient and correlation ratio $\overline{\eta}$) increases in the spring and autumn months, attaining a maximum in April ($\overline{r} = 0.61$; $\overline{\eta} = 0.62$); it decreases somewhat in summer and decreases sharply in winter with a minimum in January ($\overline{r} = 0.22$; $\overline{\eta} = 0.24$).

Thus, on the basis of measured S_M values, using the constructed graphs of the regression dependences, it is possible to estimate the H_{low} value with a stipulated probability.

In their totality the results, in the presence of cloud cover, make it possible to estimate atmospheric transparency in slant and vertical directions on the basis of the known values for horizontal transparency.

In conclusion it must be noted that although the numerical computations were made on the basis of observations in Leningradskaya Oblast, the proposed method is applicable for different geographical regions, thereby making it possible to find some general dependences.

The authors express appreciation to Professor K. S. Shifrin for useful discussions of this work, in many respects favoring an improvement in its content.

BIBLIOGRAPHY

1. Abezgauz, G. G., et al., SPRAVOCHNIK PO VEROYATNOSTNYM RASCHETAM (Handbook on Stochastic Computations), Moscow, Voyenizdat, 1970.

2. Barteneva, O. D., Dovgyallo, Ye. N. and Polyakova, Ye. A., "Experimental Investigations of the Optical Properties of the Atmospheric Surface Layer," TRUDY GGO (Transactions of the Main Geophysical Observatory), No 220, 1967.

3. Barteneva, O. D., et al., "Experimental Investigations of the Optical Properties of the Atmospheric Surface Layer," TRUDY GGO, No 220, 1967.

4. Bisyarin, V. P., et al., OSLABLENIYE LAZERNOGO IZLUCHENIYA V GIDROMETEORAKH (Attenuation of Laser Radiation in Hydrometeors), Moscow, Nauka, 1977.

5. Bozhevikov, N. S., "Correlation Between the Lower Cloud Boundary and the Range of Visibility at the Earth," TRUDY GGO, No 153, 1964.

6. Gavrilov, V. A., VIDIMOST' V ATMOSFERE (Atmospheric Visibility), Leningrad, Gidrometeoizdat, 1966.

7. Goryshin, V. I. and Korniyenko, V. I., "Variability of the Horizontal Range of Visibility," TRUDY GGO, No 324, 1974.

8. Dovgyallo, Ye. N., "Atmospheric Transparency in Vertical and Horizontal Directions," TRUDY GGO, No 169, 1965.

9. Dovgyallo, Ye. N., "Diurnal Variation of the Meteorological Range of Visibility," No 169, 1965.

10. Dovgyallo, Ye. N. and Gorb, N. N., "On the Relationship Between Visibility and the Lower Cloud Boundary," TRUDY GGO, No 153, 1964.

11. Dovgyallo, Ye. N. and Kovalev, V. A., "Results of Preliminary Tests of a 'Slant Ray' Apparatus," TRUDY GGO, No 279, 1972.

12. Dunayeva, A. V., "Variability of the Lower Cloud Boundary and its Influence on Atmospheric Transparency at the Earth," TRUDY GGO, No 184, 1966.

13. Zvereva, S. V., "Horizontal Visibility and Cloud Altitude in the Leningrad Region," TRUDY LGMI (Transactions of the Leningrad Hydrometeorological Institute), No 19, 1963.

14. Kramer, G., MATEMATICHESKIYE METODY STATISTIKI (Mathematical Methods in Statistics), Moscow, Mir, 1975.

15. Milyutin, Ye. R. and Yaremenko, Yu. I., "Experimental and Theoretical Investigation of the Distribution Law for Horizontal Atmospheric Transparency," IZV. AN SSSR: FIZIKA ATMOSFERY I OKEANA (News of the USSR Academy of Sciences: Physics of the Atmosphere and Ocean), Vol 15, No 8, 1979.

16. PERENOS MIKROVOLNOVOGO IZLUCHENIYA V ATMOSFERE (Transfer of Microwave Radiation in the Atmosphere), edited by K. S. Shifrin, TRUDY GGO, No 222, 1968.

17. Ratsimor, M. Ya., "Method for Computing Transparency and the Range of Visibility of Lights in a Slant Direction," METEOROLOGIYA I GIDROLOGIYA (Meteorology and Hydrology), No 1, 1967.

18. Ratsimor, M.Ya., "Slant and Vertical Visibility in Advective Fogs," TRUDY GIDROMETTSENTRA SSSR (Transactions of the USSR Hydrometeorological Center), No 45, 1969.

19. Reshikova, A. A. and Tonkova, Z. V., "Correlation Between the Altitude of the Lower Cloud Boundary and the Range of Visibility," TRUDY TsAO, No 7, 1952.

20. Titov, V. I., "Some Seasonal Characteristics of Weather at the Leningrad, Vnukovo, Kursk and Other Airports Determined by the Altitude of Clouds and Visibility," TRUDY NIIAKa (Transactions of the Scientific Research Institute of Aeroclimatology), No 11, 1963.

21. TRUDY GGO (Transactions of the Main Geophysical Observatory), Nos 184, 213, 220, 223, 237, 255, 279, 312, 324, 357, 384.

22. Khrgian, A. Kh., FIZIKA ATMOSFERY (Atmospheric Physics), Vol 2, Leningrad, Gidrometeoizdat, 1978.

23. Shapayev, V. M., "Influence of the Wind on Variations in Visibility and the Cloud Cover Altitude," TRUDY GGO, No 163, 1964.

UDC 519.2

RUNNING CONTROL AND EVALUATION OF ALTERNATIVE MODELS

Moscow METEOROLOGIYA I GIDROLOGIYA in Russian No 3, Mar 81 pp 39-45

[Article by N. K. Sharifullin and L. N. Romanov, candidate of physical and mathematical sciences, West Siberian Scientific Research Institute, manuscript received 21 Jul 80]

[Text]

Abstract: The article describes a method for realizing a rapid running control for the purpose of obtaining evaluations of linear alternative models. Also considered are modifications of rapid running control, making it possible to evaluate the models in a case when the initial situations are represented by a chronological series. The effectiveness of the algorithms is illustrated in the example of a short-range prediction of frosts with the use of a sufficiently long series of observations.

Introduction. An evaluation of statistical models is an important and necessary stage in their formulation. The principal difficulties in such an evaluation arise due to the shortage of a priori information, expressed in the absence of a sufficiently long series of observations. When there are limitations in the initial sample the evaluation of a model is usually made on the basis of some statistical tests. The effectiveness of such an evaluation is essentially dependent on the complexity of the simulated phenomenon. In the case of a sufficiently complex distribution of situations in multidimensional space an evaluation made using standard tests can lead to a false idea concerning its effectiveness.

The most universal method for evaluating statistical models is running control [1]. This method, making it possible to obtain adequately reliable evaluations of a model when there is a short sample of situations at the same time has limited application possibilities due to the great expenditures of computer time.

The authors of [4] presented algorithms for rapid running control making it possible to evaluate linear regression models which are formulated using a sufficiently great volume of statistical material. The use of the "ordered sorting" method [5] for the purpose of constructing a hyperplane separating classes also allows a rapid realization of running control, but such a realization is possible

only when this method is employed. In this article we describe a method for realizing rapid running control in evaluating a linear alternative rule obtained by any method. The algorithms presented in this study also make it possible to choose the optimum dimensionality of situations by successively obtaining evaluations of running control for different combinations of initial parameters.

Modifications of running control. Running control involves the successive "extraction" of situations from a teaching sample and in these situations the checking of the quality of operation of a model formulated in the remaining situations. In each case extracting one situation, it is possible to obtain evaluations of the model in all situations represented by the initial sample as if using independent material. In this procedure the length of the teaching sample is reduced by only one situation. The principal requirement imposed on the initial material in the implementation of running control is the statistical independence of the situations intended for formulating the model and evaluation of its quality. In other words, the initial situations must be obtained randomly and independently in accordance with some fixed distribution. In the formulation of a weather forecasting model the initial data usually represent synoptic situations taken successively in chronological order, as a result of which the requirement of independence of situations is not satisfied. The carrying out of running control on the basis of such material can lead to an understatement of the error in running control in comparison with the mean error of the model being tested.

Two modifications of the implementation of rapid running control are possible in order to avoid the mentioned effect. The first modification involves the successive elimination of not one situation, but some group of situations (usually groups of three situations) and computation of the error for the group in the middle. The subsequent exclusion and inclusion of situations is accomplished one-by-one in chronological order in such a way that in the teaching material in each case a group of situations of an a priori stipulated size is absent. In such a modification teaching will be accomplished using N-k situations and the error in running control involves N-k+1 situations, where k is the number of situations in the group and N is the total number of situations.

Another modification which can be used in the case of a chronological arrangement of the initial situations involves their one-by-one inclusion in the teaching material. For this purpose there must be a priori restriction of some group of situations and then situations are included in this group one by one, each time refining the model and computing the error for the situation corresponding to the later time of its appearance. If the initial group for teaching is selected from l situations, the evaluation of running control in this modification can be obtained using $N-l$ situations. For greater clarity we will call the second modification control by a refining model.

Both the above-mentioned modifications of running control allow their rapid realization if the "supplementation" method is used for this purpose [7].

Discrimination of informative situations. Assume that the hyperplane

$$\sum_{i=1}^{n} a^i x^i - c = (a\,x) + c = 0, \qquad (1)$$

constructed by any method, separates the initial set of situations $(x_1,\ldots,x_N)$ into two sets corresponding to different classes. In such cases the separation can be both complete and with errors.

We will apply the term "informative situations for a stipulated hyperplane" to those situations which unambiguously determine the hyperplane situated precisely in such a way relative to the sets to be separated. If the initial hyperplane separated sets with errors, sets should be divided with these very same errors using a hyperplane determined by informative situations.

In order to discriminate informative situations for the hyperplane (1), we will move it in multidimensional space parallel to itself until the next situation is encountered. Such a movement can be accomplished by a change in the free term c. Assume that the situation x_{k_1} was closest to the hyperplane. Setting the new position of the hyperplane at x_{k_1}, we will gradually change its orientation by a change in ^{1} until the hyperplane comes into contact with the new situation x_{k_2}. Then fixing the new approximation at the two points x_{k_1} and x_{k_2}, we similarly find a new hyperplane by a change of the coefficient ^{2}, etc. Thus, it is possible to discriminate n situations

$$x_{k_1}, \ldots, x_{k_n}, \tag{2}$$

determining the new hyperplane

$$\sum_{i=1}^{n} \beta^i x^i + D = (\beta x) + D, \tag{3}$$

having the same positioning relative to the separating sets.

Since the variation of the coefficients of the separating hyperplane (1) is possible both in the direction of their decrease and increase, the new hyperplane (3) is not unique. However, any hyperplane derived from (1) in accordance with the rule described above has the property of having the same situations, including erroneous, like the erroneous situations for the hyperplane (1).

In actual practice the discrimination of informative situations for a stipulated hyperplane can be accomplished using the "ordered sorting" method [5]. The algorithm was formulated in such a way that the initial approximation is successively improved only in the sense of a minimum number of errors and this improvement is brought about by a replacement in the system of base vectors, the final set of which constitutes the informative situations.

In exactly the same way the discrimination of informative situations can be accomplished using the algorithm described in [6].

Algorithm for rapid running control. It was demonstrated in the monograph [2] that with an error-free separation of situations by means of a hyperplane it is sufficient to carry out running control only in informative situations. Nevertheless, the process of constructing n hyperplanes in n-dimensional space can be quite unwieldy.

We will examine an algorithm which makes possible the rapid realization of the running control procedure.

Assume that the hyperplane (3), for which the informative situations are already known, is intended for separation of the sets X_1 and X_2. This means that for most of the situations from the initial sample there is the system of inequalities

$$\begin{aligned} (\beta x_i) + D > 0 \quad &\text{with} \quad x_i \in X_1, \\ (\beta x_i) + D \leq 0 \quad &\text{with} \quad x_i \in X_2. \end{aligned} \tag{4}$$

Introducing an additional parameter in each situation, equal to unity, and also changing the sign for the situations in the set X_2 to the opposite (see [3]), the inequalities (4) can be written in the form

$$(\gamma x_i) \geq 1.$$

Thus, all the initial situations can be divided into three groups in dependence on their positioning relative to the hyperplane. We assign to the first group the situations for which there are inequalities $(\gamma x_i) > 1$; to the second we assign the informative situations $(\gamma x_i) = 1$; and to the third group we assign situations for which $(\gamma x_i) < 1$. Corresponding to these groups we can form three matrices A, B and C, of which B is square and A and C are rectangular. It is evident that the first two matrices consist of properly classified situations, whereas the C matrix consists of erroneous situations.

Assume that there is inversion of the B matrix, determining the vector of the hyperplane

$$\gamma = B^{-1} I, \tag{5}$$

where I is a vector with unique components.

In order to check the next informative situation we will eliminate it from the C matrix and in its place we will alternately substitute all the situations corresponding to the rows of the A matrix and correct the vector (5) until there is a complete separation of the situations from A and B. The correction of the B^{-1} matrix is accomplished using the recurrent expression

$$B_{p+1}^{-1} = B_p^{-1} - \frac{b_l (x_k - b_l)}{x_k b_l} B_p^{-1},$$

where b_l is the l-th row of the B_p matrix, b_l is the l-th column of the B_p^{-1} matrix.

The new approximation of the γ vector is determined using the formula

$$\gamma_{p+1} = B_{p+1}^{-1} I.$$

After the approximation of the γ vector is found, the situations of the C matrix are examined and the number of those correctly recognized from C is "stored." The situation excluded from B is checked simultaneously for the correctness of recognition.

Then another situation is excluded from among the informative situations, the earlier excluded situation is put in its place, the hyperplane separating the classes is corrected, situations from C and the excluded situation are checked for

the correctness of recognition. The process of exclusion and checking is repeated n times until all the informative situations have been exhausted in this way. The probability of an erroneous classification in this case will be evaluated using the expression

$$\Phi = \frac{(\theta - t) + r}{N},$$

where θ is the number of erroneous situations in the initial matrix C, t is the total number of situations from C correctly classified after each correction, r is the number of incorrectly classified informative situations.

Experiments. The examined modifications of running control were realized in the form of programs in ALGOL language using a BESM-6 computer and were tested using data intended for a 24-hour prediction of frosts at Novosibirsk. The prediction was made using data from surface observations obtained from eight stations in southeastern Western Siberia and consisting of temperature, pressure and dew point values. Thus, each situation included 24 parameters which hypothetically should determine the presence or absence of frosts ($t \leqslant 4°C$) at Novosibirsk after 24 hours.

One of the first experiments to be carried out was one which would make it possible to confirm the assumption of an equivalence of the considered algorithm to ordinary running control. For this purpose, using a relatively small amount of statistical material (24 x 100), we carried out running control with one-by-one elimination of situations and the complete restructuring of the hyperplane for all the remaining situations. Since the initial 100 situations were divided by means of the hyperplane without error, complete running control did not involve great expenditures of computer time. The rapid running control algorithm gave a saving in computation time by a factor of 6. A comparison of the results indicated that the number of errors in the rapid running control procedure coincides with the number of errors obtained in the course of ordinary running control. We note that under conditions of absence of linear separability the gain in computation time when using rapid running control can increase substantially.

Table 1 gives the errors in separation when using a hyperplane and the errors in running control with different lengths of the initial samples. The table shows that the running control algorithm makes it possible to evaluate models on the basis of sufficiently large samples, although in this case the computation time increases nonlinearly with an increase in the number of situations.

Table 2 gives the separation errors and the running control errors in a case when there is alternate exclusion of a group of three situations arranged in chronological order and the situation situated in the middle was subject to control. The table shows that the number of errors in running control with the elimination of three situations somewhat exceeds the number of errors obtained by successive elimination of one situation for all the initial samples. This fact is naturally attributable to the statistical dependence of situations arranged in chronological order and indicates that the errors in Table 2 are more reliable than the errors in Table 1.

In investigating the behavior of the errors cited in Tables 1 and 2 we first of all note a fact which at first glance may seem to be paradoxical: the percentage of errors in running control increases with an increase in the length of the initial

sample. This effect is evidently associated with the chronological arrangement of initial situations, and also the presence of long-period weather changes which are only partially characterized by the considered samples. A lengthening of the series of observations, and also a sampling of situations from the stipulated set by means of a detector of random numbers would make it possible to reduce the mentioned effect to a minimum.

Table 1

Errors in Separation and Running Control With Successive Exclusion of One Situation

Number of situations		Separation errors		Errors in running control		Computation time
total	1st-class	total	1st kind	total	1st kind	
100	44	0	0	1	1	2'52"
200	76	6	3	10	5	5 04
250	93	12	5	9	8	8 32
300	109	20	8	30	15	12 22
400	146	34	13	52	24	15 19

Table 2

Errors in Separation and Running Control With Successive Exclusion of Groups of Three Situations

Number of situations		Separation errors		Errors in running control		Computation time
total	1st-class	total	1st kind	total	1st kind	
100	44	0	0	6	1	2'57"
200	76	6	3	18	7	6 35
250	93	12	5	30	15	9 24
300	109	20	8	32	13	13 04
400	146	34	13	53	24	19 47

Table 3

Errors in Successively Refining Model

Number of situations		Number of errors		
teaching	examination	teaching	examination	synoptic
558-594	37	57	6	8

Table 3 gives evaluations of the refining model. Initially the separation was carried out for 558 situations. Then the teaching material was gradually built up to 594 situations and an evaluation of the model was obtained using 37 situations. The table shows that then the reliability of the model was rather high, which can be attributed to the presence in the teaching material of situations closest in time to the examined situation. As a comparison, the table gives evaluations of synoptic forecasts obtained during this same period. In this case the comparison with the synoptic forecasts is interesting in that the weatherman, in forecasting, by means of allowance for the experience of the forecasts closest in time, in essence uses the same scheme of a refining model.

We note that in the described experiments there was no variation of the number of parameters determining the situation. Moreover, the choice of the initial parameters was accomplished purely formally, for the purpose of clarifying the possibilities of rapid running control.

Summary. The examined rapid running control algorithms can be used not only for evaluating linear models, but also for any alternative models formulated using the criterion of the minimum number of separation errors. In this case a changeover to an evaluation of a polynomial model requires only a preliminary transformation of the initial space for the purpose of its linearization.

The experiments described in the article are evidence of the constructive nature of the rapid running control algorithms, which gives reason to hope for their successful application for choosing the optimum number of parameters.

The authors express appreciation to G. G. Polyakov for useful consultations.

BIBLIOGRAPHY

1. Bongard, M. M., "Modeling of the Recognition Process on a Digital Computer," BIOFIZIKA (Biophysics), No 2, 1961.

2. Vapnik, V. N. and Chervonenkis, A. Ya., TEORIYA RASPOZNAVANIYA OBRAZOV (Theory of Image Recognition), Moscow, Nauka, 1974.

3. Duda, R., Khart, P., RASPOZNAVANIYE OBRAZOV I ANALIZ STSEN (Image Recognition and Scene Analysis), Moscow, Mir, 1976.

4. Polyakov, G. G. and Romanov, L. N., "Choice of Parameters in Regression Models Using Running Control," TRUDY ZAP.-SIB. RNIGMI (Transactions of the West Siberian Regional Scientific Research Hydrometeorological Institute), No 46, 1979.

5. Polyakov, G. G. and Romanov, L. N., "Separation of Classes of Situations Using Ordered Sorting," TRUDY ZAP.-SIB. RNIGMI, No 41, 1978.

6. Polyakov, G. G. and Romanov, L. N., "Minimizing the Number of Errors in Linear Alternative Models," TRUDY ZAP.-SIB. RNIGMI, No 48, 1980.

7. Fadeyev, D. K. and Fadeyeva, V. N., VYCHISLITEL'NYYE METODY LINEYNOY ALGEBRY (Computation Methods in Linear Algebra), Moscow, Fizmatgiz, 1963.

UDC 551.511.6

DETERMINATION OF TURBULENT DIFFUSION COEFFICIENTS

Moscow METEOROLOGIYA I GIDROLOGIYA in Russian No 3, Mar 81 pp 46-53

[Article by V. P. Gavrilov, candidate of physical and mathematical sciences, Institute of Experimental Meteorology, manuscript received 17 Jun 80]

[Text]

Abstract: A study was made of the dispersion of a passive impurity from an instantaneous point source in stationary and horizontally uniform surface and boundary layers of the atmosphere with a neutral stratification. Using the moments method, on the basis of the semiempirical diffusion equation expressions are derived for the coordinates of the center of gravity of the cloud of impurity and its dispersions. With the availability of experimental information on the diffusion characteristics of the cloud of impurity the derived analytical expressions make it possible to determine the turbulent diffusion coefficients.

Many studies have been devoted to an examination of the scattering of an impurity in the lower layers of the atmosphere. The diffusion of an impurity in the surface layer of the atmosphere (SLA) over an even and uniform underlying surface has been investigated relatively well experimentally and theoretically. The theoretical models of description of scattering of an impurity in the SLA for the most part are based on a semiempirical transfer equation of a parabolic type

$$\frac{\partial q}{\partial t} + v_i \frac{\partial q}{\partial x_i} = \frac{\partial}{\partial x_i}\left(K_{ij} \frac{\partial q}{\partial x_j}\right). \quad (1)$$

where q is the mean concentration of the impurity, v_i are the components of mean wind velocity, K_{ij} is the tensor of the turbulent diffusion coefficients.

The concepts of the dimensionality and similarity methods are also useful in an examination of the dispersion of an impurity in the SLA. For example, the use of the hypothesis of similarity of the Lagrangian statistical characteristics in the theory of diffusion in the SLA leads to a determination of the dispersions of the cloud of impurity created by an instantaneous point source. In addition, from these very same considerations it is possible to obtain the surface distribution of the concentration of impurity from a linear stationary source. But for an adequate description of the process of transport of an impurity this approach, like

others, is inadequate. Accordingly, it is most common to use the semiempirical diffusion equation (1), which "leads" to a detailed description of the field of concentration and use is made of additional information obtained by other methods, especially the methods of similarity theory. In this equation the wind velocity profile is rather reliably determined, but the type of diffusion coefficients remains unknown and their functional dependence is stipulated on the basis of different considerations of experimental or model representation. The problem of the choice of the type of coefficients in equation (1) constitutes a considerable, if not the principal difficulty in this method for describing the dispersion of an impurity. Dimensionality considerations simplify the problem — they fix the functional form of the diffusion coefficients but introduce a whole series of universal constants, whose values are unknown.

The dispersion of the impurity in the atmospheric boundary layer (ABL) has been investigated to a far lesser degree. The simplest ABL models as a rule "determine" the wind profile and the vertical coefficient of turbulent viscosity, which is identified with the vertical coefficient of turbulent diffusion. We do not obtain any information on the horizontal diffusion coefficients from these ABL models and therefore it is necessary to have recourse to additional hypotheses or models of horizontal scattering.

Due to the difficulty in choosing the turbulent diffusion coefficients during the scattering of an impurity in the atmosphere it is desirable to use experimental information on the diffusion characteristics of the cloud of impurity for ascertaining the type of diffusion coefficients or for determining the values of the constants determining a stipulated functional type of transfer coefficients. In this article we analyze one of the possible methods for determining the turbulent diffusion coefficients from the diffusion characteristics.

Scattering of Impurity in SLA

Now we will examine in detail the application of this method in the example of scattering of an impurity in the neutrally stratified SLA. Dimensionality considerations for the SLA lead to the following relationships for the diffusion coefficients [2]

$$K_{ij}(z, t) = \varkappa_{ij}^{(m)} u_*^{1+m} z^{1-m} t^m, \qquad (2)$$

where u_* is dynamic velocity, $\varkappa_{ij}^{(m)}$ are universal constants.

By virtue of symmetry of the flow relative to the direction of mean velocity the coefficients K_{12}, K_{21}, K_{23}, K_{32} are equal to zero. Accordingly, the transfer equation (1) for the SLA has the following form:

$$\partial q/\partial t + u(z)\partial q/\partial x = K_{11}\partial^2 q/\partial x^2 + K_{22}\partial^2 q/\partial y^2 + \partial/\partial z\,(K_{33}\partial q/\partial z + K_{31}\partial q/\partial x) + K_{13}\partial^2 q/\partial x\,\partial z. \qquad (3)$$

If the turbulent diffusion coefficients are considered turbulence characteristics, they must be represented in the form

$$K_{ij}(z) = \nu k_{ij}(zu_*/\nu), \tag{4}$$

where k_{ij} are universal functions, ν is the molecular viscosity coefficient.

Within the limits of the logarithmic region of flow, that is, with $zu_*/\nu \gg 1$, the dependence on ν must disappear, that is

$$K_{ij}(z) = \varkappa_{ij} u_* z. \tag{5}$$

The value of the constant $\varkappa_{33}$, determining vertical turbulent transfer, is best known. This constant is determined through the turbulent Prandtl number Pr_t and the Karman constant $\varkappa$ ($\varkappa_{33} = \varkappa/Pr_t$) and according to data from a large number of laboratory measurements [11], $\varkappa_{33} \simeq 0.45$-$0.47$. Among the other constants only the value of the constant $\varkappa_{13}$ can be considered at least approximately (with an accuracy to 15%) known [3, 12]: -- $x_{13} = 3.5$. This value was obtained from measurements of the horizontal turbulent flow of heat $S_x = \overline{u'T'}$ and the mean temperature profile $\overline{T}(z)$ ($K_{13} = -S_x/\partial\overline{T}/\partial z$).

Yamamoto and Shimanuki in [13] attempted to evaluate the transverse diffusion coefficient by a comparison of the empirical data on diffusion from point sources and the results of numerical solution of the stationary diffusion equation

$$u(z)\frac{\partial q}{\partial x} = \frac{\partial}{\partial y}\left(K_{22}\frac{\partial q}{\partial y}\right) + \frac{\partial}{\partial z}\left(K_{33}\frac{\partial q}{\partial z}\right) \tag{6}$$

with K_{22} values containing an undetermined parameter: $K_{22}(z) = \varkappa u_* z \alpha(\zeta_0)$, where $\alpha(\zeta_0)$ is an unknown function dependent on stratification. Then for the purpose of checking the adopted assumption concerning $K_{22}(z)$ the determined $\alpha(\zeta_0)$ values were used in theoretical computations of the distribution of the concentration along the y-axis with some x and z values, the results of which were again compared with the experimental data. For a surface concentration along the axis of the cloud of impurity with a neutral stratification and $K_{22} = 13\varkappa u_* z$ (that is, with $\frac{\varkappa_{22}}{\varkappa_{32}}$) the expression $q \sim x^{-1.78}$, agreeing well with the experimental data.

It is difficult to determine the value of the constant $\varkappa_{11}$ against the background of longitudinal advection. Indirect evaluations of the K_{11} value on the basis of laboratory measurements of the characteristics of turbulence in the boundary layer [8] lead to a value $\varkappa_{11} \sim 4.5\varkappa_{33}$. In addition, there are evaluations of $\varkappa_{11}$ based on semiempirical hypotheses [6], leading to values $\varkappa_{11}/\varkappa_{33} \sim 30$-$40$.

Data on the $\varkappa_{31}$ values are entirely lacking. There are a number of expressions derived on the basis of approximate physical or qualitative considerations of the type

$$\varkappa_{13} = \varkappa_{31}, \quad \varkappa_{31} = \frac{1}{2}\varkappa_{13}, \quad \varkappa_{31} = \frac{1}{3}\varkappa_{11}. \tag{7}$$

Thus, from a brief review of the estimated values of the constants $\varkappa_{ij}$ it follows that evaluations of these constants were obtained from a broad spectrum of empirical and semiempirical assumptions sometimes having an indirect relationship to the process of scattering of an impurity in the SLA. The values of some constants are

virtually unknown; others are not very reliable. Accordingly, it is entirely reasonable to derive expressions determining the behavior of some characteristics of a diffusing cloud of impurity, which are relatively simply and reliably determined experimentally. The constants $\varkappa_{ij}$ enter into the analytical expressions for these characteristics. Thus, having experimental information on these diffusion characteristics it is possible to obtain evaluations of the $\varkappa_{ij}$ constants.

The behavior of the coordinates of the center of gravity of the cloud of impurity from an instantaneous point source of impurity is determined by the following expressions [4, 5]:

$$X(t) = \frac{u_* t}{\varkappa}\left(\ln \frac{\varkappa_{11} u_* t}{z_0} - \varkappa\varkappa_{13} - 1 - \gamma\right). \tag{8}$$

$$Z(t) = \varkappa_{33} u_* t, \tag{9}$$

where $\gamma = -\int_0^\infty e^{-x} \ln x \, dx \approx 0.58$ is the Euler constant.

Thus, from the behavior of the trajectory of the center of gravity of the cloud of impurity it is possible to determine the values of the $\varkappa_{33}$ and $\varkappa_{13}$ constants. The $\varkappa_{33}$ value has been determined precisely in this way in laboratory measurements.

The longitudinal and vertical dispersions $\sum_{11}^2(t)$ and $\sum_{33}^2(t)$, obtained from solution of equation (3), have the form [4, 7]

$$\Sigma_{11}^2(t) = \left[\left(\frac{\pi^2}{6} - 1\right)\frac{1}{\varkappa^2} + \varkappa_{11}\varkappa_{33} - \frac{\varkappa_{31} + \varkappa_{13}}{2\varkappa}\right] u_*^2 t^2, \tag{10}$$

$$\Sigma_{33}^2(t) = \varkappa_{33}^2 u_*^2 t^2. \tag{11}$$

Using the moments method, we similarly determine

$$\Sigma_{22}^2(t) = \varkappa_{22}\varkappa_{33} u_*^2 t^2. \tag{12}$$

$$\Sigma_{13}^2(t) = \varkappa_{33}\left(\frac{1}{\varkappa} + \frac{\varkappa_{31} + \varkappa_{13}}{2}\right) u_*^2 t^2. \tag{13}$$

Thus, expressions (8)-(13) determine the behavior of the center of gravity of a diffusing cloud of impurity and its dispersions, by measuring which it is possible to determine the constants $\varkappa_{ij}$ without recourse to any additional considerations. For example, in the case of a diagonal tensor of the diffusion coefficients, that is, when $\varkappa_{13} = \varkappa_{31} = 0$, we obtain

$$\varkappa_{11} = \frac{\Sigma_{11}^2}{\Sigma_{33} u_* t} - \left(\frac{\pi^2}{6} - 1\right)\frac{1}{\varkappa^2}\frac{u_* t}{\Sigma_{33}} = \frac{\Sigma_{11}^2}{Z(t) u_* t} - \left(\frac{\pi^2}{6} - 1\right)\frac{1}{\varkappa^2}\frac{u_* t}{Z(t)}, \tag{14}$$

$$\varkappa_{22} = \frac{\Sigma_{22}^2}{u_* t \Sigma_{33}}, \tag{15}$$

$$\varkappa_{33} = \frac{\Sigma_{33}}{u_* t} = \frac{Z(t)}{u_*(t)}. \tag{16}$$

Obtaining the estimated values of the constants $\varkappa_{ij}$ from diffusion measurements, it is possible to use them for computing the concentration field in the SLA by use of equation (3). A comparison of this field with the experimental distribution makes it possible to evaluate the reliability of the initial hypothesis (5) on the functional type of the turbulent diffusion coefficients. In addition, the once-determined values $\varkappa_{ij}$ can later be used also in evaluating the diffusion characteristics of the cloud of impurity determined by expressions (8)-(13).

It must be noted that theoretical methods for determining the universal constants and functions describing turbulent diffusion of an impurity in the SLA rely on different nonrigorous semiempirical hypotheses and therefore are not precise. Accordingly, it is useful to carry out a comparison of the conclusions from different semiempirical hypotheses. The comparison makes it possible to clarify in what cases these conclusions vary little with a change in the initial hypotheses and therefore can be considered entirely reliable and in what cases they are characterized by a considerable scatter and accordingly indicate that the degree of accuracy of the used hypotheses must be checked using material from additional experimental measurements.

A similar examination of scattering of an impurity in the SLA on the basis of equation (8) with diffusion coefficients $K_{ij} = \varkappa'_{ij} u_*^2 t$, dependent only on time, leads to the following system of equations determining the behavior of the trajectory of the center of gravity of a diffusing cloud of impurity and its dispersions:

$$X(t) = \left[\frac{1}{\varkappa} \left(\ln \sqrt{\frac{\varkappa'_{33}}{2}} \frac{u_* t}{z_0} - 1 - \frac{1}{2} \right) + \sqrt{\frac{2}{\pi \varkappa'_{33}}} (\varkappa'_{13} + \varkappa'_{31}) \right] u_* t, \tag{17}$$

$$Z(t) = \sqrt{\frac{2\varkappa_{33}}{\pi}} u_* t, \tag{18}$$

$$\Sigma_{11}^2(t) = \left[\varkappa'_{11} + \frac{1}{\varkappa^2} \left(\frac{\pi^2}{8} + 1 \right) + \frac{2 \ln 2}{\sqrt{\pi \varkappa'_{33}}} \frac{(\varkappa'_{13} + \varkappa'_{31})}{\varkappa} - \frac{2}{\pi} \frac{(\varkappa'_{13} + \varkappa'_{31})^2}{\varkappa'_{13}} \right] u_*^2 t^2, \tag{19}$$

$$\Sigma_{22}^2(t) = \varkappa'_{22} u_*^2 t^2, \tag{20}$$

$$\Sigma_{33}^2(t) = \left(1 - \frac{2}{\pi} \right) \varkappa'_{33} u_*^2 t^2, \tag{21}$$

$$\Sigma_{13}^2(t) = \frac{1}{2} \left[\frac{1}{\varkappa} \sqrt{\frac{\varkappa'_{33}}{2\pi}} \ln (4e) + \left(1 - \frac{2}{\pi} \right) (\varkappa'_{13} + \varkappa'_{31}) \right] u_*^2 t^2. \tag{22}$$

If the values of the constants $\varkappa_{ij}$ and $\varkappa^0_{ij}$ are determined from one and the same mass of experimental data it is possible to draw some conclusions concerning the functional dependence of K_{ij}. In actuality, by the process of finding the distribution of the concentration with diffusion coefficients dependent only on z or

only on t, and making a comparison with the experimental distribution of the concentration, in this case proceeding on the basis of the best correspondence with the experimental data, it is possible to draw conclusions concerning the reliability of the initial hypotheses concerning the form of K_{ij}. In a case when it is found that different hypotheses on the functional form of the coefficients of turbulent diffusion lead to virtually identical results, by comparing the corresponding expressions for the dispersions we find the correlation between the constants $\varkappa_{ij}$ and $\varkappa^0_{ij}$; in particular, for the case of a diagonal tensor of the diffusion coefficients we have

$$\varkappa'_{11} = \varkappa_{11}\varkappa_{33} + \frac{1}{\varkappa^2}\left(\frac{\pi^2}{24} - 2\right), \tag{23}$$

$$\varkappa'_{22} = \varkappa_{22}\varkappa_{33}, \tag{24}$$

$$\varkappa'_{33} = \frac{\pi}{\pi - 2}\varkappa^2_{33}. \tag{25}$$

Thus, the derived systems of expressions (8)-(13) and (17)-(22), describing the behavior of the coordinates of the center of gravity of a diffusing cloud of impurity and its dispersions, make it possible to express through these characteristics the constants entering into the determination of the diffusion coefficients (2), to find the correlation between constants of a different model representation of the diffusion coefficients and with the availability of information on the field of concentration or other more complex characteristics of the cloud of impurity to evaluate the reliability of the initial hypotheses on the diffusion coefficients. This method can be used successfully in the case of scattering of an impurity in the SLA with a stratification different from neutral.

Scattering of an Impurity in a Horizontally Uniform Stationary ABL

The method described above in the example of diffusion of an impurity in the SLA is especially useful in an analysis of scattering of an impurity in the ABL since, having experimental information on the behavior of the dispersions and the measured characteristics of the ABL it is possible to obtain evaluations of the horizontal coefficients of turbulent diffusion which in contrast to the vertical coefficient are not determined by the ABL model. In actuality, the system of equations for the first two moments $q_0(z, t)$, $q_1^m(z, t)$, $q_2^m(z,t)$ $(m = 1, 2)$, through which the behavior of the coordinates of the center of gravity of the cloud of impurity and its dispersions is determined, has the following form:

$$\frac{\partial q_0}{\partial t} - \frac{\partial}{\partial z}\left(K_{33}\frac{\partial q_0}{\partial z}\right) = 0, \tag{26}$$

$$\frac{\partial q_1^m}{\partial t} - \frac{\partial}{\partial z}\left(K_{33}\frac{\partial q_1^m}{\partial z}\right) = v_m(z)\, q_0(z, t), \tag{27}$$

$$\frac{\partial q_2^m}{\partial t} - \frac{\partial}{\partial z}\left(K_{33}\frac{\partial q_2^m}{\partial z}\right) = 2K_{mm}(t)\, q_0(z, t) + 2v_m(z)\, q_1^m(z, t). \tag{28}$$

In the derivation of the equations in the system it was assumed that the components of the wind profile v_m are dependent only on z, the tensor of the diffusion coefficients has a diagonal form and $v_m(z)$ and $K_{33}(z)$ are determined from the ABL model, and K_{11} and K_{22} will be considered dependent only on diffusion time. Such an assumption for the horizontal diffusion coefficients is entirely reasonable

(for example, see [10], which gives the experimental dependences of dispersions on time for different meteorological conditions).

Integrating equation (28) for z, we obtain an equation for the dispersion $\sum^2_{mm}(t)$

$$\frac{1}{2}\frac{d\sum^2_{mm}}{dt} = K_{mm}(t) + \int_0^\infty v_m(z)\, q_1^m(z,\ t)\, dz - \frac{1}{2}\frac{d}{dt}(X_m^2), \tag{29}$$

where $X_m(t)$ are the coordinates of the center of gravity of the cloud of impurity. Hence we obtain an evaluation for the horizontal coefficients of turbulent diffusion in the ABL

$$K_{mm}(t) = \frac{1}{2}\frac{d\sum^2_{mm}}{dt} - \int_0^\infty v_m(z)\, q_1^m(z,\ t)\, dz + \frac{q_1^m(t)}{q_0}\frac{d}{dt}\left(\frac{q_1^m}{q_0}\right), \tag{30}$$

where $q_0(z, t)$ and $q_1^m(z, t)$ are determined from solution of equations (26) and (27) and the temporal behavior of the dispersions is determined from the experimental data.

Several attempts were made to evaluate the transverse diffusion coefficient K_{22} (for example, see [1], which gives the latest, most complete review of the results of experimental investigations of transverse diffusion in the ABL). These evaluations were based on a formula derived by Csanady [9] and describing the behavior of the transverse dispersion of the surface field of concentration from an instantaneous point surface source

$$\sigma_{22}^2(t) = 2K_{22}t + \frac{G^2}{f^2}F, \tag{31}$$

where G is the velocity of the geostrophic wind, f is the Coriolis parameter, and the function F describes the influence of the shear effect on the scattering process (that is, the effect of interaction between the wind profile and vertical transfer). But it must be taken into account that formula (31) was derived in an examination of scattering of the impurity in the Ekman ABL with constant (vertical and horizontal) diffusion coefficients. Accordingly, these evaluations of the transverse diffusion coefficient have a preliminary character and at best determine the order of magnitude of K_{22}, since in not one of the experiments used for evaluating K_{22} is there adherence to the conditions for the applicability of formula (31).

The turbulent diffusion coefficients obtained in this study by the considered method make it possible to avoid such incorrectness and henceforth can be used in computing the concentration field on the basis of the semiempirical equation (1). Comparison with the experimental distribution makes it possible to evaluate the reliability of the initial hypothesis that the horizontal diffusion coefficients are functions of time. The use of other model representations and hypotheses on the functional dependence of the horizontal diffusion coefficients and computations of the field of concentration on the basis of the evaluations K_{11} and K_{22} obtained for this type of coefficients, and also comparison with the measured distribution of the field of concentration make it possible to make an optimum selection of a model of scattering of an impurity in the ABL.

BIBLIOGRAPHY

1. Garger, Ye. K., "Transverse Diffusion in the Atmospheric Boundary Layer," TRUDY IEM (Transactions of the Institute of Experimental Meteorology), No 15(60), 1977.

2. Yaglom, A. M., "Equations With Time-Dependent Coefficients Describing Diffusion in the Surface Layer of the Atmosphere," IZV. AN SSSR: FIZIKA ATMOSFERY I OKEANA (News of the USSR Academy of Sciences: Physics of the Atmosphere and Ocean), Vol 11, No 11, 1975.

3. Yaglom, A. M., "Turbulent Diffusion in the Atmospheric Surface Layer," IZV. AN SSSR: FIZIKA ATMOSFERY I OKEANA, Vol 8, No 6, 1972.

4. Yaglom, A. M., "Diffusion of an Impurity From an Instantaneous Point Source in a Turbulent Boundary Layer," TURBULENTNYYE TECHENIYA (Turbulent Currents), Moscow, Nauka, 1974.

5. Batchelor, G. K., "Diffusion From Sources in a Turbulent Boundary Layer," ARCH. MECH. STOSOWANEJ., Vol 16, No 3, 1964.

6. Brutsaert, W., "On the Anisotropy of the Eddy Diffusivity," J. METEOROL. SOC. JAPAN, Vol 48, No 5, 1970.

7. Chatwin, P. C., "The Dispersion of a Puff of Passive Contaminant in the Constant Stress Region," QUART. J. ROY. METEOROL. SOC., Vol 94, No 401, 1968.

8. Corrsin, S., "Limitations of Gradient Transport Models in Random Walks and in Turbulence," ADV. GEOPHYS., Vol 18A, 1974.

9. Csanady, G. T., "Diffusion in an Ekman Layer," J. ATMOS. SCI., Vol 26, No 3, 1969.

10. Hildebrand, P. H., "A Radar Study of Turbulent Diffusion in the Lower Atmosphere," J. APPL. METEOROL., Vol 16, No 5, 1977.

11. Kader, B. A. and Yaglom, A. M., "Heat and Mass Transfer Laws for Fully Turbulent Wall Flows," INT. J. HEAT MASS TRANSFER, Vol 15, No 12, 1972.

UDC 551.(509.58+510.42)

COMPUTATION OF TRANSPORT OF SUBSTANCES CONTAMINATING THE ATMOSPHERE

Moscow METEOROLOGIYA I GIDROLOGIYA in Russian No 3, Mar 81 pp 54-58

[Article by U. Andrash, candidate of economic sciences, and R. Schenk, candidate of technical sciences, Water Management Institute, Berlin, manuscript received 1 Jul 80]

[Text]

Abstract: The article is devoted to a description of a model and computation scheme for computing the transport of atmospheric impurities in the field of a variable wind at country and regional scales. A program for computing the transport of substances contaminating the air has been developed.

A special working group of the Berlin Water Management Institute in the German Democratic Republic has carried out investigations of the transport of substances contaminating the air over great distances. The investigations were formulated in connection with the need for monitoring the transport of harmful substances not only near industries and in cities, but also in individual regions having linear dimensions of thousands of kilometers, including transport across national boundaries.

The authors here present a "fractional steps" method for solution of the three-dimensional equation for the transport of contaminating substances. It is known that the transport of impurities at different spatial and temporal scales (intra-regional, distant, etc.) is described by one and the same differential equation. Only methods for taking into account convective transport, turbulent diffusion, and chemical transformations of the transported substances are different, depending on the scale of transport. Accordingly, the method cited in the article has great universality.

Description of Transport Mechanism

The processes of transport of substances contaminating the air over short, intermediate and great distances can be described by the following equation:

$$\frac{\partial c}{\partial t} + V_x \frac{\partial c}{\partial x} + V_y \frac{\partial c}{\partial y} + V_z \frac{\partial c}{\partial z} = \tag{1}$$

$$= \frac{\partial}{\partial x}\left(K_x \frac{\partial c}{\partial x}\right) + \frac{\partial}{\partial y}\left(K_y \frac{\partial c}{\partial y}\right) + \frac{\partial}{\partial z}\left(K_z \frac{\partial c}{\partial z}\right) + Q,$$

where V_x, V_y, V_z are the wind velocity components, K_x, K_y, K_z are parameters describing turbulent transport, Q characterizes the volume of the emissions and the processes of chemical transformations of impurities.

The modeling of transport using equation (1) is based on the proposition that the impurities are transported by the air medium in which they are scattered and that the change in the velocity of movement of the impurity in comparison with the velocity of the air itself is possible only as a result of turbulent transport.

A description of the influence exerted on the characteristic motion of impurities by partial pressure and different density is possible only by use of multicomponent models. In actual practice it is better to use equation (1), taking into account the factors enumerated above in the parameters describing turbulent diffusion.

The best-known method for solving equation (1) is a description of the process of transfer by a Gaussian distribution. This method is coming into wide use and is a convenient tool for practical workers. However, if in the propagation process for such an impurity there is no symmetry and the vector field of velocities is a function of time, the volume of the computations when using a Gaussian distribution is many times greater than with the direct solution of (1).

The analogy between the processes of transport of momentum, heat and mass makes it possible, in solving equation (1), to use the same numerical methods used in solving problems in hydrodynamics. One of the most effective methods in this case is the Yanenko "fractional steps" method [2] in the form of geometric splitting. On the basis of this method it is possible to propose a difference scheme for the solution of equation (1), set forth in a study by Schenk [3].

We note that the solution (1) is based on meteorological data on the wind at different levels and a semiempirical representation of turbulent transport. According to the empirical expressions, the K_x, K_y, K_z values can be assumed proportional to velocity and distance in the coordinate.

Formulation of Problem

The processes of transport of contaminating substances correspond to the mixed problem for equation (1). With equation (1) taken into account, it is possible to write the following differential equation:

$$\frac{\partial c}{\partial t} + \left(V_x - \frac{\partial K_x}{\partial x}\right)\frac{\partial c}{\partial x} + \left(V_y - \frac{\partial K_y}{\partial y}\right)\frac{\partial c}{\partial y} + \left(V_z - \frac{\partial K_z}{\partial z}\right)\frac{\partial c}{\partial z} = \tag{2}$$
$$= K_x\frac{\partial^2 c}{\partial x^2} + K_y\frac{\partial^2 c}{\partial y^2} + K_z\frac{\partial^2 c}{\partial z^2} + Q.$$

The boundary conditions are stipulated by the equations

$$\frac{\partial c}{\partial n}\Big|_{\text{FR}} = 0, \tag{3}$$
$$\frac{\partial c}{\partial v}\Big|_{\text{OB}} = 0,$$

$$K_y \frac{\partial c}{\partial y} + \beta c = 0 \Big|_B,$$
$$c = 0 \Big|_{OB} \qquad (3)$$

and use the notations:
-- the neglecting of transport at the free boundaries FR;
-- total absorption at the upper boundary of the considered region of propagation;
-- allowance for precipitation and vertical diffusion at the earth's surface.

The initial propagation of the impurity is stipulated by the condition

$$c(x, y, z, t = 0) = 0 \Big|_{1 + FR + B}. \qquad (4)$$

The rate of dry precipitation of the impurity onto the earth's surface is taken into account by the parameter β.

Splitting Scheme

The following splitting scheme can be given for differential equation (2):

$$\frac{1}{4}\frac{\partial c}{\partial t} - Q = 0,$$
$$\frac{1}{4}\frac{\partial c}{\partial t} + \left(V_x - \frac{\partial K_x}{\partial x}\right)\frac{\partial c}{\partial x} - K_x \frac{\partial^2 c}{\partial x^2} = 0, \qquad (5)$$
$$\frac{1}{4}\frac{\partial c}{\partial t} + \left(V_y - \frac{\partial K_y}{\partial y}\right)\frac{\partial c}{\partial y} - K_y \frac{\partial^2 c}{\partial y^2} = 0,$$
$$\frac{1}{4}\frac{\partial c}{\partial t} + \left(V_z - \frac{\partial K_z}{\partial z}\right)\frac{\partial c}{\partial z} - K_z \frac{\partial^2 c}{\partial z^2} = 0.$$

Such a splitting scheme corresponds to geometric splitting. Each equation in the system (5) is solved by the scalar three-point splitting method. The solution of equations (5) gives a full description of the process of transport of impurities.

Determination of Transboundary Flows of Impurity

The introduction of linear sources for determination of transboundary flows of impurities is extremely desirable (2). Having a solution of equation (3), the intensity of the linear source can be determined using the integral

$$MD = \int_{\eta_{i1}}^{\eta_{i+1}} \int_0^H c v_n \, dy \, d\eta, \qquad (6)$$

where v_n is the projection of velocity onto the normal to the surface element $dyd\eta$; the η coordinate is situated on the integration surface bounding the space of propagation of the impurity.

The following expressions are correct for the intensity of the flows across the boundary of the space of propagation of the impurity

$$\begin{aligned} MVD &= \int_{VA} c\,\mathbf{V}_i\, d\,\mathbf{A}_i, \\ MHD &= \int_{HA} c\mathbf{V}_i\, d\,\mathbf{A}_i, \\ MRD &= \int_{RA} c\,\mathbf{V}_i\, d\,\mathbf{A}_i, \\ MLD &= \int_{LA} c\,\mathbf{V}_i\, d\,\mathbf{A}_i, \\ MUD &= \int_{BA} K_y \frac{\partial c}{\partial y_i}\Big|_B d\,\mathbf{A}_i. \end{aligned} \tag{7}$$

The subscript i means that y, V and A are vectors. Using linear sources as functions of η it is easy to determine the interregional flows.

Computation of Reliable Mean Values

In order to monitor the level of concentration of substances contaminating the air, including the prevention of dangerous situations, in principle it is necessary to know the fields of concentrations at any stipulated moment in time. However, in many cases it is possible to limit ourselves to the mean values for the sufficiently long time period T, for example, for a year. Solving equation (2) for the meteorological conditions prevailing during the period T and computing the integral

$$\overline{M} = \frac{1}{T}\int_0^T M\,dT, \tag{8}$$

we obtain the reliable mean value of the transboundary flows.

Similarly it is possible to determine the mean concentration in the propagation region

$$\overline{c}(x, y, z) = \frac{1}{T}\int_0^T c\,dt. \tag{9}$$

These mean values are of considerable importance for many practical problems. The choice of the time interval T is determined by the nature of the problem.

Use of Computers

The splitting scheme used makes it possible to employ modular programming. In particular, the program was developed for a BESM-6 electronic computer. The program makes it possible to solve the equations in a three-dimensional grid with 12,750 points of intersection; it occupies 20 000 machine words in the operational memory so that there is a reserve for broadening the propagation space. Ninety seconds of computer time is required for one iteration in the mentioned grid. Thus,

computations of the transport of an impurity over a period of 24 hours requires 72 minutes of computer time (time interval of 30 minutes). Using a curve plotter the isolines of concentrations are constructed in a regular square grid. The transboundary flows of impurities are printed out in the form of a table (in kg/sec).

The program was used successfully in computing transport over short, intermediate and great distances. In particular, the contamination of a residential quarters by the emissions of an industrial enterprise situated near this microregion was computed. Computations were made of the propagation of contaminating substances over large industrial regions, as well as over the entire territory of the GDR. Here, in addition to the fields of concentrations, it was possible to establish the magnitude of the flows between regions and across the boundaries of the country for specific meteorological conditions.

Improvement of Model and Algorithm

The results indicate the fundamental applicability of the developed model and solution method. The following refinements of the model and allowance for additional information are planned for a more adequate reflection of the true pattern:
-- transformation to curvilinear coordinates;
-- allowance for relief of the underlying surface;
-- allowance for additional meteorological parameters (changes in height of the mixing layer in space and time, zones of precipitation and its intensity, and also characteristics of the boundary layer);
-- determination of the rate of dry precipitation of impurities as a function of space and time (settling on water surfaces, snow, forested areas, etc.);
-- more precise modeling of specific processes of chemical transformations of an impurity, chemical and physical processes accompanying its washing out;
-- use of aircraft measurements for determining the vertical distribution of an impurity.

BIBLIOGRAPHY

1. Izrael, Lysak, Nazarov, Pressman and Rjaboshapko, "On National Observational System and Evaluation of the Long-Range Transmission of Pollutants," INTERNATIONAL SYMPOSIUM ON GLOBAL INTEGRATED MONITORING OF ENVIRONMENTAL POLLUTION, Riga, December 1978.

2. Janenko, DIE ZWISCHENSCHRITTMETHODE ZUR LOSUNG MEHRDIMENSIONALER PROBLEME DER MATHEMATISCHEN PHYSIK, Springer Verlag, Berlin, Gottingen, Heidelberg, 1969.

3. Schenk, NUMERISCHE BEHANDLUNG INSTATIONARER TRANSPORTVORGANGE, TH, "C. Schorlemmer" Leuna Merseburg, 1978.

4. Schenk, DREIDIMENSIONALER INSTATIONARER WARMETRANSPORT IN DURCHSTROMTEN ROHREN, ZAMW, 1977.

5. Schenk/Seidel, "Numerische Simulation von Kurz- und Lang-strecken transporten," BERICHT DER AG SCHADSTOFFAUSBREITUNG BEIM IfW, Berlin, 1978.

6. Schenk, "Instationarer, dreidimensionaler Schadstofftransport in freier Atmosphare," LUFT- UND KALTETECHNIK, 1978/1 UND ANWENDUNG DER DIGITALGRAFIK..., 1978/2.

UDC 551.(466+521+55)

TWO-FREQUENCY MICROWAVE RADIOMETRIC METHOD FOR DETERMINING WIND VELOCITY FROM A SATELLITE

Moscow METEOROLOGIYA I GIDROLOGIYA in Russian No 3, Mar 81 pp 59-67

[Article by L. M. Martsinkevich, candidate of physical and mathematical sciences, State Scientific Research Center for the Study of Natural Resources, manuscript received 26 Jun 80]

[Text]

Abstract: The article is devoted to a determination of wind velocity and wave height (with an infinite or known fetch length) from the "wave-covered sea surface - atmosphere" system thermal radioemission measured from a satellite. The author gives examples of computations of wind velocity using data from aircraft microwave measurements made during the period of the Soviet-American "SAMEX-76" experiment in the Pacific Ocean.

Different aspects of the influence of sea waves on the thermal radioemission of the sea surface have already been studied for 15 years by many scientists in our country and abroad. Most of this work has been based on the use of data from surface and aircraft microwave measurements. The authors of [1] and [5] came closest to an interpretation of the results of satellite measurements of the microwave radiation of the wave-covered sea surface.

This article is devoted to a solution of the inverse problem: determination of wind velocity and wave height (with an infinite or known fetch length) on the basis of the thermal radioemission of the "wave-covered sea surface - atmosphere" system at two wavelengths as measured from a satellite.

The fundamental premise ensuring the possibility of solving the problem is a theoretically and experimentally established law: when sighting at definite angles (close to the nadir or equal to 40-50°) the contribution of the geometric component of waves to thermal radioemission can be neglected and it is necessary to consider only the contribution of the foam cover forming with the destruction of waves and related to the wind velocity which forms the waves.

We will write a solution for the atmospheric radiation transfer equation:

$$T_{\text{a}} = \varepsilon_{\text{сум}} Te^{-\int_0^H \gamma\, dz} + \int_0^H T(z)\,\gamma\, e^{-\int_z^H \gamma\, dz} dz + (1 - \varepsilon_{\text{сум}}) \times$$

[СУМ = tot(al)]

$$\times \left(\int_0^\infty T(z)\,\gamma\, e^{-\int_0^z \gamma\, dz} dz \right) e^{-\int_0^H \gamma\, dz}, \qquad (1)$$

where T is the temperature of the sea surface, T(z) is air temperature, γ is the coefficient of attenuation of radiation in atmospheric gases, H is the altitude at which the radiation detector is situated, z is the vertical coordinate.

Modeling the sea surface by a smooth water surface, the ν-th part of which is covered by foam, we write the total emissivity of such a surface ε_{tot} in the form of the sum

$$\varepsilon_{\text{tot}} = \varepsilon(1 - \nu) + \varepsilon_{\text{foam}}\,\nu, \qquad (2)$$

where ε is the coefficient of emission of the sea surface free of foam, $\varepsilon_{\text{foam}}$ is the coefficient of emission of a sea surface completely covered by foam.

For brevity introducing the notations

$$T_1 = Te^{-\int_0^H \gamma\, dz}; \quad T_2 = \int_0^H T(z)\,\gamma\, e^{-\int_z^H \gamma\, dz} dz; \qquad (3)$$

$$T_3 = \left(\int_0^\infty T(z)\,\gamma\, e^{-\int_0^z \gamma\, dz} dz \right) e^{-\int_0^H \gamma\, dz}$$

and adhering to the calculations made in [4], we write

$$T_{\text{br}} - T_2 - T_3 - \varepsilon(T_1 - T_3) = \nu(\varepsilon_{\text{foam}} - \varepsilon)(T_1 - T_3), \qquad (4)$$

where T_{br} is the radiobrightness temperature measured from a satellite.

The expression on the right-hand side of the equation represents the increment of radiobrightness temperature of the sea surface, the ν-th part of which is covered by foam, relative to the radiobrightness temperature of a smooth, foam-free surface (radiobrightness contribution of foam).

D. T. Matveyev, on the basis of data from the "Cosmos-243" satellite, supplemented by American aircraft data and with the use of a dynamic model of foam, approximated the radiobrightness contribution of foam by a dependence on wind velocity with measurements at the nadir [6]:

$$\Delta T_f = 3 \cdot 10^{-4} T \lambda^{-0.5} (V-3)^2 \exp[-a(V-10)], \qquad (5)$$

where λ is the wave length, in cm, V is wind velocity in m/sec at a height of 20 m, a = 0 when $V<10$ m/sec and a = 0.032 when $V\geqslant 10$ m/sec.

This approximation agrees well with data from experimental observations in the range of wind velocities from 10 to 30 m/sec; roughness effects can exert a considerable influence when $V<10$ m/sec.

Writing equations (4) and (5) for the increment of the emission coefficient $\Delta\varepsilon$ and equating their right-hand sides, we obtain

[Я = br]
$$\frac{T_2-T_2-T_3-\varepsilon(T_1-T_3)}{T_1-T_3}=3\cdot10^{-4}\lambda^{-0.5}(V-3)^2\exp|-a(V-10)|. \qquad (6)$$

For solving a system of two such equations at two wavelengths it is necessary to introduce additional equations relating to one another the components of the solution for the radiation transfer equation, taking atmospheric radiation into account. Due to the impossibility of establishing analytical dependences, here it was necessary to go the way of finding the empirical relationships.

In order to investigate the atmospheric components of solution of the radiation transfer equation and establish the relationships between them we prepared a program for an electronic computer and carried out computations of atmospheric thermal radioemission from the sea surface to the upper boundary of the atmosphere with the use of radiosonde data during the period of the Soviet-American experiment "SAMEX-76" in the Pacific Ocean. An altitude 16 km was used in the computations as the upper boundary of the atmosphere; above this level thermal radioemission can be neglected.

The computations were made by the method described in [3]. In the computations an allowance was made for the absorption of radiation in oxygen, water vapor and droplet-liquid clouds; cases with precipitation were not considered.

An analysis was made of the characteristic emission of the atmospheric layer at different wavelengths (from 0.8 to 3.2 cm) between the sea surface and the radiation detector T_2, which can arbitrarily be called "radiation upward" (the second term in the solution of the radiation transfer equation); the radiation flux from the entire atmosphere, which can be called "radiation downward"; attenuation of atmospheric radiation.

An analysis of the results of computations indicated that there are some rather stable empirical relationships between the mentioned components of radiation at the upper boundary of the atmosphere.

Thus, the atmospheric radiation fluxes upward and downward differ from one another usually by not more than 2%. If we write the relationship between atmospheric radition upward T_2 and its radiation downward $T\downarrow$ in the form

$$T\downarrow=cT_2, \qquad (7)$$

the c coefficient is equal to unity with the third significant digit after the dot. This coefficient is dependent on frequency and the angle of sighting and for measurements at the nadir is determined using the following expressions:

for a wavelength 0.8 cm

$$T\downarrow = 1{,}0037 \pm 0{,}0017\ T_2; \tag{8}$$

for a wavelength 1.6 cm

$$T\downarrow = 1{,}0012 \pm 0{,}0012\ T_2. \tag{9}$$

The indicated scatter of $T\downarrow$ values with their substitution into the solution of the transfer equation leads to insignificant errors in the T_{br} values, amounting to tenths of a Kelvin.

From the physical point of view there is obviously a correlation between the characteristic radiation of the atmosphere T_2 and the integral attenuation of radiation in the atmosphere exp $(-\tau)$. There are indications of the existence of this relationship in [2, 3]. The dependence was sought in the form

$$\exp(-\tau) = 1 - b\ T_2, \tag{10}$$

where $\tau = \int_0^H \gamma dz$ is the integral coefficient of attenuation of radiation in atmospheric gases and the b values for all frequencies in accordance with the computations fall in the range 0.0036-0.0038.

This relationship has a very weak frequency and angular variation; with sighting at angles from 0 to 40-45° the latter can be virtually neglected.

For measurements at the nadir using the indicated group of materials we found the following values of the b coefficient:

for a wavelength 0.8 cm

$$b = 0{,}00371 \pm 0{,}00010; \tag{11}$$

for a wavelength 1.6 cm

$$b = 0{,}00369 \pm 0{,}00009. \tag{12}$$

An analysis of data from computations of thermal radioemission of the entire atmosphere to its upper boundary for the regions of the "SAMEX-76" polygons indicated that there is a rather stable frequency dependence for characteristic atmospheric radiation. It is very difficult to describe analytically; however, if we exclude from consideration a sufficiently narrow frequency band near the channel 1.35 cm (where the radiation is unambiguously related to the radiation in the adjacent channels) it is possible to find a rather stable coefficient relating the T_2 values in fixed pairs of channels in the range from 0.8 cm to 3.2 cm. In other words, it can be written approximately that

$$T_{2_2} = k T_{2_1}, \tag{13}$$

where $\lambda_2 > \lambda_1$, k is a dimensionless coefficient less than unity. For the pair of wavelengths 0.8 cm and 1.6 cm k is equal to 0.402, for the pair of wavelengths 1.6 cm and 3.2 cm k is equal to 0.255. Here the k coefficient is identical for all sighting angles in the range 0-45°.

The derived expressions were checked on the basis of independent computations of thermal radioemission of the atmosphere using radiosonde data (130 soundings) from weather ships in the North Atlantic (1965-1968). The results of the computations were furnished us through the courtesy of Ye. P. Dombkovskaya and V. V. Ozerkina. Checking indicated a good agreement of atmospheric radiobrightness temperatures at a wavelength of 1.6 cm, computed using radiosonde data and computed from the temperature value at a wavelength of 0.8 cm in accordance with (13).

It was found that the relative error in determining T_2 (1.6) on the basis of stipulated T_2 (0.8) in 40% of the cases is less than 5%, in 74% of the cases is less than 10%, in 90% of the cases is less than 15% and in 98% of the cases is less than 20%.

Checking of dependence (13) for pairs of more long-wave channels indicated that the relative error in determining T_2 on the average increases somewhat, but the absolute error is small. For example, whereas for the pair of channels 1.6 cm-3.2 cm according to data from weather ship B the mean relative error is 15.7%, the mean absolute error is equal to only 1.16 K, which falls within the limits of accuracy of modern radiometric instrumentation. According to data for ship L, for which the relative error for this pair of channels was small, the absolute error was only 0.38 K.

Thus, expression (13) can be used in computing characteristic atmospheric radioemission in one of the stipulated channels on the basis of the known radiation in the other channel in the range of wavelengths from 0.8 cm to 3.2 cm, with the exception of the region near the channel 1.35 cm.

Checking of expression (10) using this same independent material indicated that the values of the b coefficient do not fall beyond the limits of the already mentioned values.

It goes without saying that the derived expressions require refinement. However, the good correspondence between the results of computations for the two groups of independent materials ("SAMEX-76" expedition and the weather ships) indicated a relative stability of these relationships and the fundamental possibility of their use in global problems. It is entirely reasonable to assume that variations of the coefficients in these expressions will have a "regime" character and a rigorous geographical localization; accordingly, it is desirable to analyze the statistical material in sea polygons.

Taking expressions (7), (10), (13) into account, the components for the transfer equation T_1 and T_2, determined by formulas (3), for the stipulated pair of wavelengths λ_1 and λ_2 (here $\lambda_2 > \lambda_1$) can be written in the following way:

$$T_{1_{\lambda_1}} = T\left(1 - b_1 T_{2_{\lambda_1}}\right); \tag{14}$$

$$T_{1_{\lambda_2}} = T\left(1 - b_2 k T_{2_{\lambda_1}}\right); \tag{15}$$

$$T_{3_{\lambda_1}} = T_{2_{\lambda_1}} c_1\left(1 - b_1 T_{2_{\lambda_1}}\right); \tag{16}$$

$$T_{3_{\lambda_2}} = T_{2_{\lambda_2}} c_2\left(1 - b_2 k T_{2_{\lambda_1}}\right), \tag{17}$$

where the subscripts 1 and 2 correspond to the wavelengths λ_1 and λ_2.

The system of two equations of the type (6) for two wavelengths after the substitution of expressions (14)-(17) into them, is written in the following way

$$\frac{T_{R_{\lambda_1}} - \varepsilon_{\lambda_1} T - T_{2_{\lambda_1}}\left[1 - \varepsilon_{\lambda_1} T b_1 + c_1\left(1 - \varepsilon_{\lambda_1}\right)\right] + T_{2_{\lambda_1}}^2 c_1 b_1\left(1 - \varepsilon_{\lambda_1}\right)}{T - T_{2_{\lambda_1}}\left(T b_1 + c_1\right) + T_{2_{\lambda_1}}^2 b_1 c_1} = \tag{18}$$

$$= 3 \cdot 10^{-4} \lambda_1^{-0.5} (V-3)^2 \exp\left[-a(V-10)\right];$$

$$\frac{T_{R_{\lambda_2}} - \varepsilon_{\lambda_2} T - k T_{2_{\lambda_1}}\left[1 - \varepsilon_{\lambda_2} T b_2 + c_2\left(1 - \varepsilon_{\lambda_2}\right) + k^2 T_{2_{\lambda_1}}^2 c_2 b_2\left(1 - \varepsilon_{\lambda_2}\right)\right.}{T - k T_{2_{\lambda_1}}\left(T b_2 + c_2\right) + k^2 T_{2_{\lambda_1}}^2 b_2 c_2} = \tag{19}$$

$$= 3 \cdot 10^{-4} \lambda_2^{-0.5} (V-3)^2 \exp\left[-a(V-10)\right].$$

Thus, we obtained a system of two transcendental equations with two unknowns: wind velocity V and the characteristic radiation of the atmosphere at the wavelength λ_1 - $T_{2\lambda 1}$. This system can be reduced to one algebraic equation with one unknown $T_{2\lambda_1}$, finding the ratio of equations (18) and (19). We obtain

$$\frac{\left(\frac{\lambda_1}{\lambda_2}\right)^{0.5}\left\{T_{R_{\lambda_1}} - \varepsilon_{\lambda_1} T - T_{2_{\lambda_1}}\left[1 - \varepsilon_{\lambda_1} T b_1 + c_1\left(1 - \varepsilon_{\lambda_1}\right)\right] + T_{2_{\lambda_1}}^2 c_1 b_1\left(1 - \varepsilon_{\lambda_1}\right)\right\}}{T - T_{2_{\lambda_1}}\left(T b_1 + c_1\right) + T_{2_{\lambda_1}}^2 b_1 c_1} = \tag{20}$$

$$= \frac{T_{R_{\lambda_2}} - \varepsilon_{\lambda_2} T - k T_{2_{\lambda_1}}\left[1 - \varepsilon_{\lambda_2} T b_2 + c_2\left(1 - \varepsilon_{\lambda_2}\right)\right] + k^2 T_{2_{\lambda_1}}^2 c_2 b_2\left(1 - \varepsilon_{\lambda_2}\right)}{T - k T_{2_{\lambda_1}}\left(T b_2 + c_2\right) + k^2 T_{2_{\lambda_1}}^2 b_2 c_2}.$$

The transformation of the equation leads to an unwieldy fourth-degree equation which in a general form has no solution. However, the left- and right-hand sides of equation (20) are different functions of $x = T_{2\lambda_1}$; therefore, the solution is conveniently obtained graphically.

It is interesting that the right-hand side of the equation is the increment of the radiation coefficient at the wavelength λ_2; therefore, on the computation nomogram it is immediately possible to read the two parameters $T_{2\lambda_1}$ and $\Delta\varepsilon_{\lambda_2}$.

Figure 1 shows a computation nomogram which is a realization of the graphic solution of equation (20) for wavelengths 0.8 cm and 1.6 cm. Here along the x-axis we have plotted the increments of radiation at a wavelength of 1.6 cm due to the foam cover and along the y-axis the values of characteristic atmospheric radiation at a wavelength 0.8 cm. The series of solid curves represents a graphic realization of the left-hand side of the equation with different T_2 (0.8) values and with a definite value of the measured radiobrightness temperature of the "ocean-atmosphere" system at a wavelength 0.8, as indicated on the curve; the series of dashed curves represents a similar realization of the right-hand side of the equation with a definite value of the radiobrightness temperature measured at a wavelength 1.6 cm.

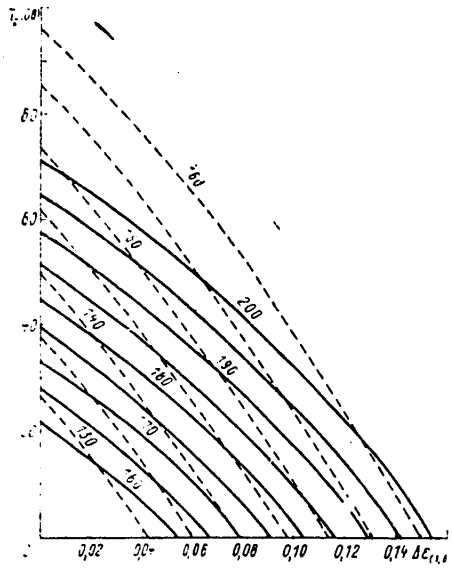

Fig. 1. Nomogram for determining characteristic atmospheric radiation at a wavelength 0.8 cm and the increment of the radiation coefficient due to waves at a wavelength 1.6 cm on the basis of satellite measurements.

The point of intersection of the corresponding pairs of curves for wavelengths 0.8 and 1.6 cm determines the atmospheric radiobrightness temperature at a wavelength 0.8 cm, which is read on the y-axis ($T_2(0.8)$), and the value of the increment of the coefficient of radiation of the wave-covered sea surface at a wavelength 1.6 cm ($\Delta\varepsilon_{1.6}$), which is read on the x-axis.

With the determined value $T_2(0.8)$ can be entered into equation (18) or (19) and it is possible to compute the wind velocity over the sea.

Working with the nomogram it can be shown that an error in measuring radiobrightness temperature by 1°K leads to an error in determining wind velocity of 3% and an error of 1.5°K leads to an error of 6%.

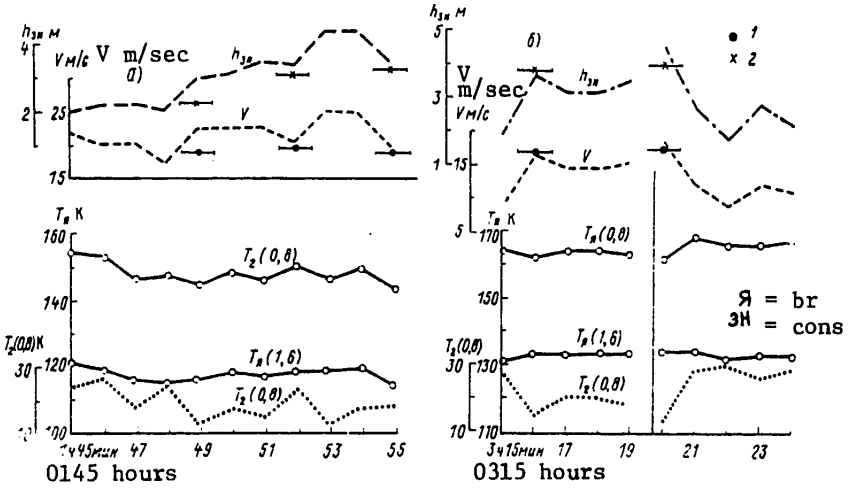

Fig. 2. Spatial changes in radiobrightness temperature at wavelengths 0.8 cm and 1.6 cm and characteristics of state of the sea surface computed from it along flight line of Il-18 aircraft. a) 11 September, b) 13 September 1976. 1) wind velocity computed from pressure gradient, 2) considerable wave height, computed from these wind velocity values.

The determined wind velocity value can be used in computing wave height in a case when fetch length can be considered infinite (completely developed waves) or known.

Thus, it was possible in general form to solve the inverse problem: determine wind velocity over the sea (and from it -- wave height) on the basis of the microwave radiation measured from a satellite.

Due to the lack of satellite synchronous microwave measurements in the selected channels the developed method for solving the inverse problem for determining wind velocity was applied to data from aircraft microwave measurements from aboard an Il-18 aircraft of the Main Geophysical Observatory during the period of the Soviet-American experiment "SAMEX-76." In the application of the "satellite" algorithm using materials from aircraft measurements the results of these measurements were "raised" to the satellite flight altitude by taking into account (on the basis of computations) atmospheric radiation in the layer 4 km (aircraft flight altitude) - 16 km (radiobrightness analogue of the atmospheric upper boundary) for each day of observations and radiation above 16 km, which was estimated approximately, on the basis of measurements with an upward-directed radiometer from aboard an American "Convair-990" aircraft during the period of the first Soviet-American "Bering" microwave experiment [8].

Figure 2 shows examples of application of the method for determining wind velocity on the basis of microwave data for specific runs of the Il-18 aircraft.

Figure 2a shows the spatial variation of radiobrightness temperatures at wavelengths 0.8 and 1.6 cm and the values of characteristic atmospheric radiation at a wavelength 0.8 cm, wind velocity along the flight line and the height of the waves (considerable) for the aircraft run of 11 September 1976 from 0145 hours to 0155 hours at an altitude of 4000 m with a sighting angle of 40° computed on their basis. The increments of the radiation coefficient, computed for an angle of 40°, were reduced to increments for the nadir by use of the Stogrun angular dependence [7]: $\Delta\varepsilon_{40^\circ} = 0.9365\Delta\varepsilon_{0^\circ}$. It was necessary to do this since the D. T. Matveyev approximation (5) relates to radiobrightness increments measured at the nadir.

Unfortunately, no instrumental measurements were made to determine wind velocity from aboard an Il-18 aircraft: therefore, as a comparison with the computed velocities, Fig. 2 gives the wind velocities and wave heights for three points computed from the pressure gradient on a surface synoptic chart; the heights were computed with allowance for fetch length. The segments of the horizontal straight lines near the wind velocity values and wave heights determined from the pressure gradient mean that it is impossible to obtain a more precise localization of the point of determination from a small-scale map.

The errors in determining wind velocity on the run are 20%, 5.2% and 5.6% for the run, provided that the wind velocity values, determined from the pressure gradient, are assumed to be true; the errors in determining the considerable height of waves are equal to 31.8%, 10% and 9.7% respectively. Thus, the errors in determining the characteristics of state of the sea surface in the second and third cases are small. The greater error in the first case does not hinder determining wind conditions as storm conditions.

In the segment of the run corresponding to the extreme right-hand side of Fig. 2a the wind velocity and the wave height decrease. This tendency corresponds to an objective evaluation of the hydrometeorological conditions with advance toward the work region of the ship, which was situated 80 km from the represented segment of the run. The wind velocity, measured from aboard the ship at the time of passage of the aircraft along the mentioned flight line, was already 13.5 m/sec and the considerable height of the wind component of waves according to data from the radar attachment to the "Don" radar set was 2.7 m (unfortunately, it was impossible to obtain wave recorder measurements of waves on this day). The indicated height agrees fairly well with the computed value 3.4 m, especially if it is taken into account that the wave height is a more conservative characteristic than the wind.

Figure 2b shows the spatial variation of radiobrightness temperatures at a wavelength 0.8 and 1.6 cm and the values of characteristic atmospheric radiation at a wavelength 0.8 cm, wind velocity along the route and considerable wave height, computed on the basis of these radiobrightness temperatures, for another run of the Il-18 aircraft which took place on 13 September 1976 (from 0315 to 0425 hours) at an altitude of 4000 m with orientation of the antenna for the radiometers to the nadir ($\theta = 0^\circ$). Here, as a comparison, we have also given the wind velocity values computed at two points on the basis of the pressure gradient and the corresponding (considerable) wave heights.

The wind velocity on the segment of the run represented in the right part of the figure is reduced, which, as in the first case, corresponds to the real situation: the aircraft is approaching the center of a cyclone.

The relative error in determining wind velocity on the basis of microwave two-channel measurements for the first control point in the measurement scheme was 1.8%. and for the second 6.7%; the error in determining wave height was 2.6% and 15% respectively.

Due to the scatter in $T\downarrow$ and b values, determined by equations (8), (9), (11), (12) the errors in determining wind velocity will deviate from the mentioned mean errors by 1-2%, which exerts virtually no influence on the possibilities of the method.

The described method for determining wind velocity from the measured radioemission of the "sea surface-atmosphere" system, as indicated above, in essence can be applied with any pair of wavelengths in the range 0.8-3.2 cm, except for a narrow frequency band near $\lambda = 1.35$ cm. The choice of the optimum pair of wavelengths can be the subject of a special investigation.

The principal difficulty in application of the method is that in the computations it is necessary to know the absolute radiobrightness temperature values and this requires very correct signal calibration.

Further work in the direction of improvement of the method should proceed along the lines of a refinement of the relationships between the atmospheric components of radiation, the careful choice of the statistics of such relationships in different regions of the world ocean and refinement of the dependence of the increment of radiobrightness temperature due to the foam cover on wind velocity.

It is also necessary to check the method on the basis of mass material from satellite microwave measurements.

BIBLIOGRAPHY

1. Basharinov, A. Ye. and Shutko, A. M., ISSLEDOVANIYE VZAIMOSVYAZI KHARAKTERISTIK POLYA TEPLOVOGO RADIOIZLUCHENIYA S SOSTOYANIYEM POVERKHNOSTI AKVATORIY (Investigation of the Interrelationship of Characteristics of the Field of Thermal Radioemission With the State of a Water Surface), PREPRINT IRE AN SSSR (Preprint of the Institute of Radioelectronics USSR Academy of Sciences), No 63, 1971.

2. Gorelik, A. G., Raykova, L. S. and Frolov, Yu. A., "Micrometric Radiometer Methods for Measuring Humidity in the Lower Troposphere," METEOROLOGIYA I GIDROLOGIYA (Meteorology and Hydrology), No 5, 1975.

3. Dombkovskaya, Ye. P., "Determination of Sea Surface Temperature and Atmospheric Moisture Content Using Measurements of Thermal Radioemission of the Earth-Atmosphere System From Artificial Earth Satellites," TRUDY GIDROMETTSENTRA SSSR (Transactions of the USSR Hydrometeorological Center), No 50, 1969.

4. Martsinkevich, L. M., "Analysis of the Characteristics of State of the Sea Surface Exerting an Influence on Thermal Radioemission in the Work Area of the Scientific Research Weather Ship 'Priboy' in the Soviet-American 'Bering' Experiment," TRUDY ZAKLYUCHITEL'NOGO SIMPOZIUMA PO ITOGAM SOVETSKO-AMERIKANSKOGO EKSPEDITSII (Transactions of the Final Symposium on the Results of the Soviet-American Expedition), Leningrad, 12-17 May 1974, Leningrad, Gidrometeoizdat, 1975.

5. Martsinkevich, L. M. and Matveyev, D. T., "Correlation Between Outgoing Microwave Radiation and the State of the Sea Surface (According to Data From the 'Cosmos-243' Satellite)," METEOROLOGIYA I GIDROLOGIYA, No 8, 1971.

6. Matveyev, D. T., "Analysis of the Results of Radiothermal Sounding of the Sea Surface During a Storm," METEOROLOGIYA I GIDROLOGIYA, No 4, 1978.

7. Stogrun, A., "The Emissivity of the Sea Foam at Microwave Frequencies," JGR, Vol 77, No 9, 1972.

8. Wilheit, T. T., Towler, M. G., Stomback, G. and Gloersen, P., "Microwave Radiometric Determination of Atmospheric Parameters During the Bering Sea Experiment," SOVETSKO-AMERIKANSKIY EKSPERIMENT "BERING" (Soviet-American "Bering" Experiment), TRUDY ZAKLYUCHITEL'NOGO SIMPOZIUMA PO ITOGAM SOVETSKO-AMERIKANSKOY EKSPEDITSIII, Leningrad, 12-17 May 1974, Leningrad, Gidrometeoizdat, 1975.

UDC 551.(465.4+466.467)(268)

DIAGNOSTIC MODEL OF WATER AND ICE CIRCULATION IN THE ARCTIC BASIN

Moscow METEOROLOGIYA I GIDROLOGIYA in Russian No 3, Mar 81 pp 68-75

[Article by V. I. Ponomarev and L. A. Glazova, Main Geophysical Observatory, manuscript received 20 Jun 80]

[Text]

Abstract: A diagnostic variant of a joint model of motion of ice and water under the influence of wind and horizontal nonuniformity of the field of masses in the ocean is examined. The authors present a method for computing the vertical component of velocity, taking into account inertial forces. The results of computations of ocean circulation in the Arctic basin with a detailed analysis of vertical movements are given.

Introduction. Concepts concerning the circulation of water and ice in the Arctic basin were obtained on the basis of observations made from the time of the remarkable drift of the "Fram" [13]. On the basis of data on the drift of ships and polar stations it was established that the principal features of macroscale circulation of ice and surface waters here are the Transarctic Current, crossing the Arctic Basin from the Chukchi Sea to Fram Strait, and the anticyclonic circulation over the Canandian Basin (see [1, 12]). The direction and velocity of propagation of Atlantic waters were evaluated for the most part by indirect methods, by an analysis of the temperature and salinity fields [8, 12]. The movement of deep waters in the Arctic Basin was the least studied due to the low measurement accuracy. The nature of the vertical circulation of waters in the entire thickness of the ocean also has remained virtually uninvestigated by empirical methods.

Theoretical investigations made it possible to obtain new concepts concerning the circulation of water and ice in the Arctic Basin. Hydrodynamic models have been the principal tool of these investigations. Using barotropic models [3, 10, 11] it was possible to describe the integral mean-term circulation of water and ice. Using diagnostic methods and models [4, 9] a study was made of the vertical structure of currents. The prognostic model in [14] made it possible to describe the process of formation of climatic fields of currents, temperature and salinity in the Arctic Ocean.

All these models best describe currents in the upper layer of the ocean. However, it is of interest to make detailed computations of currents in the layers of Atlantic and deep waters, investigate the character of vertical movements and the

interannual variability of circulation. For this purpose it is necessary to have models more precise than models used earlier, taking into account the peculiarities of the Arctic basin, the presence of an ice cover and the weak intensity of currents (the velocities of macroscale currents are several centimeters per second, and in the deep layers -- fractions of centimeters per second).

First of all it is necessary to examine the most complete and sufficiently precise diagnostic model, making it possible to compute the three components of current velocity in the entire thickness of the ocean on the basis of the stipulated density field and this article is devoted to this subject. Since within the framework of the "POLEKS-Sever" national program, beginning with 1973, regular observations have been made of the temperature and salinity fields, such a diagnostic model can be used in computing circulation for each specific year and in investigating its variability.

Principal expressions of model. As in the diagnostic models used earlier (see [7]), the initial expressions are the continuity equation for an incompressible fluid and the equations of motion in the hydrostatic and Boussinesq approximations. The derivation of the expressions for the horizontal components of current velocity is accomplished in the usual way (the assumption of quasistationarity of current velocity $\partial u/\partial t = \partial v/\partial t = 0$ is made). The equations of motion, written taking into account the equations of statics, are integrated vertically from the surface to the ocean floor. At the ocean surface ($z = 0$) and at its bottom ($z = H$) an allowance is made for the boundary conditions for frictional stresses:

$$\tau_{x,\,y}\big|_{z=0} = \tau^0_{x,\,y}; \quad \tau_{x,\,y}\big|_{z=H} = \tau^H_{x,\,y}.$$

Then a standard procedure is carried out: the stream function of total flows is introduced and the level slopes ($\partial\zeta/\partial x$, $\partial\zeta/\partial y$) are excluded from the stationary equations of motion using the vertically integrated equations of motion. This gives the following expressions for the horizontal components of current velocity (u, v):

$$u = -\frac{1}{\rho_0 l}\frac{\partial \tau_y}{\partial z} - \frac{\tau_y^0 - \tau_y^H}{\rho_0 lH} - \frac{1}{H}\frac{\partial \psi}{\partial y} - \frac{g}{\rho_0 lH}\int_0^H z\frac{\partial \rho}{\partial y}\,dz + \tag{1}$$

$$+ \frac{g}{\rho_0 l}\int_z^H \frac{\partial \rho}{\partial y}\,dz + \frac{A_L}{l}\Delta v - \frac{A_L}{lH}\Delta\left(\frac{\partial \psi}{\partial x}\right) - \frac{1}{l}N(\overline{v}) + \frac{1}{lH}\int_0^H N(\overline{v})\,dz;$$

$$v = \frac{1}{\rho_0 l}\frac{\partial \tau_x}{\partial z} + \frac{\tau_x^0 - \tau_x^H}{\rho_0 lH} + \frac{1}{H}\frac{\partial \psi}{\partial x} + \frac{g}{\rho_0 lH}\int_0^H z\frac{\partial \rho}{\partial x}\,dz -$$

$$- \frac{g}{\rho_0 l}\int_z^H \frac{\partial \rho}{\partial x}\,dz - \frac{A_L}{l}\Delta u - \frac{A_L}{lH}\Delta\left(\frac{\partial \psi}{\partial y}\right) + \frac{1}{l}N(\overline{u}) -$$

$$- \frac{1}{lH}\int_0^H N(\overline{u})\,dz,$$

where $$N(\ ) = \overline{u}\frac{\partial}{\partial x} + \overline{v}\frac{\partial}{\partial y} + \overline{w}\frac{\partial}{\partial z}.$$

If the initial equations of motion or expression (1) are reduced to dimensionless form, we obtain two small parameters: one before the inertial force (ε_1) and the other before the force of horizontal turbulent exchange (ε_2). Expanding u and v into a series for a small parameter and taking into account only the first two terms of the series, we expressed the nonlinear inertial accelerations through the first -- the linear approximations for the velocity components. (The terms containing the product $\varepsilon_1 \varepsilon_2$ are also not taken into account because they are of the same order of magnitude as terms with ε_1^2). Thus, by u, v in (1) we understand the sum of the first five terms on the right-hand side of the expressions for u and v.

The expressions for current velocities (1) satisfy a necessary condition: in the integration of the left- and right-hand sides of (1) from the surface to the bottom of the ocean these expressions become equal to identity; $S_x \equiv S_x$, $S_y \equiv S_y$, where S_x, S_y are components of the total flow vector.

In determining the integral stream function (ψ) entering into (1) use is made of the nonlinear vorticity equation, derived by cross-differentiation of the equations of motion integrated vertically from 0 to H.

The expression for vertical velocity is derived by the substitution of expressions (1) into the continuity equation, integrated vertically from 0 to z. Under the condition of a "hard top" on the ocean surface ($w|_{z=0} = 0$) the expression for w has the following form:

$$w = \frac{1}{\left(1 - \frac{\Omega_z}{l}\right)}\left\{ \frac{1}{\rho_0} \operatorname{rot}_z \frac{\tau}{l} - \frac{1}{\rho_0}\left(1 - \frac{z}{H}\right) \operatorname{rot}_z \frac{\tau^0}{l} - \right.$$

$$- \frac{z}{\rho_0 H} \operatorname{rot}_z \frac{\tau^H}{l} + \frac{z}{H}\left(u_H \frac{\partial H}{\partial x} + \right. \tag{2}$$

$$\left. + v_H \frac{\partial H}{\partial y}\right) - \frac{g}{\rho_0 l^2}\left[\frac{\partial l}{\partial x}\left(\frac{z}{H}\int_0^H (z-H)\frac{\partial \rho}{\partial y}\, dz - \right.\right.$$

$$\left.\left. - \int_0^z (\xi - z)\frac{\partial \rho}{\partial y}\, d\xi\right) - \frac{\partial l}{\partial y}\left(\frac{z}{H}\int_0^H (z-H)\frac{\partial \rho}{\partial x}\, dz - \int_0^z (\xi - z)\frac{\partial \rho}{\partial x}\, d\xi\right)\right] +$$

$$+ \frac{1}{l}\int_0^z \left(\overline{u}\frac{\partial \Omega_z}{\partial x} + \overline{v}\frac{\partial \Omega_z}{\partial y}\right) dy - \frac{z}{lH}\int_0^H \left(\overline{u}\frac{\partial \Omega_z}{\partial x} + \overline{v}\frac{\partial \Omega_z}{\partial y}\right) dz -$$

$$\left. - \frac{A_L}{l}\left(\int_0^z \Delta\Omega_z\, dz - \frac{z}{H}\Delta\Psi\right)\right\},$$

where $\Omega_z = \frac{\partial \overline{v}}{\partial x} - \frac{\partial \overline{u}}{\partial y}$,

u_H, v_H are elements of the barotropic component of current velocity, equal to the velocity at the upper boundary of the bottom friction layer (the sums of the second, third, fourth, seventh and ninth terms on the right-hand sides of formulas (1)).

In the derivation of expression (2) the inertial forces entering into (1) were taken into account partially: only the principal terms associated with vorticity advection (Ω_z) were retained (the term containing $\partial w/\partial x - \partial w/\partial y$ is not taken into account, since it is more than an order of magnitude less than vorticity advection). Thus, the derived expression for vertical velocity (2) takes into account all the principal factors responsible for macroscale circulation in the ocean, but this expression is approximate. At the same time, the used approximations are entirely valid and correct for any region in the world ocean, except for the equatorial zone, where the inertial forces evidently cannot be considered small (it is impossible to expand u and v into a series of powers of ε_1 for this reason).

It must be noted that the differences between formulas (2) and those used earlier involve not only an allowance for additional factors, but also the method for taking the principal forces into account. It follows from the formulas cited in [7] that the term caused by the divergence of drift currents is not dependent on depth, that is, in the zonal flow (for example, in the Antarctic Circumpolar Current) the vertical velocity in the entire thickness of the ocean outside the friction layers is equal to the sum of the Ekman and anemobaric components w (since $\partial\rho/\partial\lambda = 0$, $\partial\psi/\partial\lambda = 0$). In this case w does not become equal to zero at the ocean floor and does not satisfy any other physical condition.

In contrast to the formula from [7] in expression (2) the term containing the Ekman vertical velocity has the factor (1 - z/H) and therefore decreases linearly with depth from a value equal to w_E with $z = h_E$ to zero at the ocean floor. The terms associated with the β-effect and the anemobaric vertical velocity also become equal to zero at the ocean floor. In general, w in (2) satisfies the streamline flow condition when z = H:

$$w|_{z=H} = u_H \frac{\partial H}{\partial x} + v_H \frac{\partial H}{\partial y}. \qquad (3)$$

At the upper boundary of the bottom friction layer the vertical velocity is approximately equal to the sum of the friction (w_E) and orographic (w_{or}) components.

$$\vec{w}|_{z=H-h_{EH}} \approx \frac{1}{\rho_0} \operatorname{rot}_z \frac{\vec{\tau}^H}{l} + u_H \frac{\partial H}{\partial x} + v_H \frac{\partial H}{\partial y}. \qquad (4)$$

Conditions (3) and (4), denoting the presence of both friction and streamline flow on the bottom, are contradictory. This contradiction can be eliminated by introducing a boundary layer with allowance for curvature of the underlying surface of the bottom. However, in the first approximation for H it is possible to use the upper boundary of the bottom friction layer and leave the condition (4).

For closing the model relative to frictional stress at the lower surface of the ice (τ_x^0, τ_y^0) we use an extremely simple method for parameterization of the steady drift of ice examined in [6]. The ice drift velocities (u_0, v_0), the same as

the characteristics of the planetary boundary layers over the ice and under the ice, are considered quasistationary. In addition, the equations of motion for ice are written in a linear approximation without allowance for the horizontal exchange of momentum:

$$u_0 = \frac{1}{\rho_0 hl}(\tau_y^1 - \tau_y^0) + \frac{g}{l}\frac{\partial \zeta}{\partial y}; \quad v_0 = -\frac{1}{\rho_0 hl}(\tau_x^1 - \tau_x^0) - \frac{g}{l}\frac{\partial \zeta}{\partial x}, \tag{5}$$

that is, the drift velocity of ice can be represented in the form of the sum of the wind

$$\left(u_{0B} = \frac{1}{\rho_0 lh}(\tau_y^1 - \tau_y^0)\right)$$

and

$$\left(u_{0\Gamma} = -\frac{g}{l}\frac{\partial \zeta}{\partial y}\right).$$

gradient drifts [B = wind; Γ = gradient].

In such a case the frictional stresses at the lower (τ_x^0, τ_y^0) and upper (τ_x^1, τ_y^1) surfaces of the ice are determined in the following way:

$$\begin{aligned} \tau_x^i &= \rho_0^i \varkappa^2 \gamma_i^2 G_i (U_i \cos \alpha_i - V_i \sin \alpha_i), \\ \tau_y^i &= \rho_0^i \varkappa^2 \gamma_i^2 G_i (V_i \cos \alpha_i + U_i \sin \alpha_i). \end{aligned} \tag{6}$$

Here $\varkappa$ is the Karman constant, γ_i, α_i are the geostrophic friction coefficient and the angle of total rotation of the wind (i = 1) or the current (i = 0) in the planetary boundary layer (PBL). According to [2], γ and α are universal functions of the Rossby number (Ro) and the stratification parameter μ_0 (Ro = G_i/lz_0, z_0 is the roughness parameter). The functions γ(Ro, μ_0) and α(Ro, μ_0) were obtained as a result of solution of a closed system of equations for the PBL and are given in [2].

In formulas (6) with i = 1 U_1, V_1, G_1 are the components and modulus of velocity of the geostrophic wind at the upper boundary of the atmospheric PBL, with i = 0 U_0, V_0, G_0 are the corresponding differences between the drift velocities of ice and gradient currents.

It is assumed that the influence of inertial forces and horizontal turbulent exchange on the velocity of macroscale currents is small, the velocities of the gradient current at the surface approximately coincide with the velocities of gradient drift of ice

$$(u_0 = -g\frac{\partial \zeta}{\partial x}, \quad v_0 = -g\frac{\partial \zeta}{\partial y}),$$

and the vertical velocity shear in the friction layer under the ice is related only to the wind drift of ice.

It is known that the steady wind drift of ice is close to isobaric (to Zubov drift) and deviates from it by some angle γ (see [1]). Substituting (6) into (5) and reducing similar terms, it is easy to represent the wind drift of ice in the form of the sum of isobaric drift and deviations from it (as was done in [10] with use of an Ekman model for the PBL with a stipulated turbulence coefficient:

[B = wind] $$u_{0B} = C_B (U_1 \cos \gamma_B + V_1 \sin \gamma_B); \quad v_{0B} = C_B (V_1 \cos \gamma_B - U_1 \sin \gamma_B). \tag{7}$$

The expressions for the wind isobaric coefficient C_{wind} and the angle γ have the following form:

[B = wind]

$$C_B = M_1 (1 + M_0^2 + 2M_0 \sin \alpha_0)^{-1/2};$$

$$\gamma = \operatorname{arctg} \left[\frac{\cos \alpha_1 + M_0 \sin (\alpha_0 - \alpha_1)}{\sin \alpha_1 + M_0 \cos (\alpha_0 - \alpha_1)} \right], \tag{8}$$

where

$$M_i = \frac{\pi^2 \rho_i \gamma_i^2 G_i}{\zeta_a h l}, \quad i = 1, 2.$$

Thus, the already cited formulation of the diagnostic model of circulation of water and ice is a closed problem. It should be noted that formulas (8) are a special case of the expressions for C_{wind} and γ derived in [5] with allowance for the lateral friction force in the ice cover ($F_x = -ru$, $F_y = -rv$); the expression for w (2) was examined in [6], which gave computations of vertical circulation in the Arctic basin on the basis of the stipulated density field from [9] (for 1955-1956).

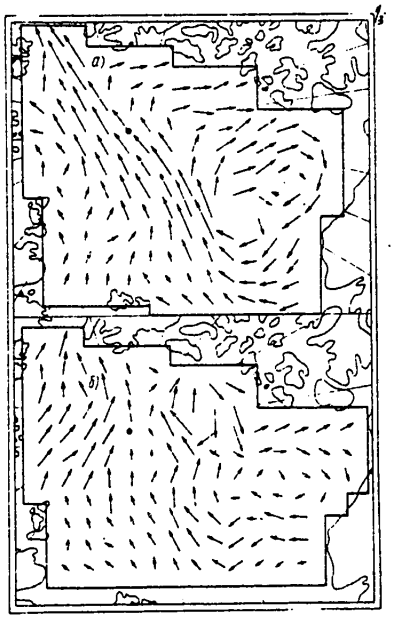

Fig. 1. Fields of velocities of gradient currents at the ocean surface. a) computed on the basis of data on density for 1958-1959 (from [9]); b) computed from density data for 1975 obtained on the "Sever-27" expedition.

In this article we give computations of the three components of current velocity and ice drift velocity on the basis of data on density obtained on the "Sever-27" expedition (carried out in 1975). The results of these computations were compared with the current velocity fields obtained in [6] on the basis of the density field

from [9], observed two decades prior to the "Sever-27" expedition.

Computations of u, v, w were made at standard horizons at the points of intersection of a uniform grid employed earlier in [3, 4, 6]; the grid interval used was 200 km. We also stipulated the discharges in straits on the basis of data from Timofeyev (see [8, 10]), the bottom relief field cited in [3] and the field of atmospheric pressure. Computations were made both with a stipulated mean long-term atmospheric pressure field, cited in [10], and with a pressure field averaged for 1974, that is, averaged for the period preceding density observations.

Results of computations. First we note that the general conclusions concerning computations of horizontal circulation in the Arctic basin and comparisons of different methods for computing currents are given in [4]. The influence of different factors on vertical velocity with a detailed analysis of all the terms in the expression for w (2) was examined in [6]. Accordingly, in this study we note only the principal conclusions pertaining to vertical circulation in the Arctic basin and we will compare the results of computations of circulation for the density fields obtained in 1958-1959 and in 1975. These results of computations differ appreciably due to important changes in the salinity field occurring over the course of 16 years.

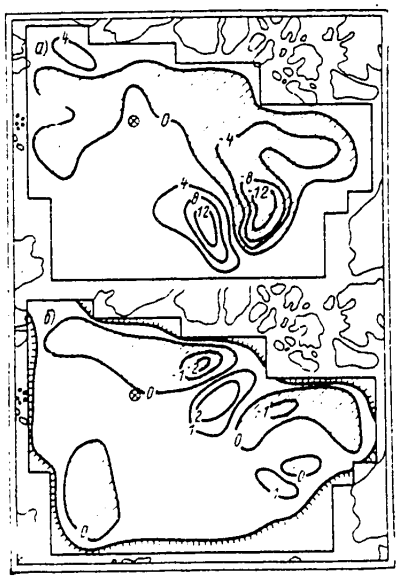

Fig. 2. Vertical velocity fields at 500-m horizon. a) computed using density data for 1958-1959, b) computed using density data for 1976. Regions of ascending movements are shaded. The north pole is designated by a dot.

Figure 1 shows that the Transarctic Current, intersecting the basin, was best expressed in 1958-1959, whereas in 1975 this current was not concentrated in a narrow zone, although everywhere in the Atlantic subbasin there was a drift with a

velocity of about 1-2 cm/sec in the direction from the Siberian shelf to the Canadian archipelago. The current was considerably intensified only in individual regions: along the Mendeleyev Range and beyond the Lomonosov Ridge. In addition, in 1958-1959 one anticyclonic circulation occupied both the region of the Pacific Ocean subbasin and the regions adjacent to the Canadian archipelago. Only over the Canadian basin in the central part of the main circulation was it possible to discriminate two anticyclonic vortices of a lesser scale (see Fig. 1a). In 1975 the anticyclonic circulation divided into two vortices; one was situated over the Canadian basin and the other, the more intense with respect to velocity and depth, but smaller in extent, was situated over the Alpha Rise, adjacent to the Canadian archipelago (Fig. 1b).

The fields of horizontal current velocity in the layer of Atlantic waters also have some differences, but less than at the above-lying horizons. It is interesting to note that in 1975 at the 500-m horizon the circulation over the Canadian basin becomes opposite, forming a cyclonic circulation, whereas over the Alpha Rise, as before, there is an intensive anticyclonic vortex.

In addition, it must be noted that the change in circulation is most appreciable and graphic in the vertical velocity field, which is the most sensitive of all the hydrological characteristics which we examined. Figure 2 shows the vertical velocity field for the 500-m horizon where it is governed for the most part by the β-effect (fifth term in expression (2), which we will denote $w_{g\beta}$). In the above-lying layers of the ocean the fields of the term $w_{g\beta}$ have the same peculiarities as the w_{500} field, but the total vertical velocity w with $z \leqslant 400$ m is also subject to a considerable influence of the divergence of drift currents (second term in (2), which will be denoted e_{E_z}).

It follows from an analysis of w_{500} (or $w_{g\beta}$) that the spatial distribution of the regions of ascending and descending movements, as well as the velocity maxima, is different in the considered years, although the general character of the vertical circulation in the thickness of the ocean, averaged in area, did not change: in the ocean area adjacent to the Canadian Arctic archipelago there is a predominance of the upwelling of waters, whereas in the region adjacent to the Siberian shelf there is subsidence of waters (see Fig. 2).

It is easy to confirm that the differences in the w fields during 1958-1959 and 1975 agree well with the differences in the fields of horizontal currents (Fig. 1), which is one of the criteria of accuracy of the model. In particular, below the region of a considerable influence of the wind (the term $w_{Ez} = w_E (1 - z/H)$) in the eastern parts of the anticyclonic vortices there is upwelling, whereas in the western parts there is a subsidence of waters governed by the β-effect.

In addition, on the axis of the Transarctic Current (see Figures 1a and 2a) the maximum horizontal gradients w, $w_{g\beta}$ and w_E are observed (the field of the Ekman vertical velocity w_E, computed from the atmospheric pressure field averaged for the 1950's, was given in [6]). It was found that the velocity w_E reverses its sign approximately on the axis of the current, $w_{g\beta}$ changes its sign to the right of the axis on the periphery of the current along the meridian, intersecting the anticyclonic circulation. The intensification of the Transarctic Current in a definite

region in all probability is associated precisely with a substantial horizontal shear and a change of the sign of W_E in this region, averaged for the preceding time period.

A comparison of the field of currents for 1975 with the w_E field, found from the atmospheric pressure field computed as an average for 1974, also confirms the conclusion that the variability of circulation in the Arctic basin is associated primarily with the mechanism of redistribution of the density field due to the vertical velocity caused by the divergence of drift currents. Thus, the wind influence to the greatest degree is determined precisely by this mechanism and not by horizontal transport of heat and salts.

Still another characteristic of the vertical movements is that the surface on which w passes through zero can be identified with a stationary front since maximum salinity and density gradients are observed near this surface.

In 1958-1959 the surface of such a large-scale front, having a considerable slope, passed through the axis of the Transarctic Current (see Fig. 1a) in the upper layer of the ocean, where $w \approx w_E = 0$, and intersected the anticyclonic circulation in the lower-lying layers approximately along the meridian 130°E at the horizon 500 m, where $w \approx w_{g\beta} = 0$.

If the steady vertical circulation in the Arctic basin is characterized as a whole, it must be noted that the vertical movements (w_{Ez}) caused directly by the prevailing wind as an average for some water area have opposite directions relative to the vertical movements caused by the β-effect ($w_{g\beta}$). The remaining factors taken into account in expression (2) exert an appreciable influence on w only in individual regions of the Arctic basin. In particular, inertial forces make an appreciable contribution to w only in the region of maximum vorticity gradients and do not exceed 20% of the contribution of the main components in (2).

In the future it is proposed that the model presented in this article be used in computations of oceanic circulation successively for each year making use of density data obtained on the "Sever" expeditions carried out by the Arctic and Antarctic Scientific Research Institute since 1973 and continuing to the present time. Such computations are necessary for investigating the year-to-year variability of circulation.

In addition, in conclusion we note the possibility of generalizing the considered model. Supplementing it with the equations of diffusion of heat and salt with the corresponding boundary conditions, we obtain a prognostic model of oceanic circulation which can be assigned to the class of filtered models cited in [7]. Using the prognostic model it is proposed that a detailed study be made of the mechanisms of variability of circulation.

BIBLIOGRAPHY

1. Gudkovich, Z. M., "Principal Patterns of Ice Drift in the Central Polar Basin," MATERIALY KONFERENTSII PO PROBLEME "VZAIMODEYSTVIYE ATMOSFERY I GIDROSFERY V SEVERNOY CHASTI ATLANTICHESKOGO OKEANA" (Materials of the Conference on the Problem "Interaction Between the Atmosphere and Hydrosphere in the Northern Part of the Atlantic Ocean"), Leningrad, No 3-4, 1961.

2. Laykhtman, D. L., FIZIKA POGRANICHNOGO SLOYA ATMOSFERY (Physics of the Atmospheric Boundary Layer), Leningrad, Gidrometeoizdat, 1970.

3. Ponomarev, V. I. and Fel'zenbaum, A. I., "Numerical Experiment on Circulation in the Arctic Basin (Barotropic Model)," MORSKIYE GIDROFIZICHESKIYE ISSLEDOVANIYA (Marine Hydrophysical Investigations), No 4(71), 1975.

4. Ponomarev, V. I., "Computations of Macroscale Circulation of Waters in the Arctic Basin Using a Diagnostic Model," PROBLEMY ARKTIKI I ANTARKTIKI (Problems of the Arctic and Antarctica), 1977.

5. Ponomarev, V. I., "Nonlinear Theory of Steady Ice Drift," Main Geophysical Observatory imeni A. I. Voyeykov, Leningrad, 1979. (Manuscript deposited at the Information Center of the All-Union Scientific Research Institute of Hydrometeorological Information-World Data Center 21 Nov 79 No 52).

6. Ponomarev, V. I., "Computations of Macroscale Vertical Circulation in the Arctic Basin," Main Geophysical Observatory imeni A. I. Voyeykov, Leningrad, 1979. (Manuscript deposited at the Information Center of the All-Union Scientific Research Institute of Hydrometeorological Information-World Data Center 19 Dec 79 No 53).

7. Sarkisyan, A. S., CHISLENNYY ANALIZ I PROGNOZ MORSKIKH TECHENIY (Numerical Analysis and Prediction of Sea Currents), Leningrad, Gidrometeoizdat, 1977.

8. Timofeyev, V. T., VODNYYE MASSY ARKTICHESKOGO BASSEYNA (Water Masses of the Arctic Basin), Leningrad, Gidrometeoizdat, 1960.

9. Treshnikov, A. F. and Baranov, G. I., STRUKTURA TSIRKULYATSII VOD ARKTICHESKOGO BASSEYNA (Structure of Water Circulation in the Arctic Basin), Leningrad, 1972.

10. Fel'zenbaum, A. I., "Theory of Steady Ice Drift and Computation of Mean Long-Term Drift in the Central Part of the Arctic Basin," PROBLEMY SEVERA (Problems of the North), 1958.

11. Campbell, W. J., "The Wind-Driven Circulation of Ice and Water in a Polar Ocean," JGR, Vol 70, 1965.

12. Coachmen, L. K. and Barnes, C. A., "The Movement of Atlantic Water in the Arctic Ocean," ARCTIC, 16(1), 1963.

13. Nansen, F., "The Oceanography of the North Polar Basin," THE NORW. N. P. EXPED. 1893-1896. SCIENTIFIC RESULTS, Vol III, London, 1902.

14. Seminer, A. I., "Numerical Simulation of the Arctic Ocean Circulation," J. PHYS. OCEANOGR., Vol 6, No 4, 1976.

UDC 551.465.72(261.2)(261.35)

COMPLEX PREDICTION OF THE INTERANNUAL VARIABILITY OF INFLOW OF NORTH SEA WATERS INTO THE BALTIC ACCORDING TO SHORE OBSERVATION DATA

Moscow METEOROLOGIYA I GIDROLOGIYA in Russian No 3, Mar 81 pp 76-79

[Article by A. Ye. Antonov, candidate of geographical sciences, Leningrad Division of the State Oceanographic Institute, manuscript received 18 Aug 80]

[Text]

Abstract: A method is described for predicting the interannual changes in bottom salinity, dissolved oxygen and the thickness of the layer of saline North Sea waters in the southern Baltic.

Water exchange through the Danish straits, and to be more precise, the entry into the Baltic of "fresh" North Sea waters with increased salinity and enriched with dissolved oxygen, is an important factor to a considerable degree determining not only the hydrological-hydrochemical conditions of this basin, but also its ecology. In any case the underflows of saline North Sea waters determine the gas and salt regimes of the bottom and deep layers of the sea, important for fishing. Therefore, the possibility of foreseeing anticipated changes in hydrological-hydrochemical conditions in this zone of the sea is of great importance.

Earlier [3, 4] we proposed a procedure for predicting the interannual variability of the position of the 10°/oo isohaline as an indicator of the intensity of the underflow of "fresh" saline North Sea waters. However, in this case it is possible to obtain only a qualitative characteristic of this phenomenon (that is, some idea as to whether a greater or lesser volume of water with a salinity greater than 10°/oo flowed in). Until now it has been impossible to predict the salinity and content of dissolved oxygen in the inflow of new North Sea waters into the Baltic Sea.

Complex investigations of the process of inflow of "fresh" North Sea waters into the Baltic Sea, and in particular, the analysis and comparison of time series of bottom salinity, thickness of saline waters, dissolved oxygen within the limits of these waters, indices of sea level and river runoff and other hydrometeorological characteristics, as well as their autocorrelation analysis, made it possible to establish good asynchronous correlations among these characteristics. They also served as a basis for developing a long-range forecast of the variability of inflow of North Sea waters through the Danish straits, making it possible to obtain a timely, multisided idea concerning the anticipated consequences of this phenomenon, especially about changes in the volume of waters with a salinity of more than 10°/oo,

about their mean salinity and the content of dissolved oxygen within the limits of these waters.

In this work we used prognostic relationships established earlier between the dynamics of sea level and the depth of the 10°/oo isohaline in the southern part of the Baltic Sea [3, 4].

Thus, for obtaining a complex idea concerning the impending entry of "fresh" North Sea waters through the Danish straits it is possible to use the prognostic equation

$$\Delta h\ 10^{0}/_{00},\ м = 0{,}14 - 0{,}486\ \Delta H, \tag{1}$$

where Δh is the increment of the mean depth of the 10°/oo isohaline in the Bornholm and Gdansk depressions in May-August of the current year in comparison with its position in the past year; ΔH is the deviation of the mean level at Kolka and Ventspils during July-December of the past year from the mean values for 1946-1965.

In the absence of data on levels at these points it is possible to use data for Kronshtadt. In this case the correlation equation has the form

$$\Delta h\ 10^{0}/_{00},\ м = -0{,}385\ H_{К}. \tag{2}$$

where Δh is the same as in equation (1) and H_K is the level increment at Kronshtadt in July-December of the past year in comparison with its position in these months in the preceding year.

The prediction of the mean salinity values in the limits of these waters can be made on the basis of one of the equations (1)-(3) proposed in [5] or it is possible to use an equation in the form

$$\Delta S^{0}/_{00} = -0{,}0011\ \Delta Q, \tag{3}$$

where ΔS is the salinity increment in the layer 60-90 m in the Bornholm depression in the current year in comparison with the past year (n - 1), whereas ΔQ is the increment of the total runoff of the Neva, Narva, Daugava, Neman and Visla in the years n - 6/n - 1 in comparison with the years n - 7/n - 2.

In order to ascertain the anticipated salinity increment in this layer it is also possible to use the formula

$$\Delta S_2 = -0{,}094\ H_{К}^{2} + 0{,}06, \tag{4}$$

where ΔS_2 are the salinity increments, averaged for two years, in the layer 60-90 m in comparison with the past (n - 1) and related to the last year (n); H_K is the increment of the mean level during July-December in n - 2/n - 1 years in comparison with its position in n - 3/n - 2 years (for Kronshtadt).

The content of dissolved oxygen in the limits of these waters, in particular, in the bottom horizons of the southern Baltic, can also be established from the "level behavior" in the preceding years. In particular, using an equation in the form

Table 1

Indices of Accuracy of Methods for Predicting Hydrological-Hydrochemical Characteristics, Their Guaranteed Probability and Effectiveness

Evaluation indices	Equations					
	(1)	(2)	(3)	(4)	(5)	(6)
Correlation coefficient	$0,82 \mp 0,05$	$0,77 \mp 0,05$	$0,71 \mp 0,08$	$0,72 \mp 0,07$	$0,71 \mp 0,06$	$0,76 \mp 0,06$
Number of years	26	28	51	30	24	23
S/σ method $\leqslant S/\sigma$ maximum admissible	$0,57 < 0,80$	$0,65 < 0,80$	$0,13 < 0,80$	$0,67 < 0,80$	$0,70 < 0,75$	$0,60 < 0,75$
Advance time, months	8	8	12	8	8	8
Admissible error, $\delta = \sigma$	6 "	6 "	0,3%	0,6%	1,0 ml/liter	0,7 ml/liter
Guaranteed probability %	92	88	80—90	86	85	90
Effectiveness %	42	40	50—60	69	69	55
Years of checking	1966—1975	—	—	—	—	—
Limits of errors	1—8 "	—	—	—	—	—
Probable success %	80	—	—	—	—	—

$$O_2 \text{ ml/liter} = 1.54 - 0.087\Delta H, \quad (5)$$
$$O'_2 \text{ ml/liter} = 1.8 - 0.087\Delta H, \quad (6)$$

where O_2 is the mean annual content of dissolved oxygen at the horizon 85/90 m in the Bornholm depression; O'_2 is the same as an average for the horizons 85/90 m in the Bornholm depression and for the horizon 100/105 m in the Gdansk depression during the course of the year; ΔH is the same as in equation (1).

An evaluation of the quality of the proposed methods for computing different hydrological-hydrochemical elements using equations (1)-(6) is given in Table 1. Its data show that the proposed procedures for predicting interannual variations in the intensity of entry of "fresh" North Sea waters through the Danish straits by means of computations of the depth of the 10°/oo isohaline, by use of the corresponding prognostic equations, as an index of the volume of North Sea waters flowing into the Baltic Sea, computations of their mean salinity and the content of dissolved oxygen within the limits of these waters are characterized by a high guaranteed probability and effectiveness. They can be used for annual correction of the super-long-range background forecast of the anticipated changes in salinity in the bottom waters of this sea [5].

In addition, the complex hydrological-hydrochemical prediction of the anticipated interannual changes in the intensity and character of entry of North Sea waters is also of independent importance, especially for fishing science and practical work. The regime of bottom and deep waters, their volume, frequency and intensity of renewal, the absolute values of salinity and dissolved oxygen within their limits are important abiotic factors to a considerable degree determining the conditions for reproduction and survival of important species of commercial fish in the Baltic Sea, such as cod and plaice [1, 2].

The broad use of the underflow of North Sea waters as a predictor of sea level indices in complex forecasting is attributable to the fact that its level is characterized by a definite universality in the reflection of hydrometeorological processes transpiring in the sea. In actuality, in characterizing the physical essence of the latter prognostic relationships (1)-(6) it should be noted that the principal predictors -- the sea level and its dynamics -- are some of the important indices of most hydrometeorological processes transpiring in the sea. The level seemingly integrates the consequences of such phenomena as continental runoff, atmospheric pressure, precipitation and evaporation from the sea surface, which in one way or another exert an influence on water exchange in the strait zone, and accordingly, on the nature and intensity of entry of North Sea waters into the Baltic Sea. Hence there is a clear relationship between dynamics of sea level and the relative volumes of inflowing North Sea waters, their salinity and dissolved oxygen within the limits of these zones.

Thus, the use of the indices of sea level dynamics (and in part the runoff of the Neva River) as a predictor makes it possible, on the basis of expressions (1)-(6), to obtain some idea concerning impending interannual changes in the underflow of North Sea waters into the Baltic Sea through the Danish straits and with an advance time of about eight months to prepare a forecast of the anticipated changes in the thickness of the layer of these waters, their mean salinity and the dissolved oxygen within their limits.

A noteworthy characteristic of the proposed procedure for the complex marine hydrological forecast is that this prediction is prepared using data from routine observations in the sea and river network of the State Committee on Hydrometeorology.

BIBLIOGRAPHY

1. Antonov, A. Ye., OKEANOLOGICHESKIYE OSNOVY RYBOPROMYSLOVYKH PROGNOZOV V YUZHNOY CHASTI BALTIYSKOGO MORYA (Oceanological Principles of Fishing Forecasts in the Southern Part of the Baltic Sea), Kaliningrad, Izd-vo Gazety "Kaliningradskaya Pravda," 1964.

2. Antonov, A. Ye., "Background Forecast of the Relative Yield of Some Commercial Fish in the Baltic Sea," RYBNOYE KHOZYAYSTVO (Fishing Industry), No 11, 1962.

3. Antonov, A. Ye., "On the Problem of the Reasons for Variation of Salinity in the Baltic Sea," RYBOKHOZYAYSTVENNYYE ISSLEDOVANIYA V BASSEYNE BALTIYSKOGO MORYA (Fishery Investigations in the Baltic Sea Basin), No 3, 1967.

4. Antonov, A. Ye., "Prognostic Relationships Between Hydrometeorological Phenomena in the Coastal Zone and in Open Regions of the Baltic Sea," TRUDY GOINa (Transactions of the State Oceanographic Institute), No 115, 1972.

5. Antonov, A. Ye., "Procedures for the Super-Long-Range Prediction of Bottom Salinity in the Baltic Sea," TRUDY GOINa, No 157, 1980.

UDC 551.464:621.039.8

STATUS OF THE STUDY OF THE ELEMENT-SALT COMPOSITION OF SEA WATERS USING NUCLEAR-PHYSICAL METHODS

Moscow METEOROLOGIYA I GIDROLOGIYA in Russian No 3, Mar 81 pp 80-85

[Article by Ye. M. Filippov, professor, Marine Hydrophysical Institute, manuscript received 25 Jul 80]

[Text]

Abstract: On the basis of computations and experimental investigations it is shown that nuclear-physical methods can be used in studying the fundamental salt composition of sea waters under natural conditions. The total salinity of the waters can be determined on the basis of the attenuation of soft gamma radiation emitted by sources with an initial energy of 100-300 KeV. The potassium in water is determined on the basis of natural radioactivity of its isotope K^{40}. The roentgenofluorescent method can be used in separate determination of chlorine, potassium, calcium and bromine and neutron methods can be used in determining chlorine, sodium and bromine. Automated systems can be created on the basis of all these methods.

There is a change in the salt composition of sea water under the influence of natural factors and anthropogenic activity [1, 3, 4]. At the present time it is being studied for the most part under laboratory conditions using chemical and physicochemical methods [5]. These methods have a high accuracy. However, they are extremely time consuming and do not make it possible to automate measurement processes. This problem can be solved on the basis of nuclear-physical methods [6-11].

It was demonstrated in [7] that for determining the total salinity of sea water it is possible to use a method based on the attenuation of soft gamma radiation in it from sources with an energy of 100-300 KeV. We will evaluate the spectrum of scattered gamma radiation on the basis of the diffusion-age equation [6], which for convenience in the computations will be represented in the form

[K = C]

$$N = \frac{Qs\,i\,(E)}{S\,\tau_k\,(E)\,\vdots\,(E)\,[\pi\theta\,(E)]^{3\,\vdots}}\,\exp\left[-\frac{r^2}{4\,\theta\,(E)} - \psi\,(E) - \varphi\,(E)\,S\right].$$

Here Q is the yield of gamma radiation from the source, s is the effective area of the detector, $\varepsilon(E)$ is detector efficiency, r is the distance between the centers of the source and detector, $\tau_C(E)$ is the linear coefficient of attenuation of gamma radiation as a result of Compton scattering, $\xi(E)$ is the mean change in the wavelength of gamma radiation as a result of scattering;

$$\Theta = \frac{1}{3}\int_{\lambda_{\gamma_0}}^{\lambda_T} \frac{d\lambda_T}{|\tau_K(\lambda_T)\,\xi(\lambda_T)|^2},$$

where $\lambda_\gamma = 511/E_\gamma$ is the wavelength of the gamma quanta.

$$\psi = \int_{\lambda_{T_0}}^{\lambda_T} \tau_\Phi(\lambda_T)\, d\lambda_T\, \tau_K(\lambda_T)\, \xi(\lambda_T).$$

This function takes into account the probability of absorption of gamma quanta on hydrogen and oxygen atoms. The function $\varphi(E)S$ is similar to ψ, but takes into account the absorption of gamma radiation on atoms of mineral salts dissolved in the water. The $\varphi(E)$ value takes into account the dependence of gamma quanta on energy and the S value determines the total salinity of water in g/liter or pro mille ($^o/oo$).

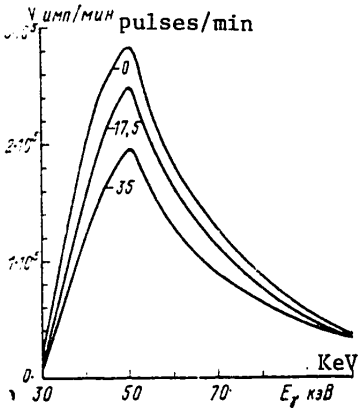

Fig. 1. Spectral distribution of scattered gamma radiation for source with initial energy of 100 KeV. The figures on the curves represent water salinity in pro mille (g/liter).

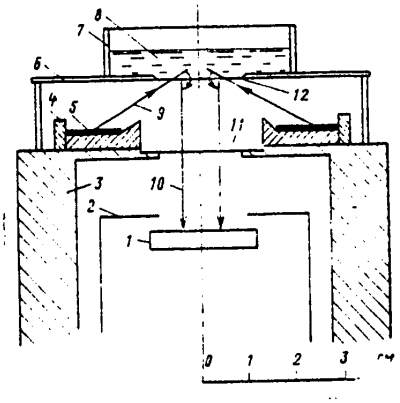

Fig. 2. Diagram of spectrometric sensor for study of element-salt composition of sea water samples. 1) Si-Li detector; 2) thermal shield; 3) detector housing; 4) capsule for annular source; 5) source; 6) support for cassette; 7) cassette with sample; 8) water sample; 9) direction of primary radiation; 10) direction of characteristic radiation; 11) Be detector window; 12) polyethylene film on cassette bottom.

The equilibrium spectrum of scattered gamma radiation, as is well known [6], is formed at distances not less than 3-4 lengths of the free path $\lambda = \tau_0^{-1}$, where τ_0 is the linear coefficient of attenuation of primary gamma radiation of the source. The spectral distribution of the scattered gamma radiation for a source with an initial energy of 100 KeV in water with different salinity is shown in Fig. 1. This figure shows that on the basis of registry of radiation in the energy range 30-70 KeV it is possible to judge the change in the salinity of sea water. With work with a source of the type Eu^{155} and Gd^{153} with a yield of about 10^9 quanta/sec and a scintillation detector the salinity of sea water can be determined with an absolute error 0.02-0.03°/oo with a duration of the measurement of approximately 5 minutes.

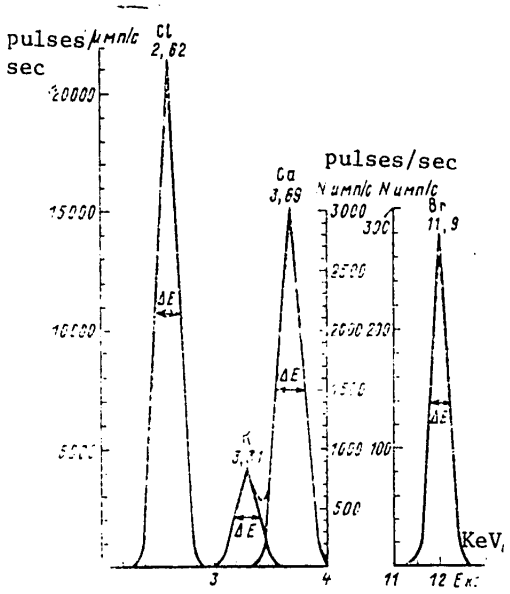

Fig. 3. Spectrum of characteristic emission of chlorine, potassium, calcium and bromine.

It was demonstrated in [3] that in the study of water salinity in the coastal marine zone the requirements on the error in measuring this parameter are reduced to 0.1°/oo. It follows from this that in measurements of salinity with a given accuracy by the considered method it was possible either to decrease the activity of the source by a factor of 25 or to decrease the duration of the measurements to 15 sec, all other conditions being equal.

The change in the potassium content in sea water can be judged from its radioactive isotope K^{40}. For example, on the basis of experimental investigations with a low-background gamma detector of the "Limon" type supplied with an NaI(Tl) crystal measuring 150 x 100 mm with a duration of measurement of one hour the K content can be determined with an absolute error 0.005°/oo [9]. For these purposes it is also

possible to create apparatus with scintillation beta counters with a developed surface.

For an express determination of other chemical elements of the fundamental salt composition it is possible to use roentgenofluorescent and neutron methods, the physical principles of which were set forth in detail in [6].

The possibilities of using proportional counters for measuring the characteristic emission of chemical elements of excited atoms of sea water were examined in [8]. There it was demonstrated that on the basis of the roentgenofluorescence (PPM) method it was possible to create automated systems for the analysis of samples under laboratory and natural conditions. In this way it is possible to determine chlorine, calcium and bromine in sea water. However, the possibilities of PPM are considerably expanded when making measurements with semiconductor silicon-lithium detectors. The author of [2] describes such detectors with thermoelectric cooling having a resolution for potassium and calcium of 243 and 245 eV respectively. On the basis of such a detector it was possible to create a sensor for measuring the element-salt composition of sea water directly aboard a ship. For the measurements it is sufficient to use water samples with a mass of 2-3 g. The measurement scheme is represented in Fig. 2. Computations for this geometry are made in accordance with [8]. We will assume that for the excitation of chlorine, potassium and calcium atoms use is made of a titanium-tritium source (T = 12.3 g, $E\gamma$ = 4.5 KeV) with a yield of $7.5 \cdot 10^6$ quanta/sec, and for the excitation of bromine -- molybdenum-93 (T = 2300 years, $E\gamma$ = 17 KeV) with a yield $1.5 \cdot 10^8$ quanta/sec. The area of the detector, in accordance with Fig. 2, was assumed to be equal to 3.8 cm^2, whereas the area of the entrance window was 2.54 cm^2.

On the basis of the considered PPM method, as demonstrated in [8], it is also possible to create submergible sensors. Such sensors can be assembled on the basis of semiconductor detectors used in field geophysical practice.

Computations of the spectral distribution of the characteristic emission of chlorine, potassium and calcium for ocean water (S = 35°/oo) are illustrated in Fig. 3. The counting rate at the photopeak of each element and the background is indicated in Table 1. The absolute (ΔC) and relative (δC) errors were computed with allowance for the background emission in accordance with [6]. The table shows that the highest accuracies in the measurements are attained when determining chlorine and calcium. When making measurements with a submergible sensor, as a result of the absorption of emission in an additional beryllium window, sealing in the sensor, the measurement errors are somewhat further increased and measurement accuracy is reduced. With an increase in source activity by an order of magnitude the measurement error can be reduced by a factor of 3.

The discussed PPM sensors can be used in a study of changes in the element-salt composition of sea water at shallow depths since otherwise they would be crushed by the hydrostatic pressure of a great thickness of water. Neutron methods can be employed in a study of sea water in an extremely wide range of depths: the neutron gamma method, based on the registry of gamma emission of the radiation capture of neutrons (NGM) and the neutron activation method (NAM).

Table 1

Results of PPM Computations and Anticipated Absolute Measurement Errors

Element	C ‰	Laboratory analysis				Submerged sensor			
		N pulses/sec	*	t sec 100	t sec 400	N pulses/sec	*	t sec 100	t sec 400
Chlorine	19	4608	1808	0,037	0,02	1475	578	0,066	0,033
Potassium	0,38	215	2136	0,012	0,006	122	1209	0,016	0,008
Calcium	0,40	773	2154	0,0037	0,002	508	1415	0,0045	0,0022
Bromine	0,065	125	800	0,0014	0,0007	121	774	0,0022	0,0011

*$N_{background/pulses}$

Table 2

Results of NAM Computations and Anticipated Measurement Errors

Element	E MeV	N pulses	N_1 pulses	N_{back} pulses	δN %	$C \pm \Delta C$ ‰
Chlorine	2,15	109500	64700	350		
	1,6	71400	36400	850	0,32	9,5±0,03
Sodium	3,85	177	52			
	2,76	47000	37780			
	1,38	74630	36100	1000	0,37	5,25±0,019
Bromine	0,62	2252	1000	850	5,2	0,0325±0,0017
Magnesium	1,013	235		1000	20	0,675±0,136
Calcium	4,68	8,32	3,36		54,6	0,2±0,109
	4,05	21,2				
	3,1	39,1				

The NGM, as demonstrated on the basis of theoretical [9, 10] and experimental investigations [11], can be used in determining chlorine. The author has demonstrated that it can be determined using a method with a californium source with a yield $\sim 1 \cdot 10^8$ neutrons/sec and a scintillation counter of the "Limon" type. With a measurement duration of 2 sec and a distance between the source and detector of 20 cm the chlorine in Black Sea water (C = 9.5‰) can be determined with an absolute error of 0.09‰ or a relative error of 0.94‰. By increasing the duration of the measurements to 8 sec the measurement errors can be cut in half.

The neutron activation method [9, 10] can be used in determining chlorine, sodium, bromine and other elements. In these studies expressions have been derived for calculating the counting rates N at the photopeaks for individual lines of activating chemical elements.

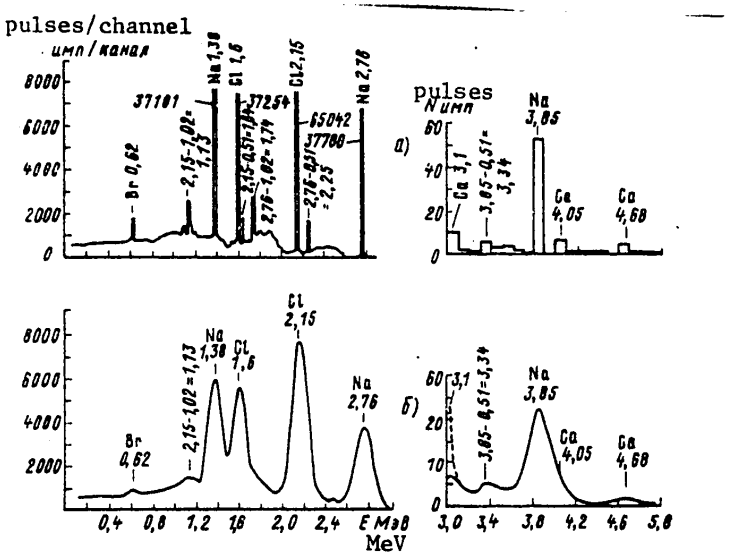

Fig. 4. Gamma spectrum of Black Sea water activated by thermal neutrons. a) for detector with ideal resolution; b) for scintillation detector of the "Limon" type.

Using these algorithms, the author, in collaboration with A. Kh. Degtyarev, made computations of the spectra of gamma radiation at the output of a "Limon" detector. The computations were made by the Monte Carlo method for an idealized case: it was assumed that all the gamma quanta hit at the center of the crystal. Due to Compton scattering and the effect of pair formation the emission reckoned at the photopeaks decreased from N to N_1 (Table 2). The resulting spectral distribution of emission is illustrated in Fig. 4. The conversion from curve a to curve b was accomplished using a Gaussian for the purpose of obtaining an "experimental" spectrum. For the left part of the spectrum the interval along the x-axis was selected equal to 20 KeV, and for the right part -- 100 KeV. The results of computations of the measurement errors are given in Table 2. Computations were made for the case of activation of water under natural conditions over a period of 30 minutes and measurements of induced activity were also made for 30 minutes. The table shows that when using the NAM method the highest accuracies are attained for chlorine and sodium and magnesium and calcium are determined less accurately.

We note on the basis of these materials that a combination of neutron methods is possible. The entire outfit for the study of sea water can be carried aboard ships, small boats, amphibian craft or rafts. A paraffin or water container with a mass of 1 ton is sufficient for storage of the neutron source. During the measurements the sensor together with the container can be lowered over the side of the ship. When the source is present in the container it is possible to determine the potassium content in sea water and evaluate the gamma background. Chlorine in sea water can be determined in the course of its irradiation in the course of a few seconds. Then after irradiation of the water and removal of the source the induced activity of the forming isotopes is measured in the container. In order for the current not to distort the measurement results the irradiated volume of water must be recorded

prior to irradiation and measurement. For this purpose it is necessary to fabricate two hemispherical containers fixing the subsurface water volume used in the measurements.

We note in conclusion that all the operations for studying the salt-element composition of the water can be automated. On the basis of specially prepared programs the data from spectrometric measurements can be processed on shipboard electronic computers, at their output giving the salinity values and the concentrations of determined elements of interest to the researcher.

BIBLIOGRAPHY

1. Baydin, S. S., "Redistribution of River Runoff Among Sea Basins and its Role in the Natural Complex of Seas and River Mouths," TRUDY GOIN (Transactions of the State Oceanographic Institute), No 143, 1979.

2. Beda, A. G., "Germanium and Silicon-Lithium Spectrometers With High Resolution for Practical Purposes," ATOMNAYA TEKHNIKA ZA RUBEZHOM (Atomic Engineering Abroad), No 9, 1979.

3. Ivanov, G. S. and Ovsyannikov, A. N., "Variability of Water Salinity in the Coastal Zone of the Sea," METEOROLOGIYA I GIDROLOGIYA (Meteorology and Hydrology), No 9, 1979.

4. Kosarev, A. N., "Problems of the Southern Seas of the USSR," ZEMLYA I VSELENNAYA (Earth and Universe), No 3, 1975.

5. RUKOVODSTVO PO METODAM KHIMICHESKOGO ANALIZA MORSKIKH VOD (Manual on Methods for Chemical Analysis of Sea Water), edited by S. G. Oradovskiy, Leningrad, Gidrometeoizdat, 1977.

6. Filippov, Ye. M., YADERNAYA GEOFIZIKA (Nuclear Geophysics), Volumes 1, 2, Novosibirsk, Nauka, 1973.

7. Filippov, Ye. M., "Possibilities for Determining the Salinity and Density of Sea Water From the Attenuation of Gamma Radiation," MORSKIYE GIDROFIZICHESKIYE ISSLEDOVANIYA (Marine Hydrophysical Investigations), Sevastopol', No 1(80), 1978.

8. Filippov, Ye. M., "Possibilities of the Roentgenofluorescent Method for Determining the Salt Composition of Sea Water," Article deposited at the All-Union Institute of Scientific and Technical Information, 12 November 1979, No 3842-79DEP.

9. Filippov, Ye. M., "Use of Californium Neutron Sources for Determining the Main Salt-Element Composition of Sea Water Under Natural Conditions," ATOMNAYA ENERGIYA (Atomic Energy), Vol 47, No 4, 1979.

10. Filippov, Ye. M., "Prospects for the Use of the Neutron Activation Method in Natural Oceanological Investigations," Article deposited at the All-Union Institute of Scientific and Technical Information, 13 February 1980, No 853-80DEP.

11. Wiggins, P. F. and Athow, K. Y., "Salt Water Chlorine Ion Determination by Neutron Capture Gamma Rays," NAVAL ENGINEERS J., No 5, 1971.

UDC 556.(166.4+047+013):551.501.81

USE OF RADAR DATA IN A HYDRODYNAMIC MODEL OF RAINWATER RUNOFF WITH DISTRIBUTED PARAMETERS

Moscow METEOROLOGIYA I GIDROLOGIYA in Russian No 3, Mar 81 pp 86-92

[Article by V. A. Rumyantsev, candidate of technical sciences, and S. A. Kondrat'yev, State Hydrological Institute, manuscript received 5 Sep 80]

[Text]

Abstract: In the example of the rainwater high-water hydrograph for the Polomet' River the authors tested a model of formation of rainwater runoff with distributed parameters which makes it possible to take into account the topography of the watershed, the spatial variability of the hydrophysical properties of soils in the basin and evaporation from the watershed surface. In the computations use was made of information on the precipitation fields determined both by the radar method and using data from the surface precipitation-gaging network. The results of the computations made it possible to detect the inadequacy of these fields, which is attributable to inadequately perfect radar set calibration.

During recent years more and more studies have appeared in the hydrological literature which are devoted to models of rain-induced runoff. These are based on the equations of motion of a fluid known from hydrodynamics [7]. However, these models have not yet been used in computations and predictions of rain-induced runoff because one of their basic advantages, the possibility of taking into account the spatial variability of the input parameters, can be realized fully only when there is thorough information on the hydrophysical properties of soil and ground and information on the field of precipitation. The latter can be obtained using the radar method for measuring precipitation. Today individual studies are known in which the materials from radar measurements are used primarily in determining the mean precipitation quantities for the basin and the conversion to the runoff hydrograph is accomplished using graphic dependences [3] with use of models of runoff with concentrated parameters [4] and linear conceptual runoff models [4, 10, 11]. In contrast to those mentioned, in this study an attempt is made in the example of the Polomet' River basin (Dvorets village) with a watershed area of

432 km^2 to demonstrate the possibility of using data on the precipitation field, obtained using the radar measurement method, in a hydrodynamic model of formation of rain-induced runoff.

An automated complex for the radar measurement of precipitation was introduced in the territory of the Valdayskaya Scientific Research Hydrological Laboratory imeni V. A. Uryvayev, situated at a distance of 10 km from the Polomet' River watershed, in July 1978. It includes a meteorological radar (MRL-2), the special "Osadki" apparatus, developed by the Central Aerological Observatory [2] and the ASVT M-6000 controlling electronic computer. The automated radar measuring complex makes it possible to measure the instantaneous intensity of atmospheric precipitation in a radius 100 km around Valday each 5 minutes and represent it at a real time scale in the form of a punched card for the mean intensity of precipitation for elementary grid squares with an area of 10 x 10 km and simultaneously in the form of punched tapes with information for grid squares with an area of 3.3 x 3.3 km for the entire territory scanned by the radar. In addition, the hourly layer of precipitation and the sum of precipitation accumulated in 6 hours are printed out and punched out. The choice of the Polomet' River as the object of investigations is also attributable to the good study of the basin, which makes it possible to stipulate the spatial distribution of watershed characteristics.

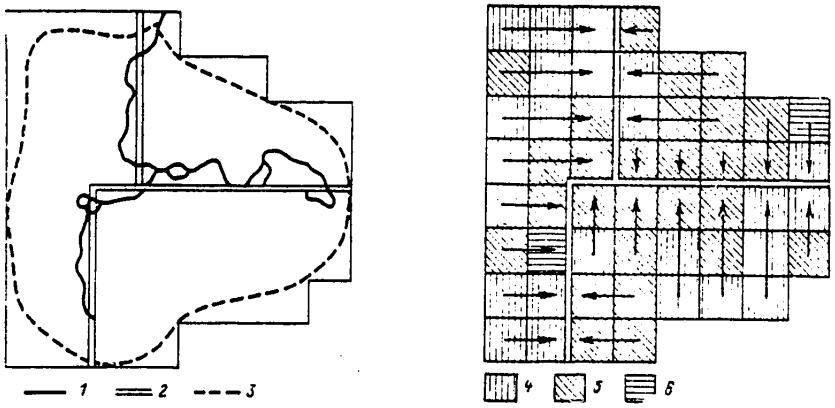

Fig. 1. Schematic representation of watershed and selected runoff directions. 1) actual channel, 2) schematic channel, 3) boundary of watershed, 4) sectors of watershed in which heavy clayey loams predominate, 5) light clayey loams and sandy loams, 6) swampy deposits.

In the Polomet' River basin surface runoff is observed extremely rarely; here there is a predominance of so-called "contact" [1] runoff. In this connection for computing the inflow into the channel network use was made of the following equation:

$$(m - W_{mmc}) \frac{\partial h}{\partial t} + \frac{\partial (kSh)}{\partial x} = R - E \qquad (1)$$

with the boundary conditions h(0, t) = h(x, 0) = 0. Here h is the intensity of "contact" runoff, m is ground porosity, W_{mmc} is minimum moisture capacity, k is a coefficient taking into account the hydraulic resistance of "contact" runoff, R and E are the intensities of precipitation and evaporation, x and t are the space and time coordinates.

In computing the transformation of the high-water wave in the channel we used the equation for a kinematic wave.

[p = ch(annel)]

$$\frac{\partial A}{\partial t} + \frac{\partial}{\partial y}\left(\frac{\sqrt{S_p}}{N}\frac{A^{\frac{5}{3}}}{P^{\frac{2}{3}}}\right) = q \qquad (2)$$

with the conditions A(0, t) = A(t), A(y,0) = A(y). Here A is the cross-sectional area, S_{ch} is channel slope, N is the Manning roughness coefficient, P is the wetting parameter, q is lateral inflow into the channel, y is the space coordinate.

The channels of the Polomet' River and its principal tributary, the Sosninka River, were approximated by linear segments (Fig. 1). In order for such an approximation not to exert an influence on the final result it is necessary to change the parameters of the schematic channel (slope and Manning roughness coefficient) in a definite way in comparison with the actual values. The relationship of the parameters can be obtained from the condition of equality of the travel time for the initial and schematic channels. For determining the travel time t_{run} we used a formula from [7]

$$t_{run} = \left(\frac{LN}{S_p^{\frac{1}{2}} q^{\frac{2}{3}}}\right)^{\frac{3}{5}}, \qquad (3)$$

where L is channel length.

By stipulating the drop in elevations Δ by the parameters of the initial channel N', S'_{ch}, L' and the length of the schematic channel by L, it is possible to determine the slope $S = \Delta/L$ and then from the condition of equality of the travel time for both cases, taking into account that $q = q'L'/L$, it is possible to obtain the relationship between the roughness coefficients

$$N = N'\left(\frac{L'}{L}\right)^{\frac{13}{6}}. \qquad (4)$$

For the approximation adopted in this problem we obtained S_{ch} = 1.5%, N = 4N'.

The computations were made for the high water passing during the period 5-20 August 1979, caused by rains falling during the period 5-7 August.

In formulating the initial conditions it was assumed that the low pre-high-water river runoff occurs at the expense of the ground water supply, virtually not changing during the time of high water. The intensity of water supply ensuring a stipulated pre-high-water discharge at the lowest-lying station was stipulated as the initial condition for channel flow. This made it possible to obtain stable values of the parameters characterizing the channel flow prior to the onset of high water and after its ending.

The slope in the direction of runoff was determined for computing the inflow into the channel network on the basis of an analysis of the topography for each of 53 grid squares with an area of 3.3 x 3.3 km covering the Polomet' River watershed.

Then a schematic mapping of soil types was carried out (Fig. 1). A determination of the soil type for each grid square was made in accordance with the maximum percentage of the area occupied by different soils. It was found that in 24 grid squares there was a predominance of heavy clayey loams, in 27 -- light clayey loams and sandy loams, and in two -- swampy deposits. We note in passing that there was not a single grid square in which sand predominated (in the watershed as a whole it occupied about 4% of the area). The grid squares were similarly classified as "field" and "wooded."

Depending on the type of soils, on the basis of observations made by N. I. Kapotova and A. A. Kapotov, specialists at the All-Union Scientific Research Hydrological Laboratory, and on the basis of data in the literature, for each grid square we established its porosity and minimum moisture capacity values: for heavy clayey loams $m = 0.33$ and $W_{mmc} = 0.27$; for light clayey loams and sandy loams $m = 0.36$ and $W_{mmc} = 0.25$; for swampy deposits $m = 0.96$ and $W_{mmc} = 0.83$. The evaporation intensities were stipulated on the basis of the mean monthly evaporation values for August as given by S. F. Fedorov [8]: for wooded sectors it was assumed that $E = 0.11$ mm/hour, for field sectors $E = 0.096$ mm/hour. The intradiurnal change in evaporation intensity was not taken into account. The initial moistening W_0 was stipulated on the basis of the moisture content in Tayezhnyy ravine (an analog for wooded sectors in the Polomet' River basin) and Usad'yevskiy ravine (an analogue for field sectors): $W_{0\ wood} = 0.209$ (3 August) and $W_{0\ field} = 0.25$ (30 July). The initial moisture reserves for swampy sectors were determined by a method proposed by O. I. Krestovskiy [5] on the basis of the pre-high-water runoff of the Polomet' River. According to an estimate which was made, the losses prior to the onset of runoff from swamps should be 75 mm. It was assumed that the runoff begins only after the moisture content attains the minimum moisture capacity values in the half-meter soil layer.

As pointed out by N. F. Befani [1], the rate of runoff of "contact" water is many times greater than the rate of ground water movement. In this connection it can be said that the k coefficient in formula (1), which when it was obtained was interpreted as the filtration coefficient, lost its initial sense here and describes the hydraulic resistance not only of intrasoil runoff, but also of the fine network of rills. Therefore, for different sectors it was stipulated in the form

$$k_i = a_i k_0,$$

here k_0 is a correction factor taking into account the runoff of water in the fine network of rills, which was assumed to be identical for different soil types.

The differences in the filtration capacity of the soils were taken into account by means of the coefficients a_i, which were stipulated from the condition of maintenance of the relationships between the filtration coefficients. On the basis of data in the literature we adopted the following values of the a_i coefficients: for heavy clayey loams $a_i = 0.1$, for light clayey loams and sandy loams $a_i = 1$, and for swampy deposits $a_i = 5$.

Thus, in the computations we took into account:
a) the spatial-temporal variability of the intensity of precipitation;
b) the spatial change in watershed surface slopes;
c) the spatial change in the hydrophysical characteristics of soils: porosity, minimum moisture capacity, filtration coefficient;

d) spatial change in the intensity of evaporation in dependence on the nature of vegetation;
e) spatial change in initial moisture supplies.

The channel roughness coefficient was taken from the tabulated data in [9] and was equal to 0.025. The k_0 coefficient was determined inversely from the condition of best agreement of the maxima of the computed and observed hydrographs [7]. A numerical realization of equations (1) and (2) was realized on the basis of an explicit finite-difference scheme for the approximation of differential operators, based on an expansion of the solution for the continuity equation

$$\frac{\partial h}{\partial t} + \frac{\partial Q}{\partial x} = q$$

into a Taylor series [7]. If the h values are known at the points of intersection of the i-th time layer of a selected uniform grid, the values at the points of intersection of the (i+1)-st layer are computed using the formula

$$h_j^{i+1} = h_j^i + \left(- \frac{Q_{j+1}^i - Q_{j-1}^i}{2\Delta x} + q_j^i \right) \Delta t + \left[\frac{D_{j+1}^i + D_j^i}{2\Delta x} \left(\frac{Q_{j+1}^i - Q_j^i}{\Delta x} - \right. \right.$$
$$\left. - \frac{q_{j+1}^i + q_j^i}{2} \right) - \frac{D_j^i + D_{j-1}^i}{2\Delta x} \left(\frac{Q_j^i - Q_{j-1}^i}{\Delta x} - \frac{q_j^i + q_{j-1}^i}{2} \right) + \tag{5}$$
$$\left. + \frac{q_j^i - q_j^{i-1}}{\Delta t} \right] \frac{\Delta t^2}{2},$$

where $D = \partial Q / \partial h$; Δx, Δt are the spatial and temporal integration intervals; j is an index for the grid points along the spatial axis.

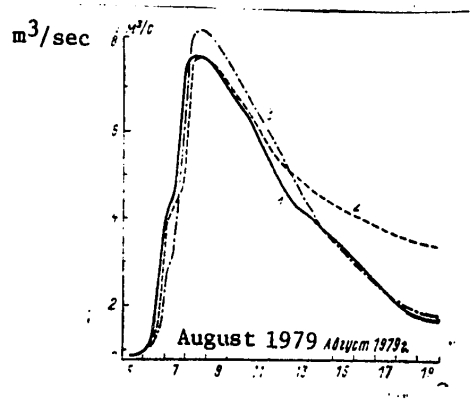

Fig. 2. Observed runoff hydrograph (1) for Polomet' River (Dvorets village) from rains of 5-7 August 1979; hydrographs computed using radar information on the precipitation fields (2) and data from surface precipitation-gaging network (3).

The runoff hydrograph, computed using radar information on the precipitation fields, is shown in Fig. 2. The value of the k_0 parameter, obtained inversely, was 3.65 m/min. The distribution of the precipitation layer over the area of the watershed, according to radar data, is shown in Fig. 3a. Comparing the constructed

hydrograph with the observed hydrograph, it is easy to see that during the dropoff the computed water discharge values somewhat exceed the observed values. The reason for this is an exaggeration of the radar data for the intensity of precipitation in the right part of the watershed, as is indicated, in our opinion, by a monotonic increase in this direction of the intensity of precipitation at any moment in time and the layer of precipitation during the entire period of falling of rain (Fig. 3a). As a confirmation of this we computed the same high water with the use of data from the surface precipitation gage network. The presence of 44 pluviographs within the Polomet' River watershed makes possible a sufficiently good description of the spatial variability of precipitation.

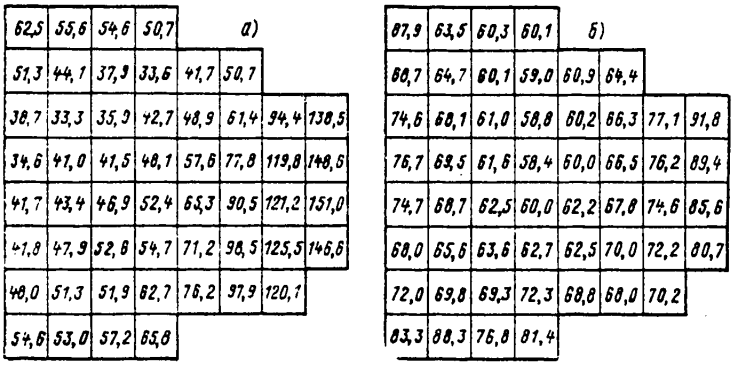

Fig. 3. Spatial distribution of precipitation layer during period 5-7 August 1979 according to radar data (a) and according to data from surface precipitation gage network (b).

The hourly precipitation layers obtained on the basis of pluviographic data were interpolated at the points of intersection in a uniform grid with an interval of 1.1 km with subsequent averaging for each of the earlier defined grid squares. The interpolation was based on an approximation of the precipitation field by a second-degree polynomial of the coordinates and was accomplished in accordance with a program prepared at the Computation Center of the State Hydrological Institute by O. M. Tolshina and N. A. Livanova. The distribution of the layer of precipitation according to surface data is shown in Fig. 3b. The hydrograph, computed using surface data with the former value of the k_0 parameter, is shown in Fig. 2. Some increase in the maximum of the computed hydrograph is attributable to the fact that in the left and central parts of the watershed the data from the surface precipitation gage network are greater than the radar data, as can be seen in Fig. 3. The good correspondence of the forms of the computed and observed hydrographs, and the coincidence of the time of onset of the maximum for both hydrographs, indicates the adequacy of the model and the correctness of a priori stipulation of the numerical values of the parameters. An improvement in the results of computations for the dropoff of the hydrograph when using data from the surface

precipitation gage network confirms the assumption made that there is an exaggeration of the radar data, and accordingly, is evidence of a definite noncorrespondence of the precipitation fields obtained using data from the surface network and by the radar method. The reason for this is that the radar was calibrated with calibration coefficients constant over the area and using precipitation layers averaged for the watershed [6], which in both cases virtually coincide. In this connection further work must be done for improving the method for radar measurement of precipitation for the purpose of obtaining calibration coefficients varying over the area of the watershed in accordance with its local orography. In the event of a successful solution of this problem it can be hoped that the accuracy of radar data on the precipitation fields will not be lower than the accuracy of the data from the surface network and due to the routineness in collection of radar information there will be a substantial broadening of the region of application of the described hydrodynamic model with distributed parameters.

At the present time work is being carried out for refining the physical picture of formation of rainwater runoff in the basin of the Polomet' River. Although work on the model was directed for the most part to solution of methodological problems, it is proposed that it be brought to the stage of introduction into practical, routine short-range forecasts for ensuring support for an optimum regime for the operation of melioration systems in the lower part of the Polomet' River basin. In addition, the model may prove useful in simulation work for evaluating the influence of different kinds of agricultural and forestry melioration measures on the formation of rainwater runoff in the basin. When carrying out numerical experiments an allowance for such measures can be made by stipulating the soil characteristics of the watershed or its topography modified for the reasons indicated above. In solving the formulated problems, in addition to improving radar calibration, it is also necessary to make an evaluation and choice of the optimum interval with stipulation of the hydrophysical characteristics of soils and topography in the watershed.

BIBLIOGRAPHY

1. Befani, N. F., PROGNOZIROVANIYE DOZHDEVYKH PAVODKOV NA OSNOVE TERRITORIAL'NO OBSHCHIKH ZAVISIMOSTEY (Prediction of Rain-Induced High Waters on the Basis of Territorially General Dependences), Leningrad, Gidrometeoizdat, 1977.

2. Beryulev, G. P., Yevpryakov, V. A., Kostarev, V. V., Mel'nichuk, Yu. V. and Chernikov, A. A., "Apparatus for Measuring the Quantity of Liquid Precipitation in an Area Using a Single-Wavelength Meteorological Radar," TRUDY TsAO (Transactions of the Central Aerological Observatory), No 121, 1975.

3. Dzhordzhevich, N. T. and Miokovich, M., "Methods for Predicting Rain-Induced High Waters With a Special Review of Experiments for Use of a Radar in Operational Forecasting," SBORNIK DOKLADOV X KONFERENTSII PRIDUNAYSKIKH STRAN PO GIDROLOGICHESKIM PROGNOZAM (Collection of Reports at the Tenth Conference of Danubian Countries on Hydrological Forecasts), Vienna, 1979.

4. Koren', V. I., "On Use of Radar Measurements of Precipitation for Predicting Rain-Induced High Waters," TRUDY GIDROMETTSENTRA SSSR (Transactions of the USSR Hydrometeorological Center), No 191, 1977.

5. Krestovskiy, O. I., "Investigation of Runoff and the Water Balance of Watersheds," TRUDY GGI (Transactions of the State Hydrological Institute), No 176, 1969.

6. Livanova, N. A. and Uryvayev, A. P., "Computation of the Intensity of Precipitation Using Data From Radar and Pluviographic Measurements," TRUDY GGI, No 258, 1979.

7. Rumyantsev, V. A. and Kondrat'yev, S. A., "Mathematical Modeling in Hydrology. Kinematic-Wave Model of Slope Runoff," GIDROMETEOROLOGIYA. GIDROLOGIYA SUSHI. OBZORNAYA INFORMATSIYA (Hydrometeorology, Hydrology of the Land, Review Information), Obninsk, No 1, 1975.

8. Fedorov, S. F., "Results of Investigation of the Hydrological Role of the Forest," TRUDY GGI, No 176, 1969.

9. Chugayev, R. R., GIDRAVLIKA (Hydraulics), Leningrad, Energiya, 1975.

10. Anderl, B., Attmannspacher, W. and Schultz, G. A., "Accuracy of Reservoir Inflow Forecasts Based on Radar Rainfall Measurements," WATER RESOUR. RES., Vol 12, No 2, 1976.

11. Schultz, G. A. and Klatt, P., "Use of Data From Remote Sensing Sources for Hydrological Forecasting," PROC. OF THE OXFORD SYMPOSIUM. IAHS-AISH PUBL. No 129, 1980.

UDC 556.164

EXPERIMENTAL SUBSTANTIATION OF COMPUTATIONS OF THE RATE OF WATER FLOW ALONG THE CULTIVATED SURFACE OF SLOPES

Moscow METEOROLOGIYA I GIDROLOGIYA in Russian No 3, Mar 81 pp 93-96

[Article by G. V. Kostsov, candidate of technical sciences, Voronezh Agricultural Institute, manuscript received 9 Jun 80]

[Text]

Abstract: On the basis of experimental investigations of the influence of runoff and slope on the rate of water flow along the cultivated surface of different types of soil and ground the author has derived a formula for computing the rate of water runoff in individual sectors of plowed slopes.

Investigations of the nature of change in the rate of water runoff along a loosened soil surface as a function of runoff discharge volume and the degree of slope were carried out experimentally in the laboratory at the Voronezh Agricultural Institute.

A special hydraulic flume was used in making the investigations. The working length of the flume was 2.0 m and its width was 0.4 m. At the head of this flume there was a device for inlet of regulated water volumes in the form of a water layer uniformly distributed in the width of the flume. Ground or soil was loaded in the trough. A screw-type hoisting mechanism made it possible to impart different slopes to the flume. A detailed description of the design of this apparatus was given in an earlier published paper [1].

The water volumes fed into the upper part of the flume were varied in the range from 0.05 to 0.26 liter/second and the surface slope was varied from 0.01 to 0.16. The number of different variations of the water quantity fed into the flume was 5 and the number of slope variations was from 6 to 8. Each experiment was repeated twice. The duration of each experiment (with a fixed discharge and slope) was 10 minutes. After its completion the ground or soil surface was restored. The runoff rate was determined in the interval from the third to the fifth minute from the beginning of each experiment by the introduction of a special dye into the water.

The runoff rate was computed using the formula

$$v = \frac{L}{t}, \tag{1}$$

where L is the length of the flume in meters; t is the time required for the dyed fluid to pass from the flume, registered by a stopwatch, in seconds.

The design of the hydraulic flume and the method adopted for carrying out the experiments ensured the formation of rates of water runoff which in absolute value were as close as possible to the local rates observed on individual slope sectors.

The ground or soil loaded into the flume was first saturated for a rather long time (not less than a day) with water to the point of total moisture capacity. The lumpy surface of the soil present in the flume had a roughness extremely close to the roughness of a plowed field. Thus, when conducting the experiments there was a sort of simulation of the conditions for the runoff of meltwater along a thawing surface of a plowed slope.

In the course of the formulated experiment we studied the nature of the change in the rate of water runoff along the loosened surface of gray forest and chernozem soils, as well as sandy ground. In addition, allowance was made for the sheet erosion of these types of soil and ground. The method for making such an allowance was set forth in studies published earlier [1, 2]. The corresponding values of the total sheet erosion obtained with identical discharges and slopes are given in the table.

In carrying out the experiments it was noted that with the runoff of water along the surface of the tested samples there is formation of a network of microjets. Their number and configuration change with time, which causes corresponding variations of different hydrodynamic characteristics. For example, the depths of the microjets, the hydraulic radii and the slopes of the forming channels change somewhat. Such a phenomenon is especially characteristic for easily eroded types of ground and soil.

The rates of water runoff observed in the course of the experiments were varied in a rather wide range. The greatest rates were observed in the case of easily eroded types of soil and ground. The minimum rates were observed with soil and ground types which are not easily eroded. The limits of variation of these rates are indicated in the table.

In virtually all cases (except for individual cases of the runoff of water in small volumes and with minimum slopes) there was a turbulent regime of water movement since the Reynolds number was more than 300.

On the basis of the results of a preliminary analysis, and also taking into account already available investigations of this question, the considered dependence was approximated in the following way:

$$v = a\, Q^m I^n, \tag{2}$$

where v is the rate of water runoff; a is a parameter characterizing the roughness of the underlying surface; Q is the runoff per unit width of slope; I is surface slope; m and n are the corresponding exponents.

The values of the parameters of this dependence were computed by the mathematical processing of data from 675 experiments carried out with a YeS-1020 electronic computer.

The established values of the exponents m and n were varied in the following range: m -- from 0.28 to 0.52; n -- from 0.36 to 0.47. Accordingly, taking into account the relatively small ranges of their variation, henceforth with some approximation we have used their mean arithmetical values, which in both cases were 0.4.

After such a transformation and the introduction of the correction factor k formula (2) was reduced to the following form:

$$v = kaQ^{0.4}I^{0.4}. \qquad (3)$$

The introduction of the factor k is attributable to the circumstance that during the period of runoff of water along the plowed slope the resistance of the underlying surface somewhat decreases with time and the rate of runoff increases because there is a gradual straightening of the runoff channels and a smoothing of roughness elements.

The value of the k factor varies in dependence on the duration of runoff and in this stage in the study can be estimated only approximately. Thus, on the basis of the materials from these investigations and generalizing already available data on this question [3] it can be assumed equal to 1.10-1.15.

In formula (3) the dimensionality of the rate of water runoff is expressed in meters per second, runoff discharge in liters per second per 1.0 m of slope width and slope in promille. The corresponding values of the a parameter are given in the table.

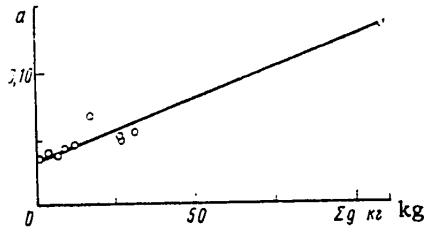

Fig. 1. Graph of the dependence of the a parameter on the degree to which different types of soils and ground are subject to sheet erosion.

A subsequent analysis indicated that the values of the a parameter are dependent on the degree to which different types of soils and ground are subject to sheet erosion, that is, on their erosional properties. The graph characterizing this dependence is represented by a straight line (see figure). The graph very clearly indicates the increase in the a parameter (decrease in roughness) with an increase in total sheet erosion ($\sum g$). This is attributable to the circumstance that during water runoff along a loosened surface of easily eroded ground and soil the water velocity will be greater than when the water flows over soils which are not easily eroded. In the latter case an influence will be exerted by the greater sinuosity

Table 1

Total Sheet Erosion ($\sum g$), Limits of Change in Observed Rates (A) and Values of a Parameter in Formula (3)

Ground, soil	$\sum g$, kg	A m/sec	a	Mean relative deviation v_{comp} from v_{obs}
Sand, medium grain size	108.89	0.17-0.56	0.132	0.083
Light gray forest sandy loam soil	16.90	0.06-0.34	0.064	0.137
Gray forest medium clayey loam soil	0.66	0.05-0.15	0.033	0.100
Leached heavy clayey loam chernozem	4.16	0.05-0.15	0.036	0.096
Leached heavy clayey loam chernozem	31.16	0.06-0.24	0.052	0.108
Leached heavy clayey loam chernozem	6.39	0.06-0.16	0.036	0.105
Typical light clayey chernozem	8.48	0.05-0.19	0.040	0.088
Typical medium clayey chernozem	11.47	0.06-0.18	0.043	0.107
Ordinary medium clayey chernozem	26.81	0.06-0.25	0.049	0.127
Southern light clayey chernozem	27.14	0.05-0.23	0.051	0.097

and roughness of the microchannels forming during water runoff along the loosened surface of these soils.

The accuracy of the computations of the rate of water runoff made using formula (3) can be evaluated on the basis of the mean relative deviations of the computed velocity values (v_{comp}) from the observed velocities (v_{obs}), the values of which are given in the table.

In the above-mentioned form formula (3) can be used in computing the rate of runoff of meltwater on individual sectors of plowed slopes. The following values of the a parameter can be used: for sandy ground -- 0.130; for sandy loam -- 0.050-0.065; for clayey loam and clayey soils -- 0.035-0.060. In the latter case the highest values of the a parameter must be used for easily eroded soils and the minimum values must be used for soils more resistant to erosion.

BIBLIOGRAPHY

1. Kostsov, G. V., "Problems and Methods for Experimental Study of the Processes of Sheet Erosion of Different Types of Soil and Ground," REGULIROVANIYE STOKA, SEL'SKOKHOZYAYSTVENNAYA MELIORATSIYA I ZASHCHITA ZEMEL' OT VODNOY EROZII V TSENTRAL'NO-CHERNOZEMNOY ZONE. NAUCHNYYE TRUDY VORONEZHSKOGO SKhI (Regulation of Runoff, Agricultural Melioration and Protection of Soils Against Water Erosion in the Central Chernozem Zone. Scientific Transactions of the Voronezh Agricultural Institute), Vol 69, Voronezh, 1975.

2. Kostsov, G. V., "Some Results of Experimental Study of the Patterns of Sheet Erosion from Slopes," ZEMEL'NYYE FONDY TSENTRAL'NO-CHERNOZEMNOY ZONY I VOPROSY IKH RATSIONAL'NOGO ISPOL'ZOVANIYA. NAUCHNYYE TRUDY VORONEZHSKOGO SKhI (Land Resources of the Central Chernozem Zone and Problems in Their Rational Use. Scientific Transactions of the Voronezh Agricultural Institute), Vol 80, Voronezh, 1976.

3. Shvebs, G. I., FORMIROVANIYE VODNOY EROZII, STOKA NANOSOV I IKH OTSENKA (Formation of Water Erosion, Runoff of Sediments and Their Evaluation), Leningrad, Gidrometeoizdat, 1974.

UDC 551.578.7:633.51

DETERMINATION OF DAMAGE TO COTTON PLANTS IN DIFFERENT DEVELOPMENT STAGES RESULTING FROM HAILFALLS

Moscow METEOROLOGIYA I GIDROLOGIYA in Russian No 3, Mar 81 pp 97-102

[Article by K. Makhmudov, Administration of the Hydrometeorological Service of the Uzbek SSR, manuscript received 8 Sep 80]

[Text]

Abstract: On the basis of experimental investigations a study was made of different aspects of the influence of mechanical damage inflicted by hail on the growth, development and yield of cotton plants. It is shown that the greatest losses from hailfalls are observed when there is severe damage to the cotton plants during the period of maturing of the bolls, whereas the minimum damage occurs in the budding phase.

Introduction. Research work for clarifying the influence of hailfalls on the growth and development of cotton plants, insofar as is known to the author, was not carried out in our country or abroad up to the 1970's.

For the first time experiments for studying the influence of mechanical damage inflicted by hail on the growth and development of cotton plants under natural conditions were carried out by B. A. Kamalov [2]. Later M. Makhmudov [3] and the author [4, 5] studied the dynamics and biology of development of damaged cotton plants. The results of these experiments indicated that hailfalls during the period of development of cotton plants cause a considerable decrease in yield and a deterioration in the quality of the raw cotton.

Unfortunately, the mentioned studies were made on the basis of limited statistical data and did not take in all the phases of cotton plant development.

In this article we give some results of investigations for clarifying the influence of mechanical damage during the entire cotton plant growing season by means of simulation of hailfalls.

Method for producing artificial hailfalls. The artificial simulation of hailfalls was used for the first time by the American researchers H. Laude and A. Pauli [7]. They inflicted mechanical damage on different varieties of winter wheat by means of

Table 1

Influence of Mechanical Damage on Development of Cotton Plants

Date of damage	Damaged plots			Undamaged plots			Lag of damaged plants in development compared with undamaged, days			Time of onset of phases from day of damage, days		
	budding	flowering	opening of bolls	budding	flowering	opening of bolls	budding	flowering	opening of bolls	budding	flowering	opening of bolls
13 V	5 VI / 16 VI	2 VII / 15 VII	20 VIII / 2 IX	22 V / 30 V	24 VI / 3 VII	13 VIII / 23 VIII	14 / 17	8 / 12	7 / 10	23 / 34	50 / 63	99 / 112
28 V	8 VI / 17 VI	8 VII / 19 VII	24 VIII / 7 IX	23 V / 31 V	24 VI / 3 VII	13 VIII / 23 VIII	16 / 17	14 / 16	13 / 15	11 / 20	41 / 52	88 / 102
12 VI	21 VI / 3 VII	23 VII / 4 VIII	9 IX / 25 IX	22 V / 30 V	24 VI / 3 VII	14 VIII / 26 VIII	30 / 34	29 / 32	26 / 30	9 / 21	41 / 53	89 / 105
27 VI	6 VII / 17 VII	8 VIII / 20 VIII	24 IX / 15 X	22 V / 31 V	25 VI / 4 VII	14 VIII / 27 VIII	45 / 47	44 / 47	41 / 49	9 / 20	42 / 54	89 / 110
13 VII	20 VII / 1 VIII	16 VIII / 31 VIII	20 X / 6 XI	22 V / 1 VI	25 VI / 4 VII	14 VIII / 27 VIII	59 / 61	52 / 58	67 / 71	7 / 19	34 / 49	99 / 116
28 VII	5 VIII / 18 VIII	2 IX / 18 IX	Did not occur	22 V / 30 V	24 VI / 3 VII	13 VIII / 25 VIII	75 / 80	70 / 77	—	8 / 21	36 / 52	Did not occur
12 VIII	20 VIII / 4 IX	29 IX / 17 X	Did not occur	22 V / 1 VI	24 VI / 3 VII	14 VIII / 26 VIII	89 / 95	97 / 106	—	8 / 23	48 / 66	Did not occur

Note. The numerator indicates the onset of the development phase (10%) and the denominator gives the extent of this phase (60%).

APPROVED FOR RELEASE: 2007/02/09: CIA-RDP82-00850R000400030065-3

FOR OFFICIAL USE ONLY

inflicting impacts on the developing ear, knocking off some of the earlets, crushing the stems, etc.

In our experiment a hailfall was simulated in the following way: small stones with a diameter of 8-15 mm were tied, each individually, to a coarse string 70-100 cm in length. The opposite ends of the strings were collected into a bundle and tied to a small stick. The experimenter, holding the stick, rotating the stones in the vertical plane and bringing them into contact with the plants, inflicts damage to them to the desired degree. The length of the tied strings was dependent on the size of the stone: the greater its size, the longer the string. This ensured the uniform striking of the stones on the surface. The size of these stones was selected in accordance with the spectrum of sizes of natural hailstones [6].

The adequacy of this method for inflicting mechanical damage to cotton plants for simulating the process of a natural hailfall is illustrated in Fig. 1. This shows a cotton farm at the Sverdlov collective farm in Namanganskiy Rayon in the Uzbek SSR, which was subjected to a natural hailfall on 13 June 1977 (Fig. 1a) and an experimental field subjected to artificial mechanical damage by the already described method on 27 June 1978 at the Kalinin kolkhoz in Chustskiy Rayon in the Uzbek SSR (Fig. 1b). Both fields were in the phase of flowering of the cotton plant at the time of damage.

As is well known, the damage to gardens, vineyards, grains, legumes and other crops such as that shown in the photographs in Fig. 1 is called "100%" and in this case they do not give any yield. However, the cotton plant with such damage still gives some repeated yield. Accordingly, the degree of damage to the cotton plant can be determined only after collection of the harvest.

In all cases of our experiment the degree of damage was such that only the damaged stems without leaves and fruits remained, as is usually observed in natural hailfalls as a result of the falling of heavy hail with a diameter up to 1 cm and large hail.

Formulation of experiment. In the experiment we selected seven experimental plots in which mechanical damage was inflicted on the cotton plants. Each experimental plot had two control plots situated alongside the experimental plot in the same line relative to the sowing. The width of both the experimental and control plots was equal to two passes of a tractor with interrow working of the fields and therefore the plots measured 4.8 x 5.2 m (25 m^2). With such a size of the experimental and control plots the mean error in determining the yield [1] of the cotton plant is 10%, maximum 24%, minimum 0.1%. However, the error in determining the times of onset of development phases does not exceed one day.

In the first experimental plot artificial damage was inflicted on the cotton plants on 13 May 1978 in the phase of two-four true leaves, in the second plot -- on 28 May in the budding phase, in the third plot -- on 12 June, etc., with a 15-day interval. In the seventh plot damage was inflicted on 12 August 1978 in the phase of onset of opening of the bolls.

During the growing season for the cotton plants all agrotechnical measures in the experimental and control plots were the same. During the maturing of the bolls in the sown field, where the experiment was carried out, there was slight development

of the cotton aphid. For this reason no measures were taken for contending with pests.

Fig. 1. Fields damaged by natural (a) and artificial (b) hailfalls.

Phenological observations. Regular phenological observations were made beginning with the time of imparting the first artificial hailfall and continued to the end of the growing season. The results of these observations are given in Table 1.

The table shows that with damage to the cotton plants by hail in the early stage of their development there is a weaker development of repeated sprouts in comparison with plants damaged at later times of development. The analysis indicates that after strong mechanical damage the cotton plant on the average after 10-11 days gives new buds, after 42 days a flowering phase begins and after 93 days

the bolls begin to open. Thus the lag in development is from 7 to 67 or more days (depending on the date of damage) in comparison with the undamaged plants. It is noted that in the damaged plants there is an increase in the duration of each development phase. This increase is the greater the later the damage is inflicted.

Table 2

Influence of Mechanical Damage on Cotton Plant Yield

Date of damage	Plot	Number of bolls		Total yield of raw cotton		Yield per boll, g		
		total	scaled to one plant	kg	tsentner/hectare	raw cotton	seeds	fiber
13 V	Damaged	1252	6,7	5,4	21,6	4,30	2,77	1,53
	Undamaged	1388	5,7	7,1	28,4	5,13	3,32	1,81
	Difference	−136	+1,0	−1,7	−6,8	−0,83	−0,55	−0,28
	%	−9,8	+17,5	23,9	−23,9	−16,2	−16,6	−15,5
28 V	Damaged	1390	5,4	6,3	25,2	4,53	3,00	1,53
	Undamaged	1438	6,0	7,8	31,2	5,44	3,53	1,91
	Difference	−48	−0,6	−1,5	−6,0	−0,91	−0,5	−0,38
	%	−3,3	−10,0	−19,2	−19,2	−16,7	−15,0	−19,9
12 VI	Damaged	1438	5,8	6,1	24,4	4,24	2,79	1,45
	Undamaged	1960	6,6	8,6	34,4	5,12	3,26	1,86
	Difference	−522	−0,8	−2,5	−10,0	−0,88	−0,47	−0,41
	%	−26,6	−12,1	−29,1	−29,1	−17,2	−14,4	−22,0
27 VI	Damaged	1237	4,3	4,6	18,4	3,69	2,45	1,24
	Undamaged	1658	6,1	9,2	36,8	5,52	3,52	2,00
	Difference	−421	−1,8	−4,6	−18,4	−1,83	−1,07	−0,76
	%	−25,4	−29,5	−50,0	−50,0	−33,2	−30,4	−38,0
13 VII	Damaged	423	1,5	1,4	5,6	3,37	2,12	1,25
	Undamaged	1599	5,8	8,8	35,2	5,52	3,56	1,96
	Difference	−1176	−4,3	−7,4	−29,6	−2,15	−1,44	−0,71
	%	−73,5	−74,1	−84,1	−84,1	−38,9	−40,4	−36,2
28 VII	Damaged	85	0,3	0,2	0,8	2,86	1,82	1,04
	Undamaged	1269	4,9	6,1	24,4	4,84	3,08	1,76
	Difference	−1184	−4,6	−5,9	−23,6	−1,98	−1,26	−0,72
	%	−93,3	−93,9	−96,7	−96,7	−40,9	−40,9	−40,9
12 VIII	Damaged	83	0,3	0,2	0,8	2,96	1,88	1,08
	Undamaged	1596	6,1	8,1	32,4	5,09	3,24	1,85
	Difference	−1513	−5,8	−7,9	−31,6	−2,13	−1,36	−0,77
	%	−94,8	−95,1	−97,5	−97,5	−41,8	42,0	−41,6

Observations of the growth and development of damaged plants indicate that strong mechanical damage in the early stage in development of the cotton plant considerably decreases the density of the plant stand. For example, at the time of inflicting the first artificial hailfall on the experimental plot, where cotton plants were damaged on 13 May 1978 in the phase of two-four true leaves, there was a total of 284 plants, and a month after damage there were 188 remaining, that is, the density of the plant stand had decreased by 33.8%, which was not observed in the case of later damage. Similar data for a definite phase in the development of the cotton plant were obtained earlier during natural hailfalls [3, 4].

Results of yield analysis. With the opening and maturing of the cotton bolls the cotton was harvested several times. The number of bolls in the experimental and control plots was counted for all the experimental variants. The results of the yield analysis are given in Table 2. The table shows that the mechanical damage inflicted on the cotton plant by hail in all phases of its development causes a decrease in the yield and a deterioration in the quality of the raw cotton. This occurs both due to a decrease in the mean number of bolls, scaled to one plant (by 15-95%), and due to a decrease in the mean weight of the raw cotton per boll (by 50-42%). It is noted that the later the mechanical damage to plants occurs, the greater are the losses and the worst is the deterioration in quality of the yield.

A decrease in cotton yield of cotton plants subjected to strong damage in the early stage of development for the most part occurs due to a decrease in the density of the plant stand. But a decrease in the density of the plant stand during this period favors the accumulation of a great number of bolls, scaled to one plant, which is not observed in other periods. As we see, the yield losses from strong mechanical damage to the cotton plants are from 19 to 97%.

On the basis of the results it was possible to ascertain the dependence of the losses to the cotton yield on the date of damage (Fig. 2). It can be seen that the maximum losses are observed when there is strong damage to the cotton plants during the period of maturing of the bolls and the minimum losses are observed when there is strong damage in the budding phase. Such a dependence is confirmed by the results of experiments carried out during natural hailfalls on cotton fields (see Fig. 2). It makes it possible to establish the magnitude of the postulated losses from hailfalls during the entire growing season for cotton plants.

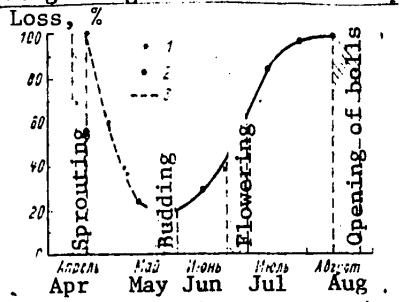

Fig. 2. Dependence of yield losses on date of hailfall. 1) results obtained during natural hailfalls on cotton fields; 2) results obtained with artificial hailfall on cotton fields; 3) losses which occur under production conditions due to resowing of cotton plants.

Summary

After analyzing the results of these experiments the following conclusions can be drawn:

1. In cases of a strong hailfall on cotton fields there is a lag in growth and development of 10-70 or more days in dependence on the date of damage.

2. Hailfalls in the early stage of cotton plant development cause a decrease in the yield for the most part due to a decrease in the density of the plant stand (by 24-44%).

3. Hailfalls exert a negative influence on the quality of the yield of cotton plants and there is a decrease in the yield of raw cotton, seeds and fiber from one boll (by 15-42%).

4. In general, the strong mechanical damage caused by hail reduces the yield of cotton by 19-97% in dependence on the date of the hailfall.

BIBLIOGRAPHY

1. Dospekhov, B. A., METODIKA POLEVOGO OPYTA (Field Experimentation Methods), Moscow, Kolos, 1968.

2. Kamalov, B. A., "Economic Effectiveness of Antihail Work," TRUDY SARNIGMI (Transactions of the Central Asian Regional Scientific Research Hydrometeorological Institute), No 16(97), 1975.

3. Makhmudov, M., "Influence of Hailfalls on the Growth and Development of Cotton," TRUDY SARNIGMI, No 35(116), 1975.

4. Makhmudov, K., "Influence of Hailfalls on the Growth and Development of Cotton Plants," TRUDY SARNIGMI, No 67(148), 1979.

5. Makhmudov, K., "Hailfalls and Cotton Yield," TRUDY SARNIGMI, No 90(171), 1980.

6. Chepovskaya, O. I., "Preliminary Results of Investigation of Hail Distribution Over the Earth's Surface," TRUDY VGI (Transactions of the High-Mountain Geophysical Institute), No 3(5), 1966.

7. Laude, H. and Pauli, A., "Simulated Hail Injures Winter Wheat," AGRICULT. EXPERT. STAT. KANSAS STATE COLLEGE OF AGRICULT., Bull. 402, 1952.

UDC 551.509.324.2(574)

IMPROVEMENT IN THE METHOD FOR PREDICTING THE INTENSITY AND QUANTITY OF PRECIPITATION IN A WARM PERIOD

Moscow METEOROLOGIYA I GIDROLOGIYA in Russian No 3, Mar 81 pp 103-106

[Article by A. T. Kenzhibayev and I. A. Petrichenko, candidate of physical and mathematical sciences, USSR Hydrometeorological Scientific Research Center, manuscript received 2 Jul 80]

[Text]

Abstract: The transformation of formulas for the prediction of precipitation is presented. These formulas are based on allowance for data on air humidity and the liquid-water content of clouds for the purpose of use of information on air humidity and temperature available under operational conditions. Analytical formulas are given for predicting the intensity, duration and quantity of precipitation and also regression analysis formulas for refining the computations applicable to the territory of Kazakhstan in the warm period.

This investigation is an improvement of the method for predicting the intensity and quantity of precipitation applicable to the territory of Kazakhstan with allowance for change in humidity and liquid-water content of clouds proposed by I. A. Petrichenko in [4]. Using this method the prediction of intensity I_h and the quantity of precipitation Q is accomplished in the coordinate system x, y, z, t using the formulas

$$I_h = -\int_h^H \rho \frac{dq}{dt}\,dz - \int_h^H M \operatorname{div}_{xy} C\,dz - \int_h^H \left(U\frac{\partial M}{\partial x} - V\frac{\partial M}{\partial y}\right)dz; \tag{1}$$

$$Q = -\int_0^t\int_h^H \rho \frac{dq}{dt}\,dz\,dt - \int_0^t\int_h^H M \operatorname{div}_{xy} C\,dz\,dt - \int_0^t\int_h^H \left(U\frac{\partial M}{\partial x} + V\frac{\partial M}{\partial y}\right)dz\,dt,$$

where ρ is air density, q is specific humidity at maximum saturation, C, U, V are velocity and the components of the velocity of movement of solid and fluid elements, M is the water mass in the liquid and solid phases in a unit air volume.

Equations (1) show that the intensity and quantity of any type of precipitation are dependent, first of all, on the decrease in specific humidity accompanying the vertical ascent of saturated air, and second, on the redistribution of water available in the clouds in the liquid and solid phases, and also on the structure of the vertical and horizontal air currents.

It should be noted that the peculiarities in the horizontal and vertical structure of air currents can be partially attributed to the lack of precipitation from already forming cloud cover over Kazakhstan in summer. Accordingly, for making computations of precipitation in this region it is desirable that equations (1) be used.

The principal difficulty in the practical realization of equations (1) involves the absence at the present time of information on the liquid-water content of clouds.

On the basis of [2, 3, 7] we have proposed a possible method for using additionally available information on air temperature and humidity instead of information on the liquid-water content of clouds.

We will use the equation for computing the liquid-water content of clouds and the continuity equation in the form

$$\frac{dM}{dt} = \frac{\partial}{\partial z}\nu\frac{\partial M}{\partial z}, \tag{2}$$

$$M\,\mathrm{div}_{xyz}\,\mathbf{C} = 0, \tag{3}$$

where M is the liquid-water content of clouds g/m^3, ν is the coefficient of vertical exchange within the clouds.

In concise form we will write the results of expansion of an individual derivative of the liquid-water content of clouds, with three-dimensional divergence of the velocity of their movement and with addition of the left- and right-hand sides of equations (2) and (3) in the form

$$\frac{\partial M}{\partial t} + \frac{\partial MU}{\partial x} + \frac{\partial MV}{\partial y} + \frac{\partial MW}{\partial z} = \frac{\partial}{\partial z}\nu\frac{\partial M}{\partial z}. \tag{4}$$

We will introduce the parameter of intensity of precipitation I equal to the value $M|W|$.

Transferring the first three terms in equation (4) into the right-hand side, we obtain the equation

$$\frac{\partial I}{\partial z} = \frac{\partial}{\partial z}\nu\frac{\partial M}{\partial z} - \frac{\partial M}{\partial t} - \left(\frac{\partial MU}{\partial x} + \frac{\partial MV}{\partial y}\right). \tag{5}$$

After integration of equation (5) from the condensation level h to the upper cloud boundary H and the assumption that the intensity of precipitation at the upper cloud cover boundary is equal to zero we have

$$I_h = \int_h^H \frac{\partial M}{\partial t}\,dz - \nu\frac{\partial M}{\partial z}\Big|_h^H + \int_h^H \left(\frac{\partial MU}{\partial x} + \frac{\partial MV}{\partial y}\right)\,dz. \tag{6}$$

We add the first equation from (1) and equation (6). After shortening of such terms the resultant intensity of precipitation at the condensation level will be determined by the equation

$$I_h = -\int_h^H \rho \frac{dq}{dt}\,dz + \int_h^H \frac{\partial M}{\partial t}\,dz - v\,\frac{\partial M}{\partial z}\Big|_h^H. \qquad (7)$$

In accordance with expression (7) the intensity of precipitation in the atmosphere is determined not only by macroscale atmospheric processes (first term), but also physical processes within the clouds (the last two terms).

In the absence of precipitation some of the atmospheric moisture content is expended on the formation and maintenance of cloud cover.

From equation (7), with some transformations taken into account, it is possible to derive prognostic equations (11)-(11'), making it possible to use information available from operational work.

In accordance with [1], the liquid-water content for cumulonimbus clouds can be expressed through the elasticity of water vapor saturation E in the following way:

$$M = 0{,}57E. \qquad (8)$$

The coefficient 0.57 was determined empirically for the territory of Kazakhstan.

The second and third terms in equation (7), taking expression (8) and the Clausius-Clayperon equation in the form $\frac{\partial E}{\partial T} = \frac{LE}{R_n T^2} = \frac{L\rho q}{T}$

into account can be represented in the following way:

$$\int_h^H \frac{\partial M}{\partial t}\,dz = 0{,}57\int_h^H \frac{\partial E}{\partial t}\,dz = 0{,}57\int_h^H \frac{\partial E}{\partial T}\frac{\partial T}{\partial t}\,dz = 0{,}57\,L\int_h^H \frac{\rho q}{T}\frac{\partial T}{\partial t}\,dz, \qquad (9)$$

$$v\,\frac{\partial M}{\partial z}\Big|_h^H = 0{,}57\,v\,\frac{\partial E}{\partial z}\Big|_h^H = 0{,}57\,v\,\frac{\partial E}{\partial T}\frac{\partial T}{\partial z}\Big|_h^H = -0{,}57\,v\,L\,\frac{\rho q}{T}\,\gamma'_{Ba}\Big|_h^H, \qquad (10)$$

where L is the specific heat of vaporization (condensation), the remaining notations are generally known.

Taking (9) and (10) into account, from equation (7) we obtain the principal prognostic equations (11)-(11'), which can be used in a numerical hydrodynamic forecast of the intensity and quantity of precipitation on an electronic computer, in particular, for the territory of Kazakhstan:

$$I_h = -\int_h^H \rho \frac{dq}{dt}\,dz + 0{,}57\,L\int_h^H \frac{\rho q}{T}\frac{\partial T}{\partial t}\,dz + 0{,}57\,L\,v\,\frac{\rho q}{T}\,\gamma'_{Ba}\Big|_h^H,$$

$$Q = -\int_0^t\int_h^H \rho \frac{dq}{dt}\,dz\,dt + 0{,}57\,L\int_0^t\int_h^H \frac{\rho q}{T}\frac{\partial T}{\partial t}\,dz\,dt + \qquad (11)$$

$$+\int_0^t 0{,}57\ L\nu\ \frac{\partial q}{T}\ \gamma'_{\text{ва}}\Big|_h^H dt. \tag{11}$$

In the coordinate system x, y, p, t the prognostic equations have the form

$$I_h = \frac{1}{g}\int_{p_0}^{p}\frac{dq}{dt}\,dp - \frac{0{,}57\,L}{g}\int_{p_0}^{p}\frac{q}{T}\frac{\partial T}{\partial t}\,dp - \frac{0{,}57\ L\nu q}{gT}\ \gamma'_{\text{ва}}\Big|_{p_0}^{p},$$

$$Q = \frac{1}{g}\int_0^t\int_{p_0}^{p}\frac{dq}{dt}\,dp\,dt - \frac{0{,}57\ L}{g}\int_0^t\int_{p_0}^{p}\frac{q}{T}\frac{\partial T}{\partial t}\,dp\,dt - \tag{11'}$$

$$-\int_0^t\frac{0{,}57\ L\nu q}{gT}\ \gamma'_{\text{ва}}\Big|_{p_0}^{p}dt.$$

[Ва = moist adiabatic]

where g is the acceleration of free falling; the remaining notations are well known.

The operational numerical synoptic-hydrodynamic scheme for the forecasting of precipitation for a time up to 36 hours, developed in the synoptic research laboratory at the USSR Hydrometeorological Center [5, 6], can serve as a base for carrying out additional computations of precipitation using formulas (11)-(11') -- the second and third terms.

In computing the quantity of precipitation a factor of more than a little importance is its duration.

The author of [3] gives a semi-empirical formula for determining the duration of shower precipitation

$$t = \frac{\varkappa\,\sigma_{1000-850}}{\bar{v}_{700-500}}, \tag{12}$$

where $\sigma_{1000-850}$ is the length of the trajectory of movement of cloud cover giving precipitation, $v_{700-500}$ is the rate of movement of the cloud cover, $\varkappa$ is a coefficient numerically equal to the ratio of the area of falling precipitation to the area of precipitation-forming cloud cover.

If the coefficient η is introduced into formula (12), it is possible to compute the duration of both strong and weak precipitation:

$$t = \frac{1}{\eta}\,\frac{\varkappa\,\sigma_{1000-850}}{\bar{v}_{700-500}}. \tag{13}$$

Now we will clarify the physical sense of the η coefficient. If in computing I_h in equations (7) we limit ourselves only to the first term, the equation can be represented in the form

$$I_h = \eta I, \tag{14}$$

where I_h is the resultant intensity of precipitation in the atmosphere at the condensation level, I is the intensity of precipitation caused by allowance only for the first term in equation (7); η is a dimensionless approximating coefficient governed by the following integral expression in accordance with equations (7) and (14):

$$\eta = 1 + \frac{\int_h^H \frac{\partial M}{\partial t}\, dz - v \frac{\partial M}{\partial z}\Big|_h^H}{-\int_h^H \rho \frac{dq}{dt}\, dz}, \tag{15}$$

It follows from expression (15) that in schemes for the prediction of precipitation it is necessary to include computations of the layer-by-layer content of moisture in the atmosphere.

For computing the duration of continuous precipitation it is also possible to use a formula from [5], for example:

[облак = cloud]

$$t_{\text{облак } 850} = t - \frac{12\, t\,(T - T_d)}{|\tau|}, \tag{16}$$

where $t_{\text{cloud } 850}$ is the duration of falling of precipitation from the 850-mb level, t is the advance time of the forecast, (T - T_d) is the dew point spread predicted at this level at a point, taking into account the advective and transformational changes in T and T_d, $|\tau|$ is the modulus of ordered ascending vertical velocity for the predicted period at the isobaric surface 850 mb.

The duration of falling of precipitation at the earth's surface is determined by the duration of precipitation at AT_{850} and AT_{700}.

It therefore follows from the above that a determination of the intensity of precipitation in the atmosphere and its duration using formulas (11), (11'), (13) or (12) makes it possible to predict the quantity of precipitation in different regions, including with a continentally arid climate, in particular, in the territory of Kazakhstan.

The prediction of precipitation for the territory of Kazakhstan on the basis of its intensity and duration computed using formulas (11)-(13) can be improved with the additional use of data from a regression analysis, making it possible to take local regional conditions into account.

For example, for one of the stations in Kustanayskaya Oblast, with use of data from automatic recorders on the intensity I, duration t and quantity Q of precipitation for the warm period of the year on the basis of observational data for 1967-1976 (100 cases were examined) a regression equation was derived in the form

$$Q = CI^a t^b, \tag{17}$$

where the coefficients C = 0.794, a = 0.748, b = 0.586 with a correlation coefficient equal to 0.68.

Substituting the I and t values, computed using formulas (11)-(13), into formula (17), we obtain the quantity of precipitation for 12-hour time intervals for an advance time up to 36-48 hours.

It should be noted that computations of precipitation on the basis of formulas (11)-(13) can be made for any forecasting regions, whereas formula (17) must be derived statistically specifically for each forecasting point.

BIBLIOGRAPHY

1. Yeviyevich, T. V., "Empirical Formulas for Determining the Total Moisture Content in the Atmosphere Over Moscow," RADIATSIONNYY REZHIM I OSADKI V MOSKVE (Radiation Regime and Precipitation in Moscow), Moscow, Izd-vo MGU, 1967.

2. Marchuk, G. I., "Theoretical Model of Weather Forecasting for a Short Time in Advance," IZV. AN SSSR: SERIYA GEOFIZ. (News of the USSR Academy of Sciences: Geophysical Series), No 5, 1964.

3. Orlova, Ye. M., KRATKOSROCHNYY PROGNOZ ATMOSFERNYKH OSADKOV (Short-Range Forecasting of Precipitation), Leningrad, Gidrometeoizdat, 1979.

4. Petrichenko, I. A., "Prediction of Precipitation Using Data on the Liquid-Water Content of Clouds," METEOROLOGIYA I GIDROLOGIYA (Meteorology and Hydrology), No 10, 1971.

5. Uspenskiy, B. D., Mertsalov, A. N., Orlova, Ye. M., Belousov, S. L., Petrichenko, I. A. and Veselova, G. K., "Synoptic-Hydrodynamic Scheme for the Quantitative Prediction of Continuous and Shower Precipitation," TRUDY GIDROMETTSENTRA SSSR (Transactions of the USSR Hydrometeorological Center), No 157, 1976.

6. Uspenskiy, B. D., Mertsalov, A. N., Orlova, Ye. M. and Petrichenko, I. A., "Peculiarities of Prediction of Precipitation in Numerical Operational Synoptic-Hydrodynamic Schemes With an Advance Time to 36 Hours," TRUDY GIDROMETTSENTRA SSSR, No 176, 1977.

7. Yudin, M. I., NOVYYE METODY I PROBLEMY KRATKOSROCHNOGO PROGNOZA POGODY (New Methods and Problems in Short-Range Weather Forecasting), Leningrad, Gidrometeoizdat, 1963.

UDC 551.594.221

POSSIBILITY OF PREDICTION OF LIGHTNING DISCHARGES

Moscow METEOROLOGIYA I GIDROLOGIYA in Russian No 3, Mar 81 pp 107-108

[Article by V. I. Arabadzhi, professor, Tula Polytechnic Institute, manuscript received 23 Jul 80]

[Text]

Abstract: The possibility of monitoring the electric field in a well-developed cumulus cloud up to the formation of a lightning discharge is examined. On this basis the author proposes prediction of development of lightning discharges in clouds.

In order to clarify the possibility of predicting lightning discharges in the weather service it is necessary to have a more complete knowledge of the conditions for the development of cumulus clouds into thunderstorm clouds. We will attempt to give some rough evaluations of this process.

We will examine a well-developed cumulus cloud, in the first approximation regarding it as a heat engine. The work performed by this engine in the separation of electric charges and in creating an electric field can be expressed by the formula

$$A = \gamma Q_1 \left(\frac{T_1 - T_2}{T_1}\right). \quad (1)$$

where Q_1 is the energy expended on charge separation in the cloud, T_1 is the temperature of the heater (the mean temperature of the lower part of the cloud), T_2 is the temperature of the cooler (the mean temperature of its upper part), γ is a factor less than unity taking into account the efficiency of operation of a real heat engine in comparison with an ideal engine (in our case it characterizes the energy losses in the formation of the electric field in the cloud).

We will compare the work according to (1) with the work which is performed in a lightning discharge. Assume that the electric energy of the cloud before and after the discharge is equal to $CV_0^2/2$ and $CV^2/2$, where C is cloud capacity and V_0 and V are its potential before and after the discharge. Then the work of the discharge is

$$A = \frac{CV_0^2}{2} - \frac{CV^2}{2} \approx CV_0(V_0 - V). \quad (2)$$

Equating (1) and (2), we obtain

Equating (1) and (2), we obtain

$$CV_0(V_0 - V) = \gamma Q_1\left(\frac{T_1 - T_2}{T_1}\right). \quad (3)$$

We will assume further that the kinetic energy of a cloud unit volume, as a result of charge separation in it, is transformed into the electric field energy in conformity to the equation

$$\gamma \frac{\rho v^2}{2} = \frac{\varepsilon\varepsilon_0 E^2}{2}, \quad (4)$$

where ρ is the density of the charged component of the aerosol medium (cloud), v is the rate of separation of charges of opposite signs, ε_0 is the electric constant, ε is the dielectric constant, E is electric field strength, γ is the already mentioned coefficient of energy losses associated with formation of the electric field in the cloud. Expressing γ from (4) and substituting the result into (3), we obtain

$$CV_0(V_0 - V) = \frac{\varepsilon\varepsilon_0 E^2}{\rho v^2} Q_1\left(\frac{T_1 - T_2}{T_1}\right). \quad (5)$$

We rewrite $Q_1(T_1 - T_2)/T_1$ in the form $S(T_1 - T_2)$, where S is the entropy lost by the heater and we will denote the mean value of lightning discharge energy, which we will use henceforth as an approximate parameter, by W. Then for the electric field developing in the cloud we will have

$$E = v\sqrt{\frac{\rho}{\varepsilon\varepsilon_0}\frac{W}{(T_1 - T_2)S}}. \quad (6)$$

Since (6) was derived with allowance for the entropic exchange in the cloud, it can be regarded as quite important for evaluating the possibility of development of a discharge. By stipulating the mean energy of the lightning discharge W and experimentally determining the ρ, v, T_1, T_2, ε and S values, using formula (6) it is possible to evaluate the degree of approximation of the electric value to that critical value which will ensure the development of a lightning discharge (we note that with allowance for a density of charged aerosols and their corona discharge typical for thunderstorm clouds the field strength responsible for a discharge in a cloud has a value of about 10^6 V/m).

For practical purposes it is important to foresee the region of the beginning of the discharge and the direction of its branching. In most cases the discharge begins in a droplet or droplet-ice part of a thunderstorm cloud where there are favorable conditions for this (additional electric fields as a result of fragmentation of the charged droplets and the falling of precipitation, some increase in the length of the free path of electrons in comparison with surface conditions, which ensure the development of the discharge channel, and a decrease in the ionization energy of molecular associations and complexes with individual molecules). The discharges, beginning and ending in the cloud or in the space directly adjacent to it, require a lesser energy for their development and therefore are observed more frequently than discharges at the ground. However, often there are discharges excited by the electric field of a thunderstorm cloud, but not beginning in the cloud, but at the ground surface -- discharges into high structures. For example, it is known that discharges into the Ostankinskaya television tower above 500 m are ascending, i.e., branch from the tower to a cloud. Discharges into the Empire State Building in the United States become ascending beginning at a height of 390

m. This effect is attributable to the high strength of the electric field at the upper parts of high buildings. In the first approximation this field increases in conformity to the law

$$E = E_0 \frac{h}{R}, \tag{7}$$

where E_0 is the field of the thunderstorm cloud at a plane earth's surface, h is height of the structure, R is the effective radius of curvature of the discharge apparatus at the top of the structure.

Assuming for the Ostankinskaya television tower h = 536 m, $R \approx 0.7$ m and at the earth's surface $E_0 \approx 4 \cdot 10^3$ V/m, for the electric field strength at the top of the tower we obtain $E \approx 10^6$ V/m. With such a field strength in dry and pure air at the earth's surface there is an electric charging of the air. At the top of the tower, for the most part due to coronal discharge suitable conditions will prevail with a lesser field strength. Thus, by knowing the height of the structure it is possible to foresee the direction of development of the lightning discharge over it.

We have briefly examined some points which can find application in work on the prediction of lightning discharges. Further research work is required for explaining the possibility of introducing these proposals into weather service practice.

BIBLIOGRAPHY

1. Arabadzhi, V. I., GROZA I GROZOVYYE PROTSESSY (Thunderstorms and Thunderstorm Processes), Minsk, 1960.

2. Gorin, V. P., Sakharova, G. S., Tikhomirov, V. V. and Shkilev, A. V., "Results of Observations of Lightning Damage From the Ostankinskaya Television Tower," SBORNIK TRUDOV GOSUDARSTVENNOGO NAUCHNO-ISSLEDOVATEL'SKOGO INSTITUTA IM. G. M. KRZHIZHANOVSKOGO (Collection of Papers of the State Scientific Research Institute imeni G. M. Krzhizhanovskiy), No 43, 1976.

UDC 556.34

DETERMINATION OF FILTRATION COEFFICIENTS OF COHESIVE SOILS IN A FROZEN STATE THROUGH THEIR KINETIC SPECIFIC SURFACE

Moscow METEOROLOGIYA I GIDROLOGIYA in Russian No 3, Mar 81 pp 109-112

[Article by V. I. Shtykov, candidate of technical sciences, Northern Scientific Research Institute of Hydraulic Engineering and Melioration, manuscript received 15 Jul 80]

[Text]

Abstract: The article describes the derivation of a dependence for determining the filtration coefficients for cohesive soils in thawed and frozen states through their kinetic specific surface. The author gives recommendations on the determination of individual characteristics of the ground entering into the cited dependences and also the results of a comparison of the filtration coefficients computed using the proposed dependences with their values obtained from experiments under laboratory conditions.

A determination of the filtration coefficients for cohesive soils in a frozen state involves great difficulties under both field and laboratory conditions. It is therefore of considerable practical interest to examine the possibility of using other methods, such as computations, when only individual characteristics of the ground in a thawed state are to be determined under laboratory conditions.

As in the case of friable soils, it is desirable to use as a point of departure a filtration scheme for the ground in which it consists of a mass of filtration passages. For friable soils we have the following dependences for determining the rate of movement and position of the percolation front with time [4]:

$$\frac{dy}{d\tau} = \frac{\gamma d_u^2}{8\pi^2\mu}\left[\frac{4A_3\cos\Theta}{d_u\gamma y} + \left(\frac{h}{y}+1\right)\right], \quad (1)$$

$$\tau = \frac{8\pi^2\mu}{\gamma d_u^2}\left(\frac{4A_3\cos\Theta + d_u\gamma h}{d_u\gamma}\ln\frac{4A_3\cos\Theta + d_u\gamma h}{4A_3\cos\Theta + d_u\gamma h + d_u\gamma y} + y\right), \quad (2)$$

where y is the distance from the ground water level to the percolation front in a vertical direction (with percolation from above, from the surface), cm; τ is time, in seconds; γ is water density, g/cm^3; d_u is the computed diameter of the filtration passage, computed from the dependence (6), cm; μ is the dynamic viscosity coefficient, g(cm·sec);

$$A = \frac{(n - i - B - \gamma_0 W_{un})\left[1 - n - \gamma_0 W_{un} + \frac{2{,}8\,(i + B)}{1 - 0{,}6\,\sqrt{i + B}}\right]}{(n - i - B)\left[1 - n - \gamma_0 W_{un} + \frac{2{,}8\,(i + B)}{1 - 0{,}6\,\sqrt{i + B}}\right]}.$$

A is a parameter taking into account the content of unfrozen water in the friable soil, which with $W_{un} = 0$ is equal to 1; σ is the coefficient of water surface tension, n/cm; θ is the wetting angle; h is the water layer at the ground surface with percolation from above (with movement from below h = 0), cm; n is porosity in fractions; i is volumetric ice content in fractions; B is the content of entrapped air in fractions.

In the case of cohesive soils the computation diameter of the filtration passage is expressed through the kinetic specific surface of the ground. We use the known fact [1] that the $2n/\varepsilon_0$ ratio is equal to the mean radius of the pores. We will assume that the above-mentioned expression is equal to the computed radius of the filtration passage when ε_0 is understood as the kinetic specific surface of the ground, that is, "dead-end" pores are excluded from consideration. Taking into account what has been said, dependence (1) for coherent soils in a dry state will have the form

$$\frac{dv}{dt} = \frac{2\,gn^3}{\pi^2 \nu \varepsilon_0^2}\left[\frac{\sigma_0 \cos\theta}{n\gamma y} + \left(\frac{h}{y} + 1\right)\right], \qquad (3)$$

where g is the acceleration of free falling, cm/sec^2; ν is the kinematic viscosity coefficient, cm^2/sec.

With $y \to \infty$, and also joining of the percolation front with the ground water level, the infiltration process passes into a filtration process and by virtue of the known expression

$$\frac{dv}{dt} = \frac{KI}{n}$$

from (3) we obtain a dependence for determining the filtration coefficient for cohesive soils.

$$K = \frac{2\,gn^3}{\pi^2 \nu \varepsilon_0^2}. \qquad (4)$$

where I is the pressure head gradient, in this case equal to 1.

In the case of clayey ground the term in parentheses in expression (3) can be neglected, and with dependence (4) taken into account we obtain the B. V. Deryagin formula [1]

$$\frac{y^2}{t} = \frac{2\,K\sigma\cos\theta}{n^2\gamma}. \qquad (5)$$

In the derivation of formula (5) the author used as a point of departure the equality of work of wetting forces and frictional forces, that is, the work of gravitational forces is neglected. Accordingly, it is rigorously applicable only to the case of horizontal percolation, and in the case of vertical percolation -- to fine-grained soils, and in particular, to clayey soils, for which the capillary potential is much greater than the gravitational potential.

Dependence (4) gives the value of the filtration coefficient at the beginning of the process of infiltration into dry ground. Upon the elapsing of some time with the saturation of cohesive soils with water the latter "loosen up." A film of bound water is formed around each of the particles and this film, with an accuracy adequate for practical purposes, can be considered immobile. With a moistening of the cohesive ground there is no substantial increase in the initial ground volume, but the total surface of the particles increases since for this we use the surface of particles with allowance for the immobile film of bound water, which leads to a decrease in the active porosity of the ground and an increase in the kinetic specific surface. An increase in the specific kinetic surface is confirmed experimentally (see Table 2, columns 3 and 4).

We will assume that in the case of cohesive ground as well the structure of the formula for determining the computation diameter of the filtration passage is the same as in the case of friable soils [5]. Then for cohesive soils in a moist state we write

$$d_u = \frac{n - B - \gamma_0 W_c}{1 - n + B + \gamma_0 W_c} C, \tag{6}$$

where γ_0 is the volumetric mass of ground in a dry state, g/cm^3; W_c is the content of firmly bound moisture in fractions of the mass of dry ground; C is a parameter dependent on the kinetic specific surface of the ground.

For cohesive ground in a dry state dependence (6) has the form

$$d_u = C \frac{n}{1 - n}. \tag{7}$$

Using the relationship between the mean radius of the filtration passage and the kinetic specific surface of the ground, we express the C parameter through ε_0:

$$C = \frac{4 (1 - n)}{\varepsilon_0}. \tag{8}$$

The value of the computation diameter of the filtration passage, computed using the dependence (6), corresponds to the kinetic specific surface of the cohesive ground in a water-saturated state (ε_W). Using the dependences (6), (8), and also the expression

$$\varepsilon_W = \frac{4 (n - B - \gamma_0 W_c)}{d_u},$$

we obtain a formula reflecting the interrelationship between the kinetic specific surface of the cohesive ground in dry and moist states,

$$\varepsilon_W = \frac{(1 - n - B + \gamma_0 W_c) \varepsilon_0}{(1 - n)}. \tag{9}$$

By analogy with moist cohesive ground, in the case of its freezing the dependences for determining the computation diameter of the filtration passage and the kinetic specific surface will have the form

$$d_u = C \frac{n - i - B - \gamma_0 W_c}{1 - n + i + \gamma_0 W_c + \frac{2,8 (i + B)}{1 - 0,6 \sqrt{i + B}}}, \tag{10}$$

$$i_{\text{д}} = \frac{4\,(n - B - i - \gamma_0 W_c)}{d_{\text{д}}}. \tag{11}$$

As a result the kinetic specific surface of cohesive ground in a frozen state is expressed through the kinetic specific surface of this same ground in a dry state in the following way:

$$s_{\text{з}} = \frac{\left|1 - n + \gamma_0 W_c + \frac{2{,}8\,(i + B)}{1 - 0{,}6\sqrt{i + B}}\right| s_0}{1 - n}. \tag{12}$$

Thus, for determining the filtration coefficients for cohesive soils in a water-saturated or in a frozen state we have the dependences

$$K_W = \frac{2g\,(n - B - \gamma_0 W_c)^3\,(1 - n)^2}{\pi^2\,(1 - n + B + \gamma_0 W_c)^2\,\varepsilon_0^2\,\nu}, \tag{13}$$

$$K_M = \frac{2g\,(n - B - \gamma_0 W_c - i)^3\,(1 - n)^2}{\pi^2\left[1 - n + \gamma_0 W_c + \frac{2{,}8\,(i + B)}{1 - 0{,}6\sqrt{i + B}}\right]^2 \varepsilon_0^2\,\nu}. \tag{14}$$

It should be noted that dependence (14) is valid only for cohesive ground in which heaving is absent. The volumetric ice content of the ground i consists of the initial i_0 ice content and the increment to ice content as a result of the partial freezing of water filtering into the ground i'. It follows from an analysis of dependence (14) that frozen friable soil can become impermeable with an i value substantially less than the porosity due to the presence of entrapped air and bound water in it.

Infiltration into frozen cohesive soils and the conditions under which it ceases were examined in a study by I. L. Kalyuzhnyy and others [3].

Table 1

Content of Unfrozen (W_{un}) and Firmly Bound (W_c) Water in Frozen Ground

Name of soil by mechanical composition	W_{un} with t = 0°C in fractions	W_c in fractions
Sandy loam	0.07	0.02
Clayey loam	0.10	0.04
Medium clay	0.20	0.08
Heavy clay	0.35	0.20

Now we will examine the problem of determining the individual parameters entering into the dependences cited above. In the absence of data on the content of entrapped air its value must be assumed equal to 0.03. Having data on the content of unfrozen water in the ground (Table 1), the initial value of the volumetric ice content can be determined using the N. A. Tsytovich formula

$$i_0 = \gamma_0(W - W_{un})/\gamma_{ice}, \quad (15)$$

where W is the total moisture content of the ground by mass in fractions; W_{un} is the content of unfrozen water by mass in fractions in the frozen ground; γ_{ice} is ice density, g/cm^3.

Table 2

Results of Determination of Filtration Coefficient of Plowed Layer in Thawed State

n	B	Kinetic specific surface of ground, cm^{-1}		Filtration coefficient 10^{-4} cm/sec	
		dry	moist	experimental	using (14)
0.484	0.020	1410	1586	5.5	5.2
0.501	0.024	1370	1550	4.9	6.0
0.498	0.031	1376	1576	5.0	5.4
0.493	0.029	1390	1589	5.3	5.2
0.489	0.034	1400	1610	4.7	4.7
0.478	0.039	1430	1660	3.9	3.9
0.473	0.032	1446	1660	3.5	3.9
0.464	0.033	1454	1670	3.8	3.6

Table 3

Results of Determination of Filtration Coefficient of Plowed Layer in Frozen State

n	*i*	*B*	Kinetic specific surface of ground cm^{-1}		Filtration coefficient, cm/sec	
			dry	frozen	experiment	using (15)
0,468	0.000	0.021	1460	1810	$1,9\cdot10^{-4}$	$2,1\cdot10^{-4}$
0,491	0.059	0,022	1400	2270	$1,3\cdot10^{-4}$	$1,1\cdot10^{-4}$
0,500	0.084	0,028	1365	2560	$0,8\cdot10^{-4}$	$0,7\cdot10^{-4}$
0.506	0,111	0.000	1353	2520	$8,0\cdot10^{-5}$	$7,8\cdot10^{-5}$
0,547	0,121	0,020	1240	3020	$5,2\cdot10^{-5}$	$5,9\cdot10^{-5}$
0,513	0,161	0,029	1330	3430	$2,4\cdot10^{-5}$	$2,0\cdot10^{-5}$
0,525	0,177	0,032	1300	3630	$1,6\cdot10^{-5}$	$1,7\cdot10^{-5}$
0,540	0,212	0,037	1260	4100	$0,8\cdot10^{-5}$	$1,0\cdot10^{-5}$
0,528	0,266	0,039	1290	4900	$2,4\cdot10^{-6}$	$2,7\cdot10^{-6}$

In conclusion we will cite experimental data for determining the filtration coefficients in cohesive soils in thawed and frozen states. The kinetic specific surface of the ground in a thawed state was determined by the B. V. Deryagin method [2] and in frozen ground was computed using the expression (12).

Tables 2 and 3 give the results of computation of the filtration coefficients for two different soil types of the plowed layer in thawed and frozen states and also data from their experimental checking.

Tables 2 and 3 show that the coincidence of the results of computations using the proposed expressions and the experimental determination of the values of the filtration coefficients for cohesive soils is entirely satisfactory.

BIBLIOGRAPHY

1. Deryagin, B. V., "Determination of the Specific Surface of Porous Bodies From the Rate of Capillary Saturation," KOLLOIDNYY ZHURNAL (Colloidal Journal), Vol VIII, Nos 1-2, 1946.

2. Kachinskiy, N. A., FIZIKA POCHVY (Soil Physics), Part I, Moscow, Vysshaya Shkola, 1965.

3. Kalyuzhina, I. L., Morozova, N. S., Pavlova, K. K. and Romanov, V. V., "Thermophysical Method for Computing the Losses of Melt Water on Infiltration Into Frozen Soil," METEOROLOGIYA I GIDROLOGIYA (Meteorology and Hydrology), No 1, 1972.

4. Shtykov, V. I., "Permeability of Frozen Friable Soils and Analysis of the Dynamics of its Change During the Period of Snow Melting and Thaws," METEOROLOGIYA I GIDROLOGIYA, No 12, 1979.

5. Shtykov, V. I., "Rate of Advance of the Percolation Front in the Ground," SBORNIK DOKLADOV PO GIDROTEKHNIKE (Collection of Reports on Hydroengineering), No 13, Leningrad, Vsesoyuznyy NII Gidrotekhniki im. B. Ye. Vedeneyeva, per I D-409, Informenergo, 1977.

UDC 556.132(571.1)

EVALUATION OF APPLICABILITY OF DIFFERENT METHODS FOR DETERMINING EVAPORATION FROM A WATER SURFACE IN A ZONE OF HUMMOCKED SWAMPS

Moscow METEOROLOGIYA I GIDROLOGIYA in Russian No 3, Mar 81 pp 112-115

[Article by Yu. P. Moskvin, State Hydrological Institute, manuscript received 8 Aug 80]

[Text]

Abstract: A study was made of the problems involved in applicability of different methods for determining evaporation from a water surface in the zone of hummocked swamps in Western Siberia. As a standard use was made of the method for determining evaporation on the basis of observational data in the GGI-3000 floating evaporator with the introduction of corresponding corrections. The accuracy in determining evaporation from a water surface is evaluated by computation methods with and without observational data over the surface of a lake.

Existing methods for computing evaporation from a water surface for the most part are based on experimental materials obtained on the basis of observations over the European USSR, in Central Asia, Kazakhstan and in the southern part of Siberia. Due to the intensive economic exploitation of regions in the Far North the need arises for developing an observation method and choice of an optimum method for computing evaporation from a water surface for these regions. The West Siberian Expedition of the State Hydrological Institute over a period of years carried out work for investigating the water balance components of hummocked swamps and in particular, for estimating evaporation from the water surface of small lakes within swamps employing a floating apparatus with a standard GGI-3000 evaporator.

The basis for this study was observational data obtained during the warm periods 1978-1979. In making the observations we selected a lake with an area of 0.178 km^2 situated within a swamp which was the most characteristic for the investigated region. This lake has an average depth of about 1 m and is situated in an unwooded complex with flat-topped hummocks. Trees with a height of 2-3 m were situated 30-80 m from the lake shore on the northern and northwestern sides and 150-200 m from the western part of the lake. There were no trees on the southern and eastern sides.

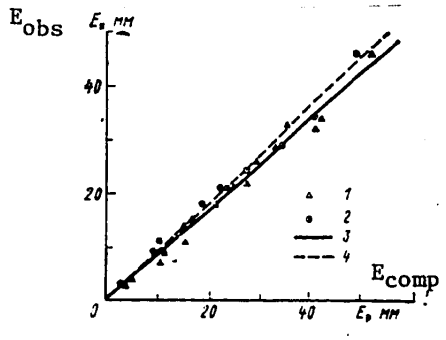

Fig. 1. Correlation graphs of 10-day sums of evaporation from water surface determined from data from observations with floating evaporator apparatus (E_{obs}) and computed using formula (2) (E_{comp}) 1978-1979. 1) observations 4 times a day; 2) observations 8 times a day; 3) correlation for observations four times a day; 4) correlation for observations eight times a day.

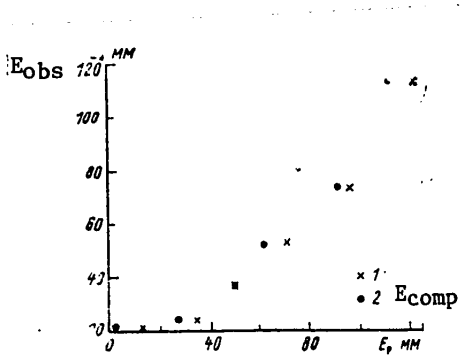

Fig. 2. Dependence of monthly sums of evaporation from water surface determined from observational data from floating evaporator apparatus and computed using data from continental station in absence of observational data for 1978-1979. 1) using formula (5), 2) using formula (2).

A full complex of observations with the floating evaporation apparatus, including observations of the meteorological elements over the water surface, were made in accordance with the INSTRUCTIONS [2]. In addition, in 1979 observations were made with continuous registry of the principal meteorological elements (wind speed, relative humidity and air temperature), which made it possible to obtain the mean daily characteristics of the mentioned elements of the meteorological regime over the water surface for eight observation times. The elasticity of water vapor over a water body was determined using psychrometric tables on the basis of data registered eight times a day on relative air humidity taken from hygrograph tapes and reduced to the readings of an aspiration psychrometer.

As a standard we employed the method for determining evaporation from a water body on the basis of observational data obtained with the GGI-3000 floating evaporator. In accordance with [1], evaporation from the lake at the site of the floating evaporator was computed using the formula

$$E = 0{,}8\,E' \frac{e_0 - e_{200}}{e'_0 - e_{200}}, \qquad (1)$$

where E' is evaporation according to the GGI-3000 floating evaporator, in mm; 0.8 is a factor taking into account the instrument correction for the GGI-3000 evaporator; e_0, e'_0 is the maximum water vapor elasticity, computed on the basis of temperature of the water surface in the water body and in the evaporator respectively, in mb; e_{200} is absolute air humidity at a height of 200 cm from the water surface on the floating evaporation apparatus, mb.

Table 1

Determination of Evaporation (mm) From Water Surface by Different Methods

Month	Ten-day period	Using (1) with GGI-3000 evaporator data	Using State Hydrological Inst. formulas with observational data, using (2)		in absence of observational data	
			8 times	4 times	using (2)	using (5)
		1978 r.				
July	2	26(8)		29(8)		
	3	33		35		
August	1	18		21		
	2	20(9)		22(9)		
	3	15		16		
	Month	53(30)		59(30)	62	72
September	1	14		15		
	2	7(9)		10(9)		
	3	4(7)		5(7)		
	Month	25(26)		30(26)	27	35
		1979 r.				
June	19—30	22	24	27	3	13
July	1	32	41	41		
	2	34	41	42		
	3	46	49	52		
	Month	112	131	135	113	123
August	1	24	27	27		
	2	29	34	33		
	3	20	22	23		
	Month	73	83	83	91	97
September	1	18	18	21		
	2	9	9	10		
	3	11	10	15		
	Month	38	37	46	50	50
October	1—3	3	3	4		
		248	278	295	257	284

Note: The number of days of observations is given in parentheses.

The evaporation quantity determined using formula (1), as a result of the insignificant area of the lake, was used as the mean layer of evaporation from the entire lake. For evaluating the applicability of the computation method when observational data are available we computed the 10-day evaporation sums using the generalized formula of the State Hydrological Institute

$$E=0{,}14\,n\,(e_0-e_{200})\,(1+0{,}72\,u_{200}), \qquad (2)$$

where n is the number of days in the computation time interval, u_{200} is the mean wind velocity over the water body at a height of 200 cm, m/sec.

In 1978 the computations were made using four observation times each day and in 1979 using eight observation times each day.

The results of the computations are given in Table 1 and are illustrated in a graph (Fig. 1). An analysis of the data in the table and graph shows that computations of evaporation using the formula of the State Hydrological Institute with the use of data from observations four and eight times each day leads to a systematic exaggeration of the results. The magnitude of the indicated exaggeration in the case of observations eight times each day averages 10-13%, and in the case of four times each day -- 17-20%. The correlation coefficients for these dependences are equal to 0.9, which makes it possible to recommend as a computation method the determination of evaporation from intraswamp lakes in the considered region using the dependences

$$E = 0.84E_{\text{four times}}, \quad (3)$$

$$E = 0.90E_{\text{eight times}}. \quad (4)$$

For evaluating the applicability of computation methods for the conditions of hummocked swamps in the absence of observations at the lake we made computations of the monthly sums of evaporation from the water surface using data from the near-lying meteorological station Tarko-Sale. In computing evaporation we used formula (2) for the conditions of absence of observations at the lake and the formula

$$E = E_{arb}K_uK_{L_{mean}}, \quad (5)$$

where E_{arb} is the evaporation from an arbitrary water body, K_u and $K_{L_{mean}}$ are coefficients taking into account the actual wind velocity and the length of the fetch over the water body.

The computations of the parameters entering into the mentioned expressions were made using data from a continental station with allowance for the transformation of meteorological elements by methods recommended in [3]. The results of the computations are given in Table 1 and in a graph (Fig. 2). The correlation coefficients for the derived expressions (Fig. 2) are equal to 0.81. The collected data give basis for assuming that the computation of the monthly sums of evaporation on the basis of meteorological data for continental stations can also be accomplished for a zone of hummocked swamps. However, final conclusions concerning the accuracy of computation of these parameters can be drawn after obtaining the necessary additional observational data.

BIBLIOGRAPHY

1. Vuglinskiy, V. S., Starovoytova, V. K. and Cherskaya, Ye. N., "Method for Evaluating Evaporation From the Surface of a Water Body Using Data From the GGI-3000 Continental Evaporator," TRUDY GGI (Transactions of the State Hydrological Institute), No 274, 1980.

2. NASTAVLENIYE GIDROMETEOROLOGICHESKIM STANTSIYAM I POSTAM (Instructions for Hydrometeorological Stations and Posts), Issue 2, Part 2, Leningrad, Gidrometeoizdat, 1961.

3. UKAZANIYA PO RASCHETU ISPARENIYA S POVERKHNOSTI VODOYEMOV (Instructions on Computing Evaporation From the Surface of Water Bodies), Leningrad, Gidrometeoizdat, 1969.

UDC 551.(524.73+507.362)

RECONCILING OF MESOSPHERIC TEMPERATURE VALUES MEASURED BY DIFFERENT ROCKET SOUNDING SYSTEMS

Moscow METEOROLOGIYA I GIDROLOGIYA in Russian No 3, Mar 81 pp 116-120

[Article by Yu. P. Koshel'kov, candidate of geographical sciences, Central Aerological Observatory, manuscript received 21 May 80]

[Text]

Abstract: The long-term atmospheric temperature values obtained at different rocket sounding stations using different measurement methods are compared. The results of these comparisons make possible the reconciling of mean data on the temperature of the mesosphere obtained at a number of stations.

Introduction. In order to construct reference models of the atmosphere, in the analysis of the temperature and pressure fields in the middle atmosphere at the scale of a hemisphere and for other purposes it is necessary to reconcile the data obtained using different rocket sounding systems, that is, obtained by different methods. At Soviet stations sounding is now accomplished using the M-100B meteorological rocket with a "361M" nosecone (prior to 1978 -- with a "361" nosecone) and using a resistance thermometer. In addition, in such work use is made of the MMR-06 rocket in which the sensing element for measuring temperature is a thermistor. In the United States it is customary to employ Super-Loci-Datasonde rockets (prior to 1970 -- the Arcasonde rocket), also employing thermistors. It is less common to use the acoustic rocket-grenade method, the method of falling gas-filled spheres, manometric methods (Pitot tubes, etc.).

It is known that data from measurements made by different methods differ above 50 km. This was confirmed in direct comparisons of rocket systems [8, 10]. However, such comparisons of necessity were based on a limited number of synchronous measurements and involved only some sounding systems. Therefore, it is desirable that their results be supplemented by "indirect" comparisons in which there is a comparison of the mean temperature values obtained at different points (or in different years) under similar atmospheric conditions, for example, in summer when the longitude temperature differences in the stratomesosphere are small (the influence of variation with latitude can be excluded by the interpolation of temperature at the necessary latitude). The temperature differences found in such comparisons are attributable both to the difference in the sounding equipment used and the residual difference in atmospheric conditions in the compared series of measurements.

The results of this sort of comparison are given below.

M-100B rockets and American network rocket systems. Table 1 gives the differences between the mean temperatures obtained using the M-100B ("361") system and American systems. For the northern hemisphere we have compared M-100B sounding data (stations at Kheys Island, Volgograd, Tumba) and Datasonde data (North American stations) for the summer of 1973-1978, in the southern hemisphere -- shipboard sounding data with the M-100B (Indian Ocean) for 1961-1977 and Arcasonde and Datasonde data (Mar Chiquita station in Argentina) for the summer of 1968-1977 at latitude 38°S and mean annual data for 1964-1975 at latitude 8°S (Easter Island).

Some of the discrepancies (Δ_1) in Table 1 can be attributed to the peculiarities of the aerodynamics of measurements of temperature by an M-100 ("361") rocket. (The Δ_1 values for winter conditions should be greater than the summer values cited in Table 1). In addition, during recent years there has been an improvement in the calibration method (the Δ_2 effect in Table 1) and there has been some refinement of the temperature restoration coefficients used in computations of the velocity correction for the M-100B rocket (Δ_3 effect). Another part of the discrepancies (Δ_4) arises as a result of the difference in the time of day when the M-100B ("361") and Datasonde rockets were launched. There are evidently also other reasons for the discrepancy in data, including those associated with errors in American measurements.

As indicated in Table 2, the data from an indirect comparison in general are confirmed by the results of the direct comparison of 1977, involving the M-100B ("361M") and Datasonde systems. Due to the approximate nature of the quantitative evaluations of the differences in the conditions for the indirect and direct comparisons (Δ_1, Δ_2, Δ_3 and Δ_4), as well as the assumptions made in the indirect comparison, one should not expect a total coincidence of the results of these comparisons.

Grenades, Pitot tubes and gas-filled spheres. A study was made of the differences between the mean temperatures determined on the basis of data from 20 rocket-grenade measurements (in 1960-1970) and 5 measurements using Pitot tubes (in 1966-1970) at Wallops Island during summer [15, 16] (see figure). The measurements made using Pitot tubes give somewhat lower temperatures than the grenade measurements in the lower mesosphere and higher temperatures in the upper mesosphere. However, the significance of these differences is great only at an altitude of 55 km. The difference decreases still more if only the grenade measurements for August (when all the measurements with the Pitot tube were made) are used. Although the volume of data is not great, it can be concluded that it is possible to make joint use of data obtained with grenades and Pitot tubes.

Measurement data obtained using spheres in the summer of 1970-1974 [12] at Woomer station (31°S), supplemented by data from a so-called "dropsonde" (in which the systematic discrepancy with spheres was eliminated [4]) and reduced to a latitude 38°, are 1-3°C warmer than grenade data for 38°N (see figure). However, the differences are not significant.

Table 1

Differences Between Mean Atmospheric Temperature Values (°C) Obtained Using Datasonde Data (With Correction [11]) and Arcasonde Data (With Correction [1]) and Data for M-100B Rocket (With "361" Nosecone) During Summer (at 8°N as Average for Year)

Altitude, km	Latitude					Mean
	80° N	49° N	9° N	8° S	38° S	
70	32,5	23	29,5	—	—	28,5
65	38	30	33	—	—	33,5
60	27,5	22,5	27,5	26,5	24,5	25,5
55	15	11	15	16,5	15	14,5
50	4,5	5	4,5	7	7	5,5
45	1	0,5	—0,5	4	1	1,5

Table 2

Differences (Δ_{ind}) Between Mean Atmospheric Temperature Values (°C) According to Datasonde and M-100B ("361") Rockets With Indirect Comparison; Evaluations of Influence of the Aerodynamic Changes for Summer Conditions (Δ_1) [1], Calibration (Δ_2) and the Coefficients of Temperature Restoration (Δ_3) for the M-11B System and Diurnal Variation [9, 14] (Δ_4) and the Temperature Difference for the Datasonde-"361M" Systems (Δ_{dir}) in Direct Comparisons 1977 (With Standard Processing of "361M" Data)

Altitude, km	Δ_{ind}	Δ_1	Δ_2	Δ_3	Δ_4	$\Delta_{ind}-(\Delta_1+\Delta_2+\Delta_3+\Delta_4)$	Δ_{dir}
70	28.5	9	2	0	1.5	16	11
65	33.5	13	2.5	4	1.5	12	14
60	25.5	12	3	3	0.5	7	6
55	14.5	7	2	1.5	0.5	3.5	5
50	5.5	2	1	0.5	1	1	2

FOR OFFICIAL USE ONLY

APPROVED FOR RELEASE: 2007/02/09: CIA-RDP82-00850R000400030065-3

Table 3

Differences Between Mean Temperature Values (°C) Obtained by Grenade Measurements (in 1960's) and Thermistor Measurements (in Numerator -- According to Datasondes With Correction [11], in Summer 1973-1979 for the Northern Hemisphere, Mean Annual Values for 1971-1978 for 8°S; in Denominator -- According to Arcasondes With Correction [7], in Summer 1965-1968 for the Northern Hemisphere, Mean Annual Values for 1965-1968 for 8°S)

Altitude, km	Latitude				Mean
	38° N	59° N	71°N	8°S	
70	—3,5/—	—10,5/—	—10/—		—8/—
65	—4/—	—4,5/—	—7/—	—6,5/—	—5,5/—
60	—3/—5	—1/—3	—3/—6	—1,5/—5,5	—2/—4
55	0,5/—1	—0,5/—2	—0,5/—2	0/—1,5	0/—1,5
50	2,5/—1	0,5/—1	1/—2	—0,5/—1	0,5/—1
45	1,5/—1	1/0	2/0	—1/—3,5	1/—1

Table 4

Differences Between Temperature Values According to Grenade Measurements (Pitot Tubes, Australian Spheres) and Data (1978) for M-100B ("361") Rocket in Summer (at Equator -- for Year). The Values in Parentheses are the Mean Differences Between Grenade Data and Data (for 1979-1980) Obtained by M-100B ("361-M") Rocket

Altitude, km	30° S	Equator	49° N	80° N	Mean
75	10,5	9,5	8,5	8	9 (5)
70	19	18	20,5	26,5	21 (8)
65	20	22	22	30	23,5 (10)
60	19	20,5	20	25	21 (7)
55	10	11,5	9,5	16	12 (6)

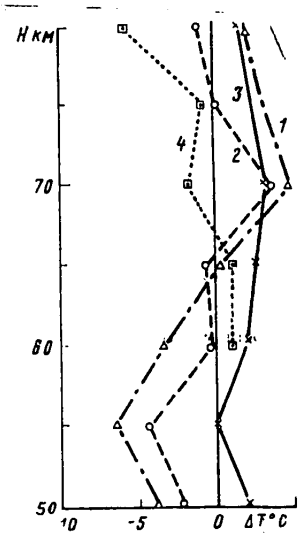

Fig. 1. Deviations of mean temperatures obtained using Pitot tubes and gas-filled spheres from grenade data during summer months. 1) data from Pitot tubes for August and grenade data for June-August; 2) data from Pitot tubes for August and grenades for August; 3) data from Australian spheres for December-February and grenades for June-August; 4) data for American spheres and grenades for June-August.

The mean long-term temperatures measured with American spheres in the subtropics in the upper mesosphere were lower than the temperature measured using grenades (see figure). Some of the differences, however, must be attributed to the diurnal variation of temperature because the spheres were launched for the most part at 0500-1200 hours (LT) whereas the grenades were launched more uniformly in the course of the day. An influence of the 11-year cyclicity of temperature in the stratomesosphere is also possible [3, 5, 13].

Grenades (spheres) and Datasondes (Arcasondes). The differences between summer temperatures according to grenade measurements and data from Datasonde and Arcasonde probes for North America were important at the level 60 km and above (Table 3). During the winter and transitional seasons the "grenade-Datasonde" differences for 38 and 59°N were somewhat greater: -1 - -3°C at the level 55 km, -3 - -6°C at 60 km and -8 - -9°C at 65 km. The influence of the diurnal variation and the possible 11-year cycle on the accuracy of the comparisons in this case should not be great.

According to data from about 200 paired launchings of Datasondes and spheres in the United States during 1971-1978 [18] at latitudes 22, 28 and 34°N the spheres give lower temperature values than the Datasondes (with the correction [11]): on the average by 4°C at the level 45 km, 5.5°C at 50 km, 3°C at 55 km, 0.5°C at 60 km and (with a reduction of the number of pairs to 35) 4°C at 65 km. These results agree with the "grenade-sphere" differences.

Grenades (Pitot tubes, spheres) and M-100B rockets. The differences between the temperature values estimated on the basis of grenade measurements (also using Pitot tubes and Australian spheres) [12, 15, 16] for the latitudes of the Soviet stations and determined using the M-100B ("316") rocket are maximum for 80°N (Table 4). The reason for this may be an inaccuracy in the extrapolation of grenade data to 80°N, the small volume of data, etc. At the 80-km level the values of the differences are variable.

When using the modernized "316M" nosecone with the M-100B rocket (instead of the "361") the discrepancies with grenade data are reduced, but their values are preliminary.

M-100B and MMR-06 rockets. Table 5 shows that the temperature values according to MMR-06 data in the lower mesosphere are somewhat higher than according to M-100B ("361M") data by approximately 1°C at altitudes 45-50 km and 6°C at 55 km. With the results given in Table 4 we find that the temperatures measured with the MMR-06 rocket and with use of grenades are in agreement with one another at altitudes 50-55 km.

Summary. Our analysis systematizes the discrepancies in long-term data from rocket measurements of temperature in the mesosphere carried out at a number of stations using different methods and apparatus. This makes possible the reconciled use of data from different sources. However, there is no unanimous opinion concerning the choice of a reference method because investigations of the errors of individual methods have not been completed. In the formulation of standard and reference models of the mesosphere it has become the practice to use data on temperature obtained by the grenade method as the fundamental data [2, 6, 17]. Accordingly, in the formulation of new models a continuity is best ensured by continuing to employ data obtained by the grenade method as the reference data for the mesosphere (Table 6). Data obtained with the MMR-06 rocket, Australian spheres (in the 1970's) and Pitot tubes on the average agree with grenade data. In the case of the M-100 rocket reconciling corrections in Table 6 are considerably smaller for data obtained at the present time using the "361M" nosecone than for archival data (prior to 1978) accumulated using the "361" nosecone.

We note that grenade observations in general are complex and expensive and for all practical purposes are not being made at the present time. In choosing a method as a reference (for example, M-100 ("361-M") data) the values of the reconciling corrections vary in accordance with the differences between the temperatures obtained using this and the grenade method.

****

Table 5

Differences Between Atmospheric Temperature Values (°C) Measured Using MMR-06 Rocket and M-100B ("361M") Rocket

Period	Region	Altitude, km			
		40	45	50	55
Summer 1979-1980	Middle latitudes	0.5	1.5	2.5	5
May 1979	Equator	-3.5	0	-0.5	8
February 1980	Equator	1.5	2.5	1.5	7

Table 6

Reconciling Empirical Increments (°C) to Long-Term Temperature Values Obtained in Former Years by Various Rocket Measurement Methods (Using Grenade Measurements as Reference Values)

Altitude, km	M-100B		Datasonde	Arcasonde		Sphere (USA)
	"361" (summer)	«361M»	with correction [11]	without correction [7]	with correction [7]	
80	—	—	—	—	—	6
75	9	5	—	—	—	0
70	21	8	—7	—	—	0
65	24	10	—5	—	—	—2
60	21	7	—3	—15	—3	—2
55	12	6	—1	—8	—1	2
50	5	4	0	—5	—1	5
45	2	1	0	—3	—1	4

BIBLIOGRAPHY

1. Avdeyev, V. N., Lysenko, Ye. V. and Chernova, G. G., "Aerodynamic Error in Temperature Measurements in the Atmosphere With a Rocket Thermometer," TRUDY TsAO (Transactions of the Central Aerological Observatory), No 144, 1980.

2. GOST 4401-73. STANDARTNAYA ATMOSFERA (State Standard 4401-73. Standard Atmosphere), Moscow, Izd-vo Standartov, 1974.

3. Kokin, G. A., Bugayeva, I. V., Ryazanova, L. A. and Speranskiy, K. Ye., "Correlation Between Stratospheric Processes and Solar Activity," METEOROLOGIYA I GIDROLOGIYA (Meteorology and Hydrology), No 7, 1977.

4. Koshel'kov, Yu. P., "Mean Monthly Temperature in the Southern Hemisphere Mesosphere," TRUDY TsAO, No 140, 1978.

5. Angell, J. K. and Korshover, J., "Recent Rocketsonde-Derived Temperature Variations in the Western Hemisphere," J. ATMOS. SCI., Vol 35, 1978.

6. COSPAR INTERNATIONAL REFERENCE ATMOSPHERE 1972 -- CIRA 1972, Berlin, Akademie-Verlag, 1972.

7. Exemenary, F. R. C., "On the Magnitude and Uncertainties of Corrections to Arcasonde 1 A Temperatures," J. APPL. METEOROL., Vol 11, No 4, 1972.

8. Finger, F. G., et al., "Compatability of Meteorological Rocketsonde Data As Indicated by International Comparison Tests," J. ATMOS. SCI., Vol 32, No 9, 1975.

9. Hoxit, L. R. and Henry, R. M., "Diurnal and Annual Temperature Variations in the 30-60 km Region as Indicated by Statistical Analysis of Rocketsonde Temperature Data," J. ATMOS. SCI., Vol 30, No 5, 1973.

10. Ivanovsky, A. I., et al., "Preliminary Results of the Intercomparison Test of US and USSR Meteorological Systems at the Wallops Island in August 1977," Preprint to XXI COSPAR, Innsbruck, 1978.

11. Krumins, M. V. and Lyons, W. C., "Corrections for the Upper Stratosphere Temperatures Using a Thin Film Loop Mount," MOLTR 72-152. Naval Ordnance Laboratory, Md., 1972.

12. Pearson, P. H., TECHNICAL NOTES, Weapons Res. Establish., Salisbary, Australia, 1970-1975.

13. Quiroz, R. S., "Stratospheric Temperatures During Solar Cycle 20," JGR, Vol 84, 1979.

14. Schmidlin, F. J., "Diurnal Tidal Analysis in the Equatorial Stratosphere and Mesosphere," Preprint to COSPAR XIX, Philadelphia, 1976.

15. Smith, W. S., et al., "Temperature, Pressure, Density and Wind Measurements in the Upper Stratosphere and Mesosphere," NASA TECHN. REPORTS R-211, R-245, R-263, R-288, R-316, R-340, R-360, R-391, 1964-1972, Wash. D. C.

16. Theon, J. S., et al., "The Mean Observed Meteorological Structure and Circulation of the Stratosphere," NASA TR R-375, Wash. D.C., 1972.

17. US STANDARD ATMOSPHERE, 1976, NOAA, NASA, USAF, Wash., D.C., 1976.

18. World Data Center A, METEOROLOGY. HIGH ALTITUDE METEOROLOGICAL DATA, Asheville, N. C., 1965-1977.

UDC 551.508.29

RADIO DEVICE OF A SYSTEM FOR THERMAL SOUNDING OF THE ATMOSPHERE BY THE RADIOACOUSTIC SOUNDING METHOD

Moscow METEOROLOGIYA I GIDROLOGIYA in Russian No 3, Mar 81 pp 120-123

[Article by V. M. Bovsheverov, M. A. Kallistratova and L. V. Knyazev, candidates of physical and mathematical sciences, A. G. Gorelik, professor, and M. Yu. Yegorov]

[Text]

Abstract: Radioacoustic sounding (RAS) is a promising method for prolonged measurement of the temperature profile in the atmospheric boundary layer. The authors examine the various aspects of design of the receiving and transmitting radio elements of a radioacoustic sounding system. The optimum specifications for these devices are set forth. An experimentally determined temperature profile is given and this is compared with radiosonde results.

Radioacoustic sounding (RAS) is an effective method for long-term monitoring of the temperature profile T in the atmospheric boundary layer at a real time scale. The method is based on measurement of the speed of sound v_s in the atmosphere,

$$v_s = 20.05\sqrt{T},$$

which is determined from the Doppler frequency shift f_D of an electromagnetic signal reflected from an acoustic wave. A distinguishing characteristic of the RAS system is that it effectively functions near the synchronism $2\lambda_s = \lambda$ [5, 6], when the electromagnetic energy reflected from each of the acoustic wave fronts arrives in the receiver antenna in phase. In this case

$$f_D = 2v_s/\lambda = v_s/\lambda_s = f_s,$$

where λ and λ_s are the wavelengths of the electromagnetic signal and sound.

A highly important problem in developing the radio device for the RAS system is the choice of a working wavelength. The systems described in the literature have used either very short electromagnetic waves (about 3 cm, 10 cm [2, 3]) or very long waves (0.7 m, 8 m [4, 5]). In the first case it is impossible to obtain a reflection with great ranges since the acoustic wave rapidly attenuates; in the second

the acoustic wave almost does not attenuate during propagation, but the realization of such a system requires the construction of unwieldy narrow-beam radio and acoustic antennas.

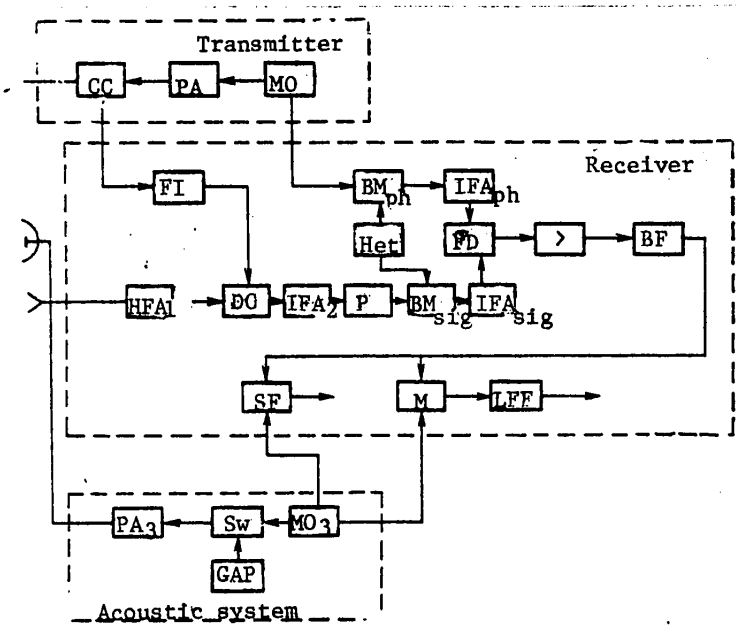

Fig. 1. Block diagram of RAS system radio complex. CC) capacitive coupling; PA and PA_3) power amplifiers for transmitter and acoustic system; MO and MO_3) master oscillators; PI) phase inverter; HFA) high-frequency amplifier; DC) directional coupling; P) preselector; BM_{sig} and BM_{ph}) balance mixers of signal and phase channels of receiver; Het) heterodyne; IFA_{sig}, IFA_{ph}) intermediate frequency amplifiers; PD) phase detector; BF) band filter; SF) synchronous filter; M) multiplier; LFF) low-frequency filter; Sw) switch; GAP) generator of acoustic pulses.

The developed RAS system operates at a wavelength of 30 cm. This is a compromise in the effort to obtain a significant effective range of the RAS system with relatively small dimensions of the antenna system.

According to [5], for the reception of a signal from a kilometer range with an acoustic power of about 5 W and with an antenna directional diagram of about 10° the ratio of the power of the electromagnetic signal P_{rec} reflected from the acoustic pulse to the transmitter power P_t (radar potential) should be not less than 140 db. This does not take into account the attenuation of the signal caused by turbulence and the shift of the acoustic pulse relative to the radio antenna ray by the horizontal wind component. The attenuation of the reflected signal caused by the enumerated factors

is 50 db or more. The required potential is therefore -190 db.

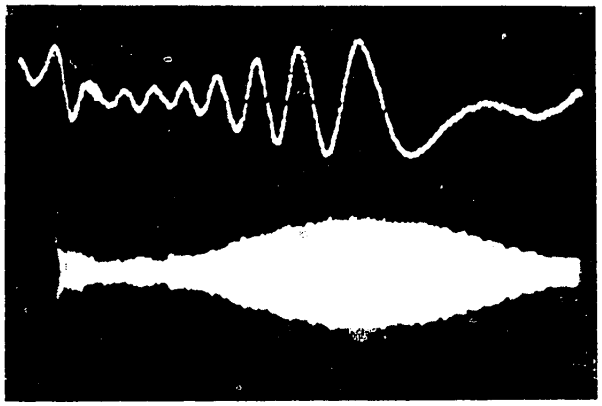

Fig. 2. Output voltages of circuit for synchronous shift of Doppler frequency and band filter. The scale 0.2 sec/cm corresponds to a range scale 70 m/cm.

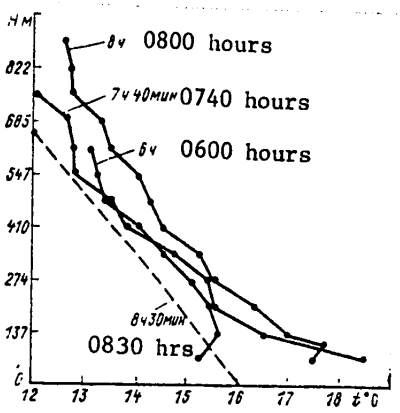

Fig. 3. Temperature profiles obtained with one registry of acoustic pulse from synchronous drift circuit. Radiosonde measurement (dashed line) was made at a distance of 40 km from the place where radioacoustic sounding took place.

The potential of any continuous radar is determined primarily by the "creeping" of transmitter noise from the transmitter antenna to the receiver antenna. With f_D 2200 Hz and an effective width of the receiver band Δf = 30 Hz the power of this noise is below the power of the carrier frequency of the transmitter by about 100 db. If the decoupling of the receiving and transmitting antennas is inadequate, it

is precisely this noise which determines the real receiver response. With a good decoupling of the antennas the potential will be determined by the P_t value and receiver response W_{rec}. In our case the decoupling value, with allowance for compensation, was not less than -110 db. This excluded the influence of transmitter noise.

Under these conditions it is possible to ensure the potential (-190 db) by several methods: the first involves an increase in receiver response, the second requires an increase in the radar transmitter power P_t, and the third necessitates an increase in the directivity of the radio and acoustic radiation source. The possibilities for the second method are extremely limited because with an increase in P_t there is an increase in a direct "creeping" of the transmitter signal to the receiver input, which in the last analysis leads to a saturation of the receiver amplification channel. An increase in the directivity of the antennas is possible only to a definite limit (in the case of narrow-beam antennas the wind influence increases sharply and the adjustment of the entire RAS system is complicated).

Accordingly, the most justified approach is a maximum increase in receiver response.

Now we will briefly discuss the principal technical specifications of the developed RAS system radio complex (Fig. 1).

The centers of the radio antennas were situated at a distance of 4 m from the center of the acoustic antenna, on either side relative to the latter. An electromagnetic screen with an absorbing upper edge was installed in the middle. The height of this screen was 4 m. The absorbing edge makes it possible to reduce diffraction phenomena arising at the screen edges. In this way there was a decoupling between the antennas $\alpha_{de} = -74$ db.

In order to reduce the influence of the HF channel the high-frequency amplifiers HFA_1, HFA_2 and the directional coupler (DC) were mounted on the receiving antenna. The compensation circuit made it possible to reduce the undesirable influence of direct "creeping" of the signal into the receiver; some of the transmitter power was fed through an adjustable capacitive coupler (CC) and phase inverter (PI) via the directional coupler into the receiver amplification channel and it was really possible to compensate the direct "creeping" of the signal by an additional 30-40 db. The resulting decoupling and compensation made it possible to work with a power level in the transmitting antenna of 1 W.

At the output of the band filter (BF) the signal was suitable for analysis for the purpose of obtaining geophysical data on the atmosphere. The band 200 Hz covers all possible f_D values in the real temperature range without readjusting the outfit. From this output at altitudes up to 250 m a signal was received which exceeds the noise by 40-30 db. However, this is not the limit: using the synchronism property, only with which reliable reception is possible, there can be a further increase in receiver response.

Since $f_D = f_S$, it is desirable to use a narrow-band filter (SF) with tuning changing synchronously with f_S. With an average temperature gradient 6°C/km in the altitude range 1 km the width of the filter transmission band is

$$\Delta f = 20.05/\lambda \Delta T/\sqrt{T} \approx 24 \text{ Hz}.$$

Tuning for synchronism was accomplished by a change in f_s. At the selected altitude the moment of synchronism was determined on the basis of zero beats at the output of the Doppler spectrum synchronous drift circuit for the reflected signal (photomultiplier). The circuit also makes it possible to exclude an excess of information in statistical processing of the reflected signal. The measures described above made it possible to bring the potential to -190 db.

The developed apparatus was employed for geophysical measurements in the atmosphere beginning in July 1979. Temperature profiles to an altitude of 1 km were obtained which agree well with data from radiosonde measurements. Figure 2 shows the characteristic appearance of a reflected signal at the output of the band filter and the output of spectrum synchronous drift circuit and Fig. 3 was constructed on the basis of the output signal of this circuit. The latter figure shows temperature profiles based on one passage of the acoustic pulse along the path. The minimum sounding altitude was 50 m. The results of field measurements are discussed in greater detail in [1].

BIBLIOGRAPHY

1. Azizyan, G. V., Bovsheverov, V. M., Gorelik, A. G., Yegorov, M. Yu., Kallistratova, M. A., Karyukin, G. A. and Knyazev, L. V., "Experience in Measuring Temperature Profiles in the Lower Troposphere by the Radioacoustic Sounding Method," IZV. AN SSSR: FIZIKA ATMOSFERY I OKEANA (News of the USSR Academy of Sciences: Physics of the Atmosphere and Ocean), No 2, 1981.

2. Babkin, S. I., Kutsenko, V. I., Pakhomov, Yu. A., Proshkin, Ye. Ye. and Ul'yanov, Yu. N., "System for Radioacoustic Sounding of the Atmosphere in the Centimeter Wavelength Range," TEZISY V VSESOYUZNOGO SIMPOZIUMA PO LAZERNOMU I AKUSTICHESKOMU ZONDIROVANIYU ATMOSFERY. CH. III (Summaries of Reports at the Fifth All-Union Symposium on Laser and Acoustic Sounding of the Atmosphere. Part III), Tomsk, SO AN SSSR, IOA, 1978.

3. Makarova, T. I., "Use of the DISS-3P Station in a Radioacoustic Sounding System," TEZISY V VSESOYUZNOGO SIMPOZIUMA PO LAZERNOMU I AKUSTICHESKOMU ZONDIROVANIYU ATMOSFERY. CH. III, Tomsk SO AN SSSR, IOA, 1978.

4. Frenkel, M. S., Chang, N. J.,and Sander, M. F. (Jr.), "A High-Frequency Acoustic Sounder for Remote Measurement of Atmospheric Wind and Temperature," BULL. AMER. METEOROL. SOC., Vol 58, No 9, 1977.

5. Marshall, J. M., Peterson, A. M. and Barnes, A. A., "Combined Radar-Acoustic Sounding System," APPL. OPTICS, Vol 11, No 1, 1972.

6. North, E. M., Peterson, A. M. and Parry, H. D., "RASS, a Remote Sensing System for Measuring Low-Level Temperature Profiles," BULL. AMER. METEOROL. SOC., Vol 54, No 9, 1973.

REVIEW OF MONOGRAPH BY V. R. ALEKSEYEV AND B. L. SOKOLOV: POLEVYYE ISSLEDOVANIYA NALEDEY (FIELD INVESTIGATIONS OF ICE ENCRUSTATIONS), LENINGRAD, GIDROMETEOIZDAT, 1980

Moscow METEOROLOGIYA I GIDROLOGIYA in Russian No 3, Mar 81 pp 124-125

[Review by M. Sh. Furman, candidate of geographical sciences, Irkutsk Hydrometeorological Observatory]

[Text] In connection with the intensive exploitation of the natural resources of Siberia and the Far East engineering field workers, planners and construction men are encountering the need for study of the ice encrustation phenomena, which have a widespread occurrence, for developing measures to provide safeguards against their unfavorable influence on engineering structures, transportation routes, populated places, etc. The construction of the Baykal-Amur Railroad and the implementation of plans for the economic development of adjacent regions have provided a new momentum for a more active and planned study of ice encrustations.

Until now field investigations of ice encrustations have been scattered; investigations of this phenomenon are made by different scientific and engineering organizations and specialists in different fields.

The collection of reliable scientific information on ice encrustations and ice encrustation processes is possible only with a standardization of field observations, on the basis of a unified geographical-hydrological method and their investigation with a multisided study of all environmental components.

Along these lines a positive fact was the publication of the monograph FIELD INVESTIGATIONS OF ICE ENCRUSTATIONS by the Gidrometeoizdat in 1980. It was prepared by scientists and specialists of the State Hydrological Institute of the State Committee on Hydrometeorology, the Institute of Geography of Siberia and the Far East of the Siberian Department USSR Academy of Sciences and the "Priroda" State Center of the Main Administration of Geodesy and Cartography.

The authors of the book generalized available experience in work on study of ice encrustations in different regions of Siberia and the Far East and established the principal aspects of the field research method.

In the first chapter the authors examine the fundamental concepts and terms related to field investigations, primary processing and analysis of data from field observations. The principal patterns of interrelationship between ice encrustations and the environment are presented and on their basis it is emphasized that there is a need for multisided study of ice encrustation phenomena, which leads to obtaining reliable data for the solution of practical and scientific problems.

The second chapter examines the objectives, content and methods of field investigations of ice encrustations.

The following directions in the study of ice encrustations are fundamental in the solution of different problems: 1) clarification of the patterns of geographical distribution of ice encrustations over an area; 2) study of the dynamics of ice encrustation processes in their annual and long-term cycles; 3) their prediction, taking into account man's economic activity, evaluation and allowance for the influence of ice encruscations on the environment and engineering structures. The authors propose that these directions be pursued by solving a whole series of interrelated problems: study of the territorial distribution of ice encrustations, investigation of the physical and geochemical processes of ice encrustation formation, the laws governing the regime of ice encrustations, etc. as a result of the interaction of all natural processes. Particular attention must be given to the accuracy of field measurements, evaluation of the use of the results of complex observations for different purposes and application of the general patterns determined from studied ice encrustations to unstudied formations.

The authors have developed a general basis of the work method and provided a list of the necessary methods for field investigations which are differentiated as surface and remote. The book examines all types of standard observations and experimental investigations, each of which solves an individual part of the overall problem.

At the present time remote methods for the study of ice encrustations are only beginning to enter the arsenal of researchers and for this reason great attention is given to this problem in the third chapter. The characteristic features of remote methods are examined. These make it possible simultaneously to obtain information on a great number of features scattered over an area, ensure a uniformity of measurement data and the possibility of obtaining additional information on the processes accompanying the formation of ice encrustations which are difficult to study by surface methods. In examining the advantages of these methods, the authors point out for what purposes they are most effective (preparation of catalogues, surveys, atlases, etc.) in evaluating the temporal and areal ice encrustation of a territory, etc.

On the basis of their own experience and the work of different organizations the authors describe methods for making observations from the air and by landing of aircraft in the investigated areas. They discuss aerial photographic surveys of ice encrustations, reveal the distinguishing characteristics of this work, interim use of these methods, interpretation criteria, etc.

A new method is examined for a study of ice encrustations -- radar sounding of ice. Its fundamental physical principles are discussed, a block diagram of the radar apparatus is given, the experience in carrying out such work in the mountainous regions of the zone of the Baykal-Amur Railroad is described, and the principal requirements on equipment for the sounding of ice encrustations from an aircraft are set forth.

The fourth and fifth chapters examine methods for reconnaissance and stationary investigations. These give an analysis of the specifics of work for the study of ice encrustations formed from ground and surface waters, validate the choice of features

for observation, and describe the makeup and content of such studies (general and specialized), as well as explaining the placement of measurement rods on ice encrustations, etc. A method for evaluating the errors in measuring different characteristics of ice encrustations is given for validation of an observation network with determination of the optimum number of observation points.

Fully understanding the complexity of a thorough substantiation of field investigations of ice encrustations and the overall state of the discussed problem, the authors call upon specialists in different lines of work who are concerned with the study and exploitation of regions in Siberia and the Far East to broaden their work in developing a unified method for the field study of ice encrustations and ice encrustation processes.

The publication of the book by V. R. Alekseyev and B. L. Sokolov is very timely. In this book the first attempt is made at generalizing existing experience for the field study of ice encrustations and ice encrustation processes. The individual shortcomings of the book and disputable points are related primarily to the fact that ice encrustation processes have still been studied very little, only general ideas exist concerning some of them and individual aspects of this phenomenon have only appeared recently.

The reviewed book can become the basis for creating a manual for study of ice encrustations in the network of stations and posts of the State Committee on Hydrometeorology, taking into account the specifics of implementation of network observations.

FIFTIETH ANNIVERSARY OF THE LENINGRAD HYDROMETEOROLOGICAL INSTITUTE

Moscow METEOROLOGIYA I GIDROLOGIYA in Russian No 3, Mar 81 pp 126-127

[Article by B. Ya. Tolstobrov, prorector, Leningrad Hydrometeorological Institute]

[Text] During the period 27-28 November 1980, at the Leningrad Hydrometeorological Institute (LHMI), there was a solemn conference and session of the Scientific Council devoted to the 50th anniversary of this academic institute. The institute was organized in Moscow on 23 July 1930 on the basis of the Geography and Geology Faculties at First Moscow State University and at that time was called the Moscow Hydrometeorological Institute (MHMI). It moved to Leningrad in the autumn of 1944.

Representatives of the Ministry of Higher and Special Education RSFSR, the State Committee on Hydrometeorology, USSR Academy of Sciences, Ministries of Defense, Civil Aviation, Power and Electrification and other departments participated in the anniversary solemnities.

At the solemn session a report on the activity of the institute in its 50 years was presented by its rector, Doctor of Geographical Sciences N. P. Smirnov. He noted that the LHMI was the country's and world's first specialized hydrometeorological college. Over the period of a half-century its personnel carried out much work for the training of personnel, for different branches of the national economy and for national defense. Since the time of its founding the institute has trained more than 10,000 specialists with higher skills -- meteorologists, hydrologists and oceanologists -- furnishing hydrometeorological information and forecasts to aviation and agriculture, industry and the power industry, construction and transportation in all regions of our great country and far beyond its limits.

During the period of the Great Fatherland War the MHMI, transformed in the summer of 1941 into the Higher Military Hydrometeorological Institute (HMHMI), was completely switched over to the training of military hydrometeorological engineers for the armed forces of our country. The graduates of the institute successfully supported at the fronts the combat operations of the Soviet Army, the Air Forces and the Navy and thereby made a weighty contribution to the victory of our people over the German-Fascist invaders.

During the years which followed the institute continued to develop: there was improvement in its structure, the content of the lecture courses and the instruction method, the staff increased in size, the material-technical base was strengthened, the quality of preparation of the graduated specialists increased and international relationships were developed.

At the present time the institute has three faculties: meteorological, hydrological and oceanological, responsible for training in the three fields of specialization and in several narrower areas of specialization (numerical forecasting methods, long-range forecasts, hydrometeorological measurements and instruments, physical oceanology and marine chemistry). Since 1981 there has been a faculty for upgrading skills for supervisory personnel and specialists of the State Committee on Hydrometeorology. There are 21 departments at the institute where there are about 180 instructors, of which more than 100 have academic degrees and titles, including 25 professors and doctors of sciences. By a resolution of the Collegium of the Ministry of Higher and Intermediate Special Education RSFSR the LHMI has been assigned the functions of the main council on hydrometeorological education in our country.

The institute also heads work of the Council on the Problem "Preservation and Rational Use of the Atmosphere" in the USSR Ministry of Higher and Intermediate Special Education system.

The LHMI is widely known for its international relationships. Each year about 150 foreign citizens (students and graduate students) from 45 countries of Asia, Africa, Latin America and Europe study within the walls of the institute.

The staff of instructors and service organizations and students devote much attention to the training of skilled specialists for foreign countries, seeing this as their international duty and an important means for educating young people.

The body of scientists at the institute is carrying out much scientific research work. The merits of institute scientists in the field of writing of textbooks and study aids in hydrometeorological disciplines are great and widely recognized. Institute specialists have met this anniversary with new successes in academic, scientific and instructional work, the adoption of additional obligations in honor of the 26th CPSU Congress.

The first rector of the institute, Professor V. A. Belinskiy, the former rectors Docent V. I. Poltavtsev and Corresponding Member USSR Academy of Sciences O. A. Alekin and others participated in the anniversary session.

A member of the Collegium, the head of the Administration of Personnel and Academic Institutes of the State Committee on Hydrometeorology A. N. Chilingarov, the president of the USSR Geographical Society and Director of the Arctic and Antarctic Scientific Research Institute Corresponding Member USSR Academy of Sciences A. F. Treshnikov, the director of the Main Geophysical Observatory Professor Ye. P. Borisenkov, the director of the State Hydrological Institute Professor A. A. Sokolov, the director of the State Meteorological Publishing House Merited Worker in Culture RSFSR Yu. V. Vlasova, representatives of many other scientific research institutes, the Ministry of Higher and Intermediate Special Education and academic institutes presented greetings to the personnel of the LHMI. The institute received more than 200 congratulations and telegrams. These included greetings from the chairman of the USSR Council of Ministers, the chairman of the State Committee on Science and Technology Academician G. I. Marchuk, the chairman of the State Committee on Hydrometeorology Corresponding Member USSR Academy of Sciences Yu. A. Izrael', chairman of the

earth sciences section of the Presidium USSR Academy of Sciences, Vice President of the USSR Academy of Sciences Academician A. V. Sidorenko, Academician-Secretary of the Division of Oceanology, Physics of the Atmosphere and Geography of the USSR Academy of Sciences Academician L. M. Brekhovskikh, director of the Institute of Applied Geophysics Academician Ye. K. Fedorov. The specialists and students of the LHMI were warmly and sincerely congratulated by the Ministry of the Ship Building Industry, the Ministry of Power and Electrification, the Ministry of Fisheries, the Ministry of Defense, the Ministry of Civil Aviation, the Design Bureau imeni A. N. Tupolev and many others. Many congratulatory telegrams were also received from the hydrometeorological services of the socialist countries. The graduates of the institute sent warm greetings to the LHMI staff.

At the anniversary session of the scientific council of the institute reports were presented on several directions of work carried out in the scientific program of the institute by: Meritorious Worker in Science RSFSR, Professor L. T. Matveyev, Professor V. G. Morachevskiy, Professor L. G. Kachurin, Professor A. R. Konstantinov and Docent I. P. Spitsyn, Professor Yu. P. Doronin, and Professor B. N. Belyayev.

An All-Union Conference of the Student Scientific Society was also held. It was devoted to the 50th anniversary of the Komsomol organization at the institute. Reports were presented to the conference by students at the Leningrad Hydrometeorological Institute, Odessa Hydrometeorological Institute and a number of universities of the country.

The institute is faced with major tasks in the field of further improvement in the academic process, the communist education of students and the development of fundamental scientific research.

NOTES FROM ABROAD

Moscow METEOROLOGIYA I GIDROLOGIYA in Russian No 3, Mar 81 pp 127-128

[Article by B. I. Silkin]

[Text] The nitrogen oxides and sulfur emitted into the atmosphere in the course of industrial activity, entering into interaction with the moisture present in the air, form corresponding acids. The farther these concentrations of substances move away from the source, the greater is the quantity of acid which they create. As a result, in regions remote from factories and electric power stations there can be acidic precipitation which exerts a destructive effect on the plant and animal world.

In NEW SCIENTIST, Vol 87, No 1215, 1980 it is reported that the largest supplier of such substances to air space is the United States, where each year about 26 million tons of sulfur dioxide and 22 million tons of nitrogen oxide enter the atmosphere. Their principal source is thermoelectric power stations operating on coal. The metallurgical plants of Canada add their own, although lesser fraction to it. As a result of the distant transport of contaminating agents the problem of the acidity of precipitation has become international in North America. The Minister for Environmental Affairs of Canada, J. Roberts, declared that that country in the next 20 years must expend not less than 400-500 million dollars annually for the prevention of acidic precipitation; the cooresponding expenditures for the United States must be approximately eight times greater. If this process is not stopped the losses inflicted on lakes, soil, harvests, structures and human health will lead to equivalent losses.

***

As reported in SCIENCE, Vol 209, p 491, 1980 and in NEW SCIENTIST, Vol 87, No 1212, p 366, 1980, the first evidence appeared in 1975 that fluorocarbons, forming a part of household aerosols, can cause substantial harm to the ozone layer which safeguards the earth against receipts of excess quantities of solar UV radiation. Taking into account that such a phenomenon should lead to an increased occurrence of cases of skin cancer, a number of countries adopted measures for banning the production of aerosols containing fluorocarbons.

Now a scientific specialist of the United States Geological Survey D. Johnston has concluded that in the course of an average year the materials ejected into the atmosphere in the course of volcanic eruptions can cause destruction of the earth's ozonosphere to an equal degree as all the fluorocarbons entering into air space in 1975, being a period of maximum use of aerosols.

Until recently the quantity of chlorine entering the atmosphere as a result of explosive volcanic activity remained poorly studied.

According to an approximate evaluation by D. Johnston, in the entire world on the average each year there should be one explosive eruption similar to that which occurred in 1976 in Augustine Volcano in Alaska. This eruption, judging from all available data, led to the ejection of a quantity of HCl which substantially exceeds the quantity of fluorocarbons released as a result of human activity in 1975. Between 17 and 36% of this volcanic ejecta entered directly into the earth's stratosphere.

An eruption occurring about 700,000 years ago in California evidently led to the settling of approximately 100 km^3 of volcanic ash onto its surface. It should have released into the stratosphere six times more chlorine than did anthropogenic factors in 1975.

The figures cited by D. Johnston are approximate. However, it is clear that the regular entry of a large quantity of chlorine into the earth's air space, caused by volcanic activity, must be seriously taken into account by meteorologists and specialists in physics of the atmosphere in modeling the chemistry of the planet's air envelope.

OBITUARY OF MAKSIM SAVVICH KULIK (1907-1980)

Moscow METEOROLOGIYA I GIDROLOGIYA in Russian No 3, Mar 81 p 128

[Article by agrometeorologists of the USSR Hydrometeorological Center and the All-Union Scientific Research Institute of Agricultural Meteorology]

[Text] Soviet agrometeorology has experienced a severe loss: Maksim Savvich Kulik, one of the leading agrometeorologists of our country, died on 8 August 1980.

M. S. Kulik gave about 50 years to the development of Soviet agrometeorology. Heading the Agrometeorological Section of the Ukrainian Administration of the Hydrometeorological Service in 1932, his scientific and organizational activity was inseparably related to problems in agrometeorology.

During the years of the Great Fatherland War Engineer-Major M. S. Kulik directed meteorological support of the army.

During the first post-war years he was Deputy Chief of the Ukrainian Administration of the Hydrometeorological Service and at the same time was a senior scientific specialist of the Geography Institute of Kiev University. In 1948 Maksim Savvich

successfully defended his candidate's dissertation and beginning in 1949, for a period of 15 years, was deputy director of the Central Interest of Forecasts, heading a large group of agrometeorologists. At this time, under his direct leadership and with his participation a validation was given for state measures directed to the upgrading of agriculture. Agrometeorological observations and forecasts were developed and improved. Maksim Savvich created a method for evaluating and predicting the effectiveness of application of mineral fertilizers in dependence on weather conditions, making it possible to increase the effectiveness of fertilizers during spring top dressing of winter crops in the nonchernozem zone, which gives a yield increase of not less than 20%.

The teaching activity of M. S. Kulik was highly diversified. An excellent lecturer and propagandist, he gained merited fame by presenting lectures at courses for upgrading the skills of specialists of the Hydrometeorological Service and other organizations.

He trained a whole group of young scientists, eleven of whom have successfully defended candidate's and doctor's dissertations. The numerous scientific studies of M. S. Kulik (there are more than 80 of them) are widely known in our country and abroad.

He was an active worker in the international agencies of the WMO and a participant in many international conferences.

In 1964 M. S. Kulik headed a laboratory in the Obninsk Affiliate of the Institute of Applied Geophysics, successfully combining much scientific work with public activity, being a member of the executive committee and a deputy of the city soviet.

Maksim Savvich devoted much effort to scientific editing and preparations for the printing of scientific papers, over a period of many years being a member of the editorial board of the journal METEOROLOGIYA I GIDROLOGIYA and serving as chairman of the agrometeorology section of the editoral council of the Hydrometeorological Publishing House. In 1967 he was awarded honorary diplomas of the Presidium of the Supreme Soviet RSFSR and the Obninsk City Committee CPSU, and in 1976 for successes in the implementation of the Ninth Five-Year Plan -- the Order "Emblem of Honor."

The bright memory of Maksim Savvich Kulik, a talented scientist, a good, responsive person, will long remain in the hearts of his numerous students, fellow workers and followers.

5303
CSO: 1864/8

- END -